5-2015

TWO-COLOR FLUORESCENT ANALYSIS OF CONNEXIN 36 TURNOVER AND TRAFFICKING – RELATIONSHIP TO FUNCTIONAL PLASTICITY

Yanran Wang

TWO-COLOR FLUORESCENT ANALYSIS OF CONNEXIN 36 TURNOVER AND TRAFFICKING – RELATIONSHIP TO FUNCTIONAL PLASTICITY

by

Yanran Wang

APPROVED:

_____
Supervisory Professor: John O'Brien, PhD

_____
Joseph L. Alcorn, PhD

_____
Steve Massey, PhD

_____
Christophe P. Ribelayga, PhD

_____
Eric C. Swindell, PhD

APPROVED:

_____
Dean, The University of Texas
Graduate School of Biomedical Sciences at Houston

TWO-COLOR FLUORESCENT ANALYSIS OF CONNEXIN 36 TURNOVER AND TRAFFICKING – RELATIONSHIP TO FUNCTIONAL PLASTICITY

A DISSERTATION

Presented to the Faculty of
The University of Texas
Health Science Center at Houston
and
The University of Texas
MD Anderson Cancer Center
Graduate School of Biomedical Sciences
in Partial Fulfillment

of the Requirements

for the Degree of

DOCTOR OF PHILOSOPHY

by

Yanran Wang
Houston, Texas

May, 2015

Acknowledgements

I would like to thanks my advisor, Dr. John O'Brien for his mentorship. I cannot express enough gratitude for his guidance and help throughout the years. With great patience, he has taught me a lot of scientific knowledge and skills, writing and presentation skills, also the right attitude and mindset facing challenges and setbacks. He set a great example on how to face difficulties and pressure in career and in life. I am not only a better scientist, but a better person because of him.

I also would like to thank the other members of my thesis committee. Dr Joseph Alcorn, Dr. Steve Massey, Dr. Christophe Ribelayga, and Dr. Eric Swindell have provided me with critiques and advice over the years. They gave me a lot of brilliant ideas on carrying forward with my project, pointed out weaknesses where I have overlooked, and challenged me to give better presentations.

The fellow members of the O'Brien lab, both past and present, have provided me with supports. These include Dr. Wade Kothmann, Dr. Hongyan Li, Ya-Ping Lin, Cheryl Mitchell, Alex Vila and Dr. Keith Moore. Dr. Christopher Whitaker and Dr. Gina Nobles, past and present post-docs of the ophthalmology department, have given me great advice on scientific writing and presentation. My fellow neuroscience students have always been a great support system. I could not have made it through the much dreaded candidacy exam without their candid advice and critiques. All of them have been not only great lab-mates, co-workers, classmates, but also great friends in life that I can share laughs with and count on when I need help.

My parents, Xianhong Zhou and Xudong Wang, have been there for me all my life through thick and thin. Being away from home since young age, I have always felt their constant love and support, no matter how far away from home I am. They have always encouraged and challenged me to better myself. My fiancé Daniel, and my future in-laws, the Burtons, have given me support and encouragement even when I doubted myself. I could not have achieved this without my family, both present and future.

TWO-COLOR FLUORESCENT ANALYSIS OF CONNEXIN 36 TURNOVER AND TRAFFICKING – RELATIONSHIP TO FUNCTIONAL PLASTICITY

Yanran Wang

Supervisory Professor: John O'Brien, PhD

Gap junctions (GJ) formed of Cx36 show tremendous functional plasticity on several time scales. Changes in connexin phosphorylation modify coupling in minutes through an order of magnitude, but recent studies also imply involvement of connexin turnover in regulating cell-cell communication. We utilized Cx36 with an internal HaloTag to study Cx36 turnover and trafficking in cultured cells to discriminate newly formed and pre-existing Cx36. New Cx36 in cargo vesicles was added directly to existing gap junctions and newly made Cx36 was not confined to points of addition, but diffused throughout existing gap junctions. Existing connexins also diffused into photobleached areas with a half-time of less than 2 seconds. Recovery of connexin was impaired when laser power was focused and phototoxicity may be responsible. To better understand mechanisms of turnover we studied the role of cytoskeletal elements, actin filaments in particular, in Cx36 vesicle trafficking and GJ mobility. Phalloidin labeling showed that thick actin bundles connected all edges of GJ plaques, but actin filaments were rare within. Actin filaments were found associated with small, chase-labeled delivery vesicles. Many GJs showed substantial numbers of finger-like filadendrites extending from both the edges and the center of the plaques, and the morphology of these filadendrites changed at a fast pace. Double labeling of HaloTag ligand and phalloidin showed that these filadendrites colocalized with thin actin filaments. Disruption of actin filaments with Cytochalasin D caused loss of GJ at cell-cell contacts. Treatment with Latrunculin A, which prevents new actin elongation, did not disrupt GJ

plaques and only partially suppressed Cx36 turnover, but eliminated the filadendrite extensions. In conclusion, studies of Cx36-HaloTag revealed novel features of connexin trafficking and demonstrated that phosphorylation-based changes in coupling occur on a different time scale than turnover. The role of rapid mobility of elements of GJ plaques in functional plasticity is unknown, but we hypothesize that it may relate to the mechanisms that control turnover of connexin protein.

Table of Contents

LIST OF FIGURES

Chapter One

Chapter Two

Chapter Three

Chapter Four

Chapter Five

LIST OF TABLES

List of Abbreviations

BFA: Brefeldin A

cAMP: Cyclic adenosine monophosphate

CT: C-terminal

Ctrl: Control

Cx: Connexin

Cy-D: Cytochalasin D

DMSO: Dimethyl Sulfoxide

ER: Endoplasmic Reticulum

EPSP: Excitatory Postsynaptic Potential

FRAP: Fluorescence Recovery After Photobleaching

GJ: Gap Junction

GST: Glutathione S-Transferase

Halo-EV: HaloTag Empty Vector

IPL: Inner Plexiform Layer

La-A: Latrunculin A

MEM: Minimum Essential Medium

NA: Numerical Aperture

OG: Oregon Green

OPL: Outer Plexiform Layer

PBS: Phosphate Buffered Saline

PBST: Phosphate Buffered Saline with Tween 20

PKA: Protein Kinase A

PM: Plasma Membrane

PP2A: Protein Phosphatase 2

ROI: Region of Interest

ROS: Reactive Oxygen Species

Rp: Rp-8-cpt-cAMPs

Sp: Sp-8-cpt- cAMPs

TBST: Tris-Buffered Saline with Tween 20

TGN: trans-Golgi network

TMR: Tetramethylrhodamine

WT: Wild Type

ZO-1: Zonula Occludens-1

Chapter One

Overview

In the nervous system, neurons pass down information through two types of synapses: chemical synapses and electrical synapses. In chemical synapses, there are distinct pre-synaptic and post-synaptic sides. Information is carried by chemical transmitters known as neurotransmitters. These neurotransmitters are released from the pre-synaptic side into the synaptic clefts, where they diffuse across to bind specific active targets on the post-synaptic side called receptors (Pereda, 2015). There are two types of neurotransmitter receptors, the ionotropic receptors, and metabotropic receptors. Ionotropic receptors are ligand-gated ion channels that generate currents quickly upon ligand binding (Connolly and Wafford, 2004). Metabotropic receptors, or G-protein linked receptors, most often interact indirectly with ion channels through G protein and release second messenger chemical (Conn and Pin, 1997). The binding between neurotransmitters and receptors trigger a series of downstream responses. Electrical synapses, on the other hand, consist of gap junctions (GJs) that provide a direct pathway of low resistance. The direct pathway allows much faster communication; the synaptic delay is only a fraction of a millisecond (Furshpan and Potter, 1959).

GJs are composed of membrane proteins that form a specialized intercellular channel that connects the cytoplasm of two adjacent cells. They allow direct transfer of ions and small molecules including metabolites and second messengers (Saez et al., 2003). They are diverse and ubiquitous and play an important role in cell-to-cell communication. Connexin is the single building block of a GJ. There are 21 connexin genes in the human genome. Connexins are four transmembrane domain proteins, with two extracellular loops for docking and one intracellular loop for functional regulation. Both the carboxyl terminus (C-terminus) and amino terminus (N-terminus) are in the cytoplasm (Figure 1.1A). Six connexin proteins oligomerize to form a hexameric structure called a connexon, or a hemichannel. Two hemichannels from adjacent cells

insert themselves into the plasma membrane and dock together to form a functional GJ channel (Figure 1.1B) (Ahmad et al., 1999a; Thomas et al., 2005; Zhang et al., 1996). When channels are functional, they allow communication between cells, called GJ coupling.

The formation of a hemichannel can be among the same type of connexin subunit (homomeric) or different types (heteromeric). The coupling of two hemichannels can be between the same type of connexons (homotypic) or different types (heterotypic) (Figure 1.1A) (Bloomfield and Volgyi, 2009). In homotypic electrical synapses, the steady state relationship between the GJ conductance and trans-junctional voltage is generally symmetrical. This allows the passage of current and small molecules to be bi-directional. Heterotypic GJ channels, however, can exhibit voltage-dependent rectification of conductance (Bukauskas et al., 1995).

A.

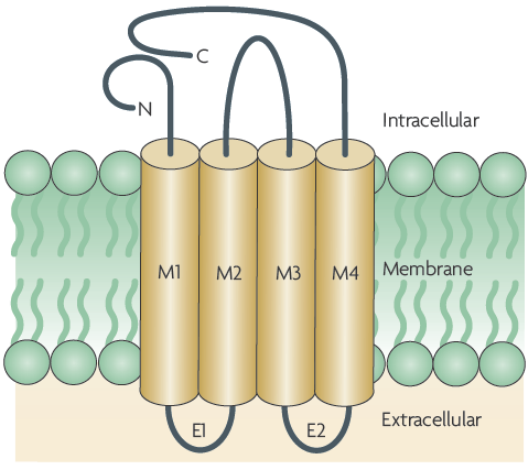

B.

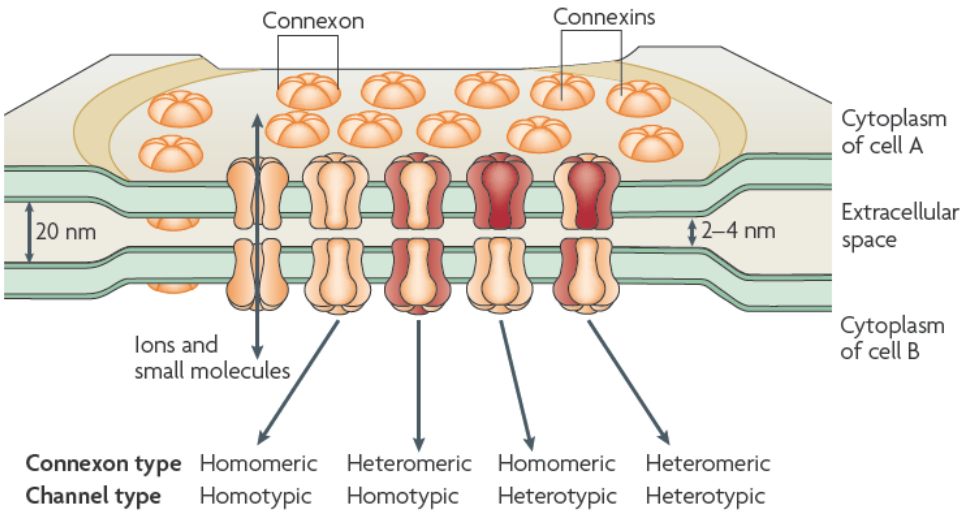

Figure 1.1: structure and molecular organization of GJs. (A) Ribbon structure of a typical connexin. (B) Formation of GJ between two cells and various GJ types. From Bloomfield and Volgyi, 2009 (Originally published in Nature Reviews in Neuroscience, image reproduce with permission from Nature Publishing Group) (Bloomfield and Volgyi, 2009).

Regulation and trafficking of ion channels and receptor proteins in chemical synapses have been studied extensively and have been proven to be an important aspect of chemical synaptic strength and plasticity. Like chemical synapses, electrical synapses are dynamic and

highly plastic. However, we are still in the process to decipher what contributes to the plasticity and strength of electrical synapses. In our study, we focused on synaptic plasticity of GJs made of Cx36, the most abundant neuronal connexin in the central nervous system. Cx36 (Cx35 is the non-mammalian homolog) GJs are widespread in the central nervous system. They can be found in the retina (Deans et al., 2002; Bloomfield and Volgyi, 2009), olfactory bulb (Christie et al., 2005), neocortex (Deans et al., 2001; Blatow et al., 2003), hippocampus (Belluardo et al., 2000; Hormuzdi et al., 2001; Belluardo et al., 2000), inferior olive (Long et al., 2002; De Zeeuw et al., 2003), and cerebellum (Belluardo et al., 2000). Retina is a good system for studying Cx36 GJs, where they are responsible for the coupling of many neurons including AII amacrine cells and photoreceptors (Lee et al., 2003; Kothmann et al., 2009; O'Brien et al., 2012; Li et al., 2013). Cx36 GJs between rods and cones are strongly modulated by light adaptation and a circadian rhythm; Cx36 coupling can change up to 20 fold when light state changes (Figure 1.2A and B) (Li et al., 2013). AII amacrine cells, also coupled by Cx36, show significant plasticity when the phosphorylation states of Cx36 are regulated by domapine receptor activity (Figure 1.2C and D) (Kothmann et al., 2009).

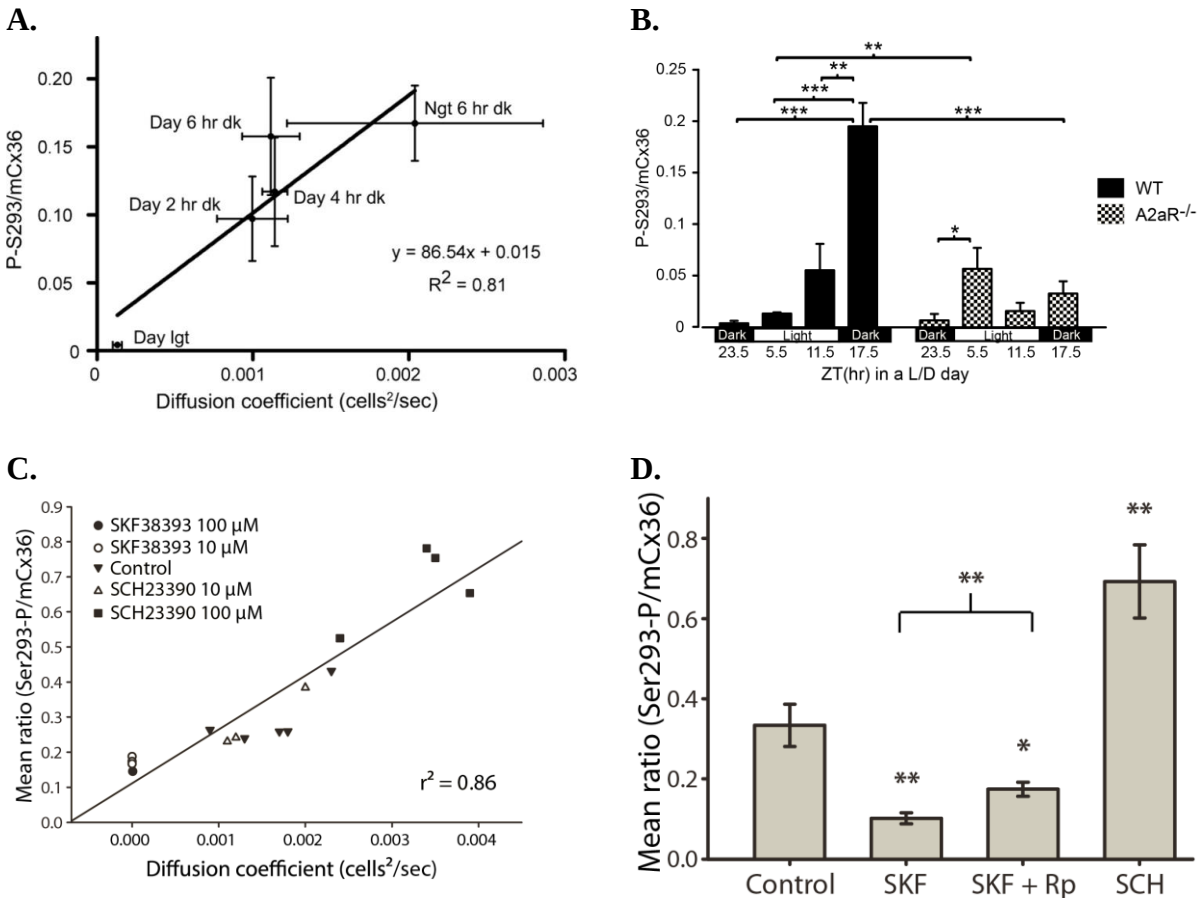

Figure 1.2. Cx36 shows a wide range of plasticity in the retina. (A-B) Cx36 phosphorylation and tracer coupling of photoreceptors are positively correlated. The coupling of Cx36 can increase up to 20 fold between day time and night time (Li et al., 2013) (Originally published in the Journal of Neuroscience). Cx36 phosphorylation and tracer coupling of AII amacrine cells are positively correlated. The coupling of Cx36 was regulated by dopamine receptor activity (Kothmann et al., 2009) (Originally published in the Journal of Neuroscience). (Images reproduced with permission from The Journal of Neuroscience).

The changes in coupling shown above are due to changes in the phosphorylation of Cx36 at regulatory serines (S110 and S276) regulated by protein kinases and phosphatases (Kothmann et al., 2007; Kothmann et al., 2009), but we believe that turnover and trafficking can also play a signficant role in Cx36 synaptic plasticity. To date, very few studies have investigated the link between Cx36 turnover and functional plasticity. Turnover rates of connexin proteins are usually exceptionally high. Previous studies reported connexin half-lives in different tissues varied from

one hour to ten hours, with one exception in the lens cells (Table 1.1). The majority of reports showed a half-life between 1.5 and 3.5 hours. Table 1 is a summary of selected reports of connexin half-lives.

Cx	Modification	Half-lives (h)	Cells or tissues	Reference
Cx26		5	Adult mouse hepatocytes	(Fallon and Goodenough, 1981)
		1.3-2	Cultured mouse hepatocytes	(Traub et al., 1989)
Cx31		4.1	HeLa cells	(Diestel et al., 2004)
		6	HeLa cells	(He et al., 2005)
Cx32		4-6	Rat hepatocytes	(Traub et al., 1983)
		2.5-3	Mouse embryo hepatocytes	(Traub et al., 1987)
		~3	PC12 cells	(VanSlyke et al., 2000)
	Cx32T-GFP	3.3	Hepatocellular carcinoma-derived PLC cells	(Windoffer et al., 2000)
	Flagged Cx37	3	BWEM cells	(Larson et al., 2000)
Cx43		1.5	Chick lens epithelial cells in culture	(Musil et al., 1990)
		3.1	Novikoff hepatoma cells	(Lampe, 1994)
		~1.5	BICR-M1Rk cells	(Laird et al., 1995)
		2.5	E36 Chinese hamster ovary cells	(Laing and Beyer, 1995)
		3.27	Bovine aortic endothelial cells in culture	(Larson et al., 1997)
		2.7	Cultured leptomeningeal cells of newborn rat	(Hertzberg et al., 2000)
		2.66 to 3.95	MC3T3 osteoblastic cells	(Yamaguchi and Ma, 2003)
		2	SK-HEP-1 cells	(Thomas et al., 2003)
		~1	BWEM cells	(Laing et al., 1997)
		2.3	Bovine retinal endothelial cells	(Fernandes et al., 2004)
		1-2	Newborn rat cardiac myocytes	(Laird et al., 1991)
		1.9	Newborn rat cardiac myocytes	(Darrow et al., 1995)
		1.4	Newborn rat cardiac myocytes	(Laing et al., 1998)
		1.3	Adult rat heart	(Beardslee et al., 1998)
	Cx43-GFP	2-3	HeLa cells	(Hunter et al., 2005)
Cx45		4.2	HeLa cells	(Hertlein et al., 1998)
		2.9	Newborn rat cardiac myocytes	(Darrow et al., 1995)
Cx45.6		2.5	Lens of embryonic chicken in culture	(Yin et al., 2000)
	Cx49-GFP	10	HeLa cells	(Breidert et al., 2005)
Cx56		2-3 (1^{st} pool) 48 (2^{nd} pool)	Chicken lens cultured cells	(Berthoud et al., 1999)

Table 1.1. Comparison of the half-lives reported for different connexins or modified connexins in cells and tissues. From Herve et al., 2007 (Originally published in and adapted from Journal of Membrane Biology) (Table reproduced with permission from Springer).

In our previous studies, we have created a new fusion protein, Cx36-Halo, to study the turnover rate of Cx36 in HeLa cells. Utilization of the HaloTag provided us with a highly

efficient and specific way to visualize Cx36, and allowed us to differentiate Cx36 synthesized from different time points. This fusion protein will be introduced in detail in Chapter Two under Material and Methods. We used the Cx36-Halo fusion protein to calculate the turnover rate of Cx36 in HeLa cells by performing pulse-chase experiments. Cx36 has a turnover rate of 3.1 hours in HeLa cells, and this rate is consistant with the fast turnover rates that other connexin proteins have shown.

Short term plasticity is regulated by protein kinases and phosphatases. Cx36 turnover rate is too slow to contribute significantly to short term plasticity that is neurotransmitter driven. Cx36 turnover will most likely contribute to long term plasticity of Cx36 GJs. Changes in abundance of Cx36 have been proposed to contribute to plasticity of coupling in mouse photoreceptors (Katti et al., 2013). It is possible that Cx36 turnover rate could be altered in response to the changes in levels of neurotransmitters such as dopamine and adenosine, which are key regulators to Cx36 coupling (Li et al., 2009a; Kothmann et al., 2009; Li et al., 2013). This leads us to a number of questions that we are trying to address in this study.

How is new GJ material added to the GJ plaques? The ability to differentiate new and old GJ material by using different ligands provided us with new insight into how Cx36 protein was added. In our previous pulse-chase experiments, we observed new GJ material being inserted into the GJ plaques in small solid vesicles from both the edges and the internal portion of the plaques. New Cx36 diffused throughout the GJ plaques. This observation contradicted the previously reported behavior of Cx43 on which the common framework of understanding of connexin trafficking and turnover is based. Cx43 was observed to accrete on the edges of existing GJ plaques and was unable to diffuse (Simek et al., 2009). On the other hand, our observation is consistant with those of Shaw and colleagues, who found that Cx43 cargo vesicles

were targeted directly to adherens junctions adjacent to GJ plaques through microtubule plus-end tracking proteins (Shaw et al., 2007). In this study, we will determine whether the lateral diffusion of Cx36 was a real phenomenon. In Chapter Two, we will introduce the two types of experiments we used to determine whether these tagged connexins diffuse through GJ plaques. First, we performed pulse-chase analysis of turnover with Cx36-Halo and Cx43-Halo constructs in both HeLa and HEK293 cells. Second, we performed live fluorescence recovery after photobleaching (FRAP) experiments of Cx36-Halo in HeLa cells and both Cx36- and Cx43-Halo in HEK293 cells. During our FRAP experiments, we have used a wide range of parameters to perform the photobleaching and noticed potential effects of phototoxicity and their influence on current live cell imaging. We will discuss that in Chapter Three.

The next question we were trying to answer was: what is the transportation pathway of Cx36? Cx36 has a high turnover rate. In order to understand the mechanism of such high turnover rate, we need to study the biosynthesis and transportation of Cx36 in HeLa cells. Cx36 is synthesized and co-translationally inserted into the endoplasmic reticulum (ER) as four trans-membrane integral membrane proteins. The oligomerization of connexins into connexons occurs primarily in the trans-Golgi-network (TGN) (Koval et al., 1997; Musil and Goodenough, 1993) with the exception of Cx26 and Cx32, which happens primarily in the ER (Falk and Gilula, 1998; Falk et al., 1994; Falk et al., 1997). It also has been shown that Cx26 can bypass TGN and directly insert hemichannels into the plasma membrane from the ER (Ahmad and Evans, 2002; George et al., 1998; Evans et al., 1999; George et al., 1999; Martin et al., 2001). In this study, we will determine whether the insertion of Cx36 into the plasma membrane involves the traditional ER-Golgi-TGN-PM pathway.

Transportation of vesicles inside a cell usually involves the cytoskeleton. Cytoskeleton machinery has been shown to play an important part in protein trafficking. Both the microtubule and actin cytoskeleton have essential contributions to intracellular vesicle trafficking. In our preliminary imaging of the cytoskeleton in HeLa cells expressing Cx36-Halo, we found that actin filaments were closely associated with the plasma membrane, where GJs were located. There have been extensive studies on the role of microtubules in trafficking (Thyberg and Moskalewski, 1999; Musch, 2004; Palmer et al., 2005; Vaughan, 2005) and the role of actin filaments has been attracting more attention. Actin is a globular multi-functional protein that is involved in many important cellular processes. Actin cytoskeleton remodeling provides the force required for a variety of cellular processes based on membrane dynamics, such as endocytosis, exocytosis, and vesicular trafficking at the Golgi (Lanzetti, 2007). The role of actin filaments has been tested in the transport of vesicles from Golgi to plasma membrane (Hirschberg et al., 1998; Cao et al., 2005), as well as their removal to early and late endosome in association with microtubules (Apodaca, 2001; Brown and Song, 2001; Mundy et al., 2002). In Chapter Four, we will determine how the cytoskeleton, actin filaments in particular, plays a role in Cx36 trafficking and turnover.

We have identified a few key components that participate in Cx36 plasticity. One important factor of Cx36 plasticity is the phosphorylation state of Cx36. Changes in Cx36 phosphorylation state are regulated by protein kinases and phosphatases. Experimental results from mutagenesis studies showed that the Cx36 C-terminus regulates coupling. Results from previous chapters indicated that Cx36 trafficking is associated with actin filaments. How do these components fit in the big picture of electrical synaptic plasticity? - Do they affect plasticity individually or do they regulate each other? It is important to determine the potential interaction

and inter-regulation among these elements of plasticity. In Chapters five and six I discuss how the C-terminus of Cx36 influences coupling and whether disrupting actin filaments interferes with Cx36 coupling and Cx36 turnover rate.

Cx36 plasticity is extremely complex, and studies investigating the regulators of Cx36 plasticity have barely scratched the surface. Through this study, we can hopefully gain more insight into the factors contributing to electrical synaptic plasticity and their roles in regulating cell-cell communication.

Here we go…

Chapter Two

Cx36 Dynamics and Mobility - Lateral Diffusion of Cx36

Part of the study in this chapter was published in my Dissertation of Master's Degree.

Introduction

Turnover rate of Cx36

The regulation of the biosynthesis and degradation of GJ protein is an essential element in the control of intercellular communication (Thomas et al. 2002). Connexins are synthesized and co-translationally inserted into the endoplasmic reticulum (ER) as four trans-membrane integral membrane proteins. They are post-translationally assembled into hexamers, known as hemichannels or connexons. The hemichannels insert themselves into the plasma membrane and form functional GJs with hemichannels from the adjacent cells (Ahmad et al., 1999a; Thomas et al., 2005; Zhang et al., 1996). Assembly of connexins into GJs usually involves the traditional ER-Golgi-TGN-plasma membrane pathway.

Turnover rates of connexins are exceptionally high compared to other membrane proteins. Connexin half-lives reported in the literature range from 1 to 10 hours, with one exception in cultured lens cells (48hrs). The turnover of Cx36, the most abundant neuronal GJ protein, has not been well studied. The Pereda group studied the connection between GJ turnover and electrical synaptic strength for the first time in goldfish Mauthner cells by showing that reduced exocytosis weakened electrical transmission (Flores et al., 2012), providing evidence that turnover and trafficking of GJ protein can affect electrical synaptic plasticity.

Understanding the trafficking and regulation of Cx36 will be an important first step in understanding whether connexin turnover rate affects electrical synaptic plasticity, and the ability to specifically label proteins is key to revealing the dynamics and functions of protein. In our previous study, we created a fusion protein of Cx36 and HaloTag to provide better visualization of the protein of interest. HaloTag protein is a 34kDa monomeric protein. It is derived from a

prokaryotic hydrolase which is not endogenous to eukaryotic cells, allowing high specificity (Los et al. 2005). It is genetically engineered to form a covalent bond with specific, synthetic HaloTag ligands (Figure 2.1A). The HaloTag ligands are chloroalkanes that are modified to carry a variety of functional chemical tags for different types of studies (Los et al., 2008; Los and Wood, 2007). In this study, we used two cell permeable HaloTag fluorescent ligands, Oregon Green (OG) and tetramethylrhodamine (TMR), to label Cx36-HaloTag fusion protein (Figure 2.1B).

A.

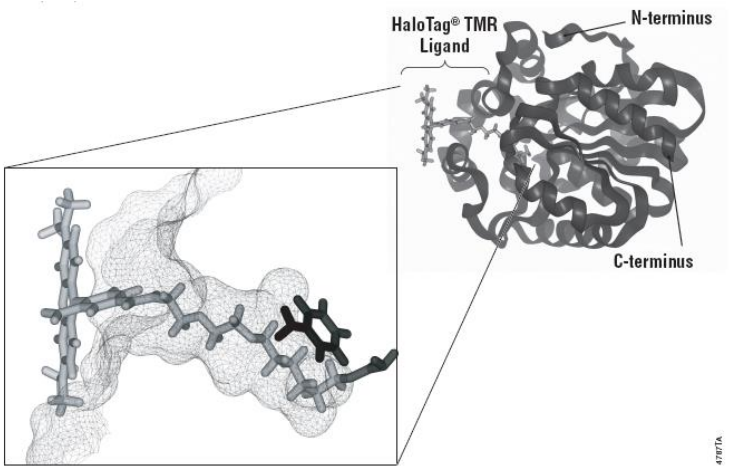

B.

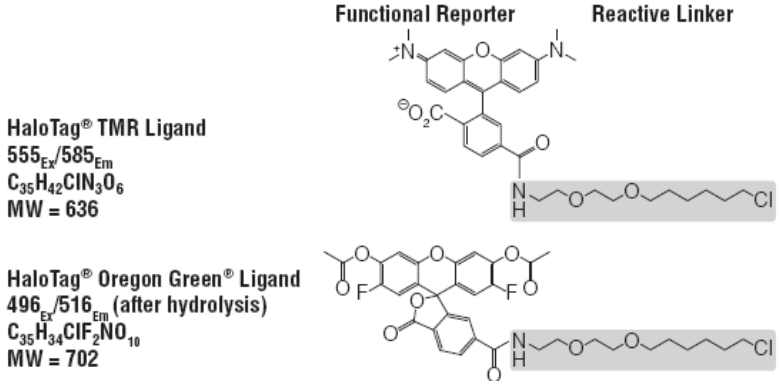

Figure 2.1: HaloTag technology. A) Ribbon structure of HaloTag protein, the enlarged picture shows the active binding site between HaloTag protein and HaloTag TMR ligand. B) Structure of HaloTag TMR ligand and HaloTag Oregon Green Ligand. Originally published on Promega website (Images reproduced with permission from Promega Corporation).

To study Cx36 without interfering with its protein-protein interactions, we had to carefully choose a site to insert the HaloTag open reading frame where it is not too close to the functional or regulatory amino acids. The insertion site was in the internal site of the C-terminus of Cx36, between the two important serine sites (S293 and S315) (Figure 2.2).

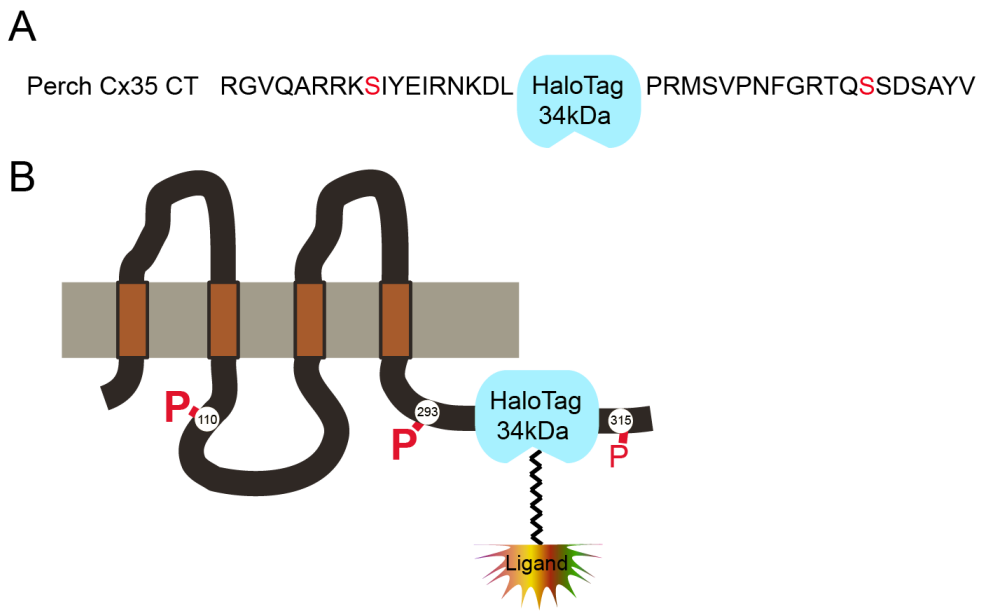

Figure 2.2: Construction of the Cx36-HaloTag fusion. (A) Sequence of perch Cx35 C-terminus indicating the insertion point of the HaloTag open reading frame. Regulatory serine phosphorylation sites (S276 and S298) are indicated in red type. (B) Ribbon structure of Cx36 showing the relative locations of HaloTag and regulatory phosphorylation sites. HaloTag ligands are covalently bound to the HaloTag protein when applied and become permanently attached to the Cx36-Halo protein. Ribbon structure depicts mouse Cx36, where S293 and S315 are equivalent to S276 and S298 in perch Cx35.

In this chapter, I will present the validation experiments we performed to confirm the functionality of the Cx36-Halo construct, and how we used this construct to perform pulse-chase analysis for a direct measurement of Cx36 half-life in HeLa cells. These results have been previously published in my thesis for my Master's degree. They are included here to provide a better foundation for the following data. During the pulse-chase analysis, we observed interesting dynamics of Cx36 trafficking due to the ability of label Cx36 protein at different time point in HeLa. I will focus on the dynamics and trafficking of Cx36 protein in this chapter.

Methods and Materials

Connexin-HaloTag constructs

The HaloTag open reading frame was inserted into an internal site in the C-terminus of perch Cx35 (non-mammalian homolog of Cx36) in pcDNA 3.1 Zeo (O'Brien et al., 2004). The location of the insertion was chosen so as not to disrupt the regulatory C-terminal phosphorylation sites nor block the C-terminal PDZ interaction motif (see Figure 1.2).

Cx35 pcDNA was split in its C-terminus using whole plasmid PCR amplification with primers TTCAGAGCCCGAGGATGAGTGTGCC (forward) and TCTGCCATCAAGTCCTTATTTCTGATCTC (reverse). The HaloTag open reading frame was amplified by PCR from the HaloTag-N vector (Promega, Madison, WI) with primers AGGACTTGATGGCAGAAATCGGTACTGGC (forward) and ATCCTCGGGCTCTGAAAGTACAGATCCTCAGTG (reverse). Phusion high-fidelity polymerase (New England Biolabs, Ipswitch, MA) was used for both PCR reactions. The purified PCR products were cloned using cold fusion cloning (System Biosciences, Inc., Mountain View, CA). This clone is called Cx36-Halo-C-IN, and referred to as Cx36-Halo throughout the manuscript.

A conventional C-terminal fusion of the HaloTag open reading frame to perch Cx35 was made using Cx35 in the EGFP-N1 vector (Clontech, Mountain View, CA). EGFP was deleted with SmaI and NotI. The HaloTag open reading frame was cut out from the HaloTag-C vector (Promega) with XhoI, filled in with Klenow polymerase, cut with NotI, and cloned into the Cx35-containing vector. This clone is called Cx36-Halo-C-END (Figure 2.3).

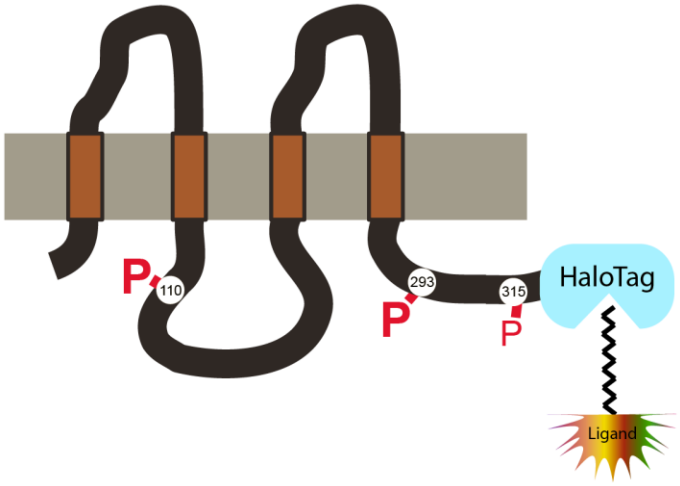

Figure 2.3. Ribbon structure of Cx36-Halo-C-END showing relative location of HaloTag.

A human Cx43 cDNA clone (NM_000165.3) in pReceiver-M02 was purchased from Genecopoeia (Rockville, MD). Two constructs containing the HaloTag at internal sites within the C-terminus were created using native XcmI and EcoRI restriction sites. HaloTag was amplified from HaloTag-N (Promega) with primer pairs TTCCCCGATGATAACCAGATGGCAGAAATCGGTACTGGCT (forward) and AGCAGCTAGTTTTTTAGAATTCTCGCCGGAAATCTCGAGC (reverse) for EcoRI and AGCGACCCTTACCATGCGATGGCAGAAATCGGTACTGGCT (forward) and GGCTCAGCGCACCACTGGTCTCGCCGGAAATCTCGAGC (reverse) for XcmI using Q5 polymerase (New England Biolabs), and cloned into the respective restriction sites of Cx43 using Gibson Assembly (New England Biolabs). A C-terminal fusion of Cx43 was produced by amplifying Cx43 with primer pair GCAAAGCGATCGCTTCCGGAGTTCGAACCATGGGTGACTG (forward) and GATCCTCAGTGGTTGGCTCGAGGATCTCCAGGTCATCAGGCCG (reverse) using Q5

polymerase and cloning into EcoRI and XhoI sites of pHaloTag-N using Gibson Assembly. All clones were fully sequenced through the connexin-HaloTag fusion open reading frames.

Cell culture and reagents

All media, fetal bovine serum and cell culture reagents were obtained from Invitrogen (Grand Island, NY). HeLa cells (Cat# CCL-2) and Hek-293 cells (Cat# CRL-1573) were obtained from American Type Culture Collection (Rockville, MD,). Cells were grown in complete MEM supplemented with 10% fetal bovine serum and 1% antibiotic-antimycotic (penicillin/streptomycin/amphotericin B). Cells were plated on 12 mm cover glasses, grown to 75% confluence overnight in 35 mm culture dishes, and transiently transfected with 2 μg of plasmid DNA per 35 mm culture dish using GenePORTER® 2 transfection reagent (Genlantis, San Diego, CA). Plasmids transfected included the connexin-HaloTag constructs described above, untagged Cx36 in pcDNA (Cx36 wild type) or HaloTag-N empty vector (control). Experiments were conducted 24 hours after transfection.

General lab chemicals were obtained from Sigma (St. Louis, MO). PKA activator, Sp-8-cpt-cAMPS and PKA inhibitor, Rp-8-cpt-cAMPS, were from Alexis (San Diego, CA). HaloTag ligands Oregon Green (OG) and tetramethylrhodamine (TMR) were purchased from Promega, and Brefeldin A was purchased from Cell Signaling Technology (Danvers, MA).

Tracer coupling

Transfected HeLa cell cover glasses were maintained in oxygenated Ringer's medium at 35°C. The medium was supplemented with 0.05% Neurobiotin and cells were scraped with a 25-

gauge needle. Incubation with Neurobiotin was continued for 10 minutes to allow loading and diffusion. Cells were then washed twice with 0.1 M phosphate buffer to remove excess Neurobiotin and fixed with 4% paraformaldehyde (Electron Microscopy Sciences, Hatfield, PA) in 0.1 M phosphate buffer. When used, the PKA activator Rp or inhibitor Sp was added to the oxygenated incubation medium 10 minutes before the scrape for pre-incubation and replaced with fresh drug upon Neurobiotin addition. PKA regulating drugs were present throughout the 10 minute tracer diffusion period. Following fixation, cells were probed with streptavidin-Cy3 (Jackson ImmunoResearch, West Grove, PA) and photographed on a Zeiss (Thornwood, NY) fluorescence microscope (Axiovert 200 with 40x, 0.5 NA Hoffman Modulation Contrast objective) with a Hamamatsu C4742-95 digital camera using HCImage software (Hamamatsu, Sewickley, PA). Five images were taken of different patches of loaded cells for each experiment and treated as replicates in the data analysis.

The diffusion coefficient of Neurobiotin through the coupled network of HeLa cells was determined from fluorescence intensity data using a compartmental diffusion model (Zimmerman and Rose, 1985). The analysis utilizes a linear 25-compartment diffusion model to fit Neurobiotin concentration and diffusion distance measurements (O'Brien et al., 2004). This model has been applied to neural networks to assess GJ coupling in the retina (Mills and Massey, 1998; O'Brien et al., 2004; Li et al., 2009a). The movement of tracer between adjacent compartments is described by a series of 25 differential equations that are solved for tracer flux given the total amount of diffusion time and a diffusion coefficient, k. The diffusion coefficient k represents the proportion of tracer that diffuses from the first compartment to the next per second. Optimal fitting of intensity data to the model was determined in MatLab (Mathworks, Natick, MA) by varying the diffusion coefficient k and another parameter, bo, the bolus loading

rate. The parameter bo is defined as the rate of addition of tracer to the initial compartment for the loading period, which was assumed to be 1 minute in the scrape-loading experiments, and was set to zero thereafter. Data fits were determined by plotting cell intensities on a log intensity axis and determining the diffusion coefficient k that best fit the rate of decline of tracer intensity with distance from the cell of origin, and the rate of delivery, bo, that fit the overall tracer concentration (Mills and Massey, 1998; O'Brien et al., 2004; Ouyang et al., 2005; Li et al., 2009a). Replicate measurements were averaged to yield a single value for each treatment condition in each experiment. Diffusion coefficients were compared under different drug treatment conditions using a mixed effects model.

A.

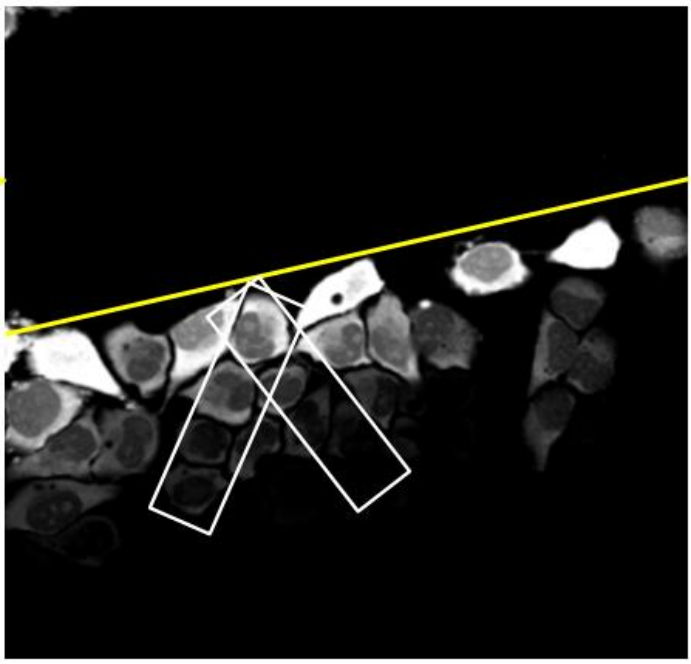

B.

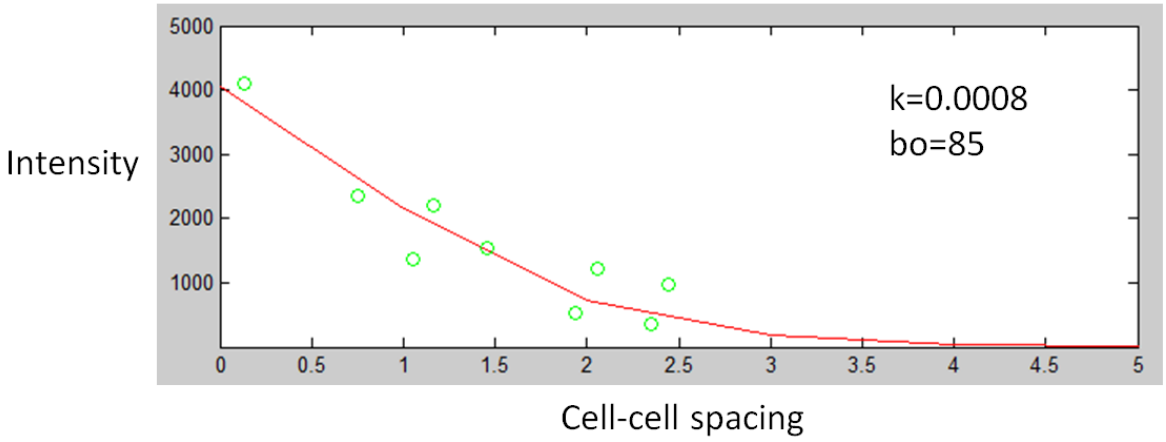

Figure 2.4. Scrape-loading analysis. A) Picking compartments. In this experiment, compartment represents one HeLa cell that is coupled to two neighbors in a linear array via a coupling resistance (a GJ) characterized by the diffusion coefficient. B) Intensity data are plotted vs. distance from the cut edge in cell-to-cell spacing (mean of spacing measured from the same image). The data are fit to the model by systematic adjustment of the k (diffusion coefficient) and bo (tracer loading rate into the initial compartment at the cut edge) parameters. Diffusion time for the model is set by the actual time from cutting to fixation of the sample (16 minutes in this experiment).

Labeling, immunostaining and imaging

Transfected HeLa cell cover glasses were incubated in Ringer's medium containing 5 µM HaloTag TMR fluorescent ligand for 15 minutes. Cover glasses were then washed with ligand-free medium to remove unbound ligand and transferred to a microscope to capture live images.

After live cell imaging, cells were fixed with 4% paraformaldehyde in 0.1 M phosphate buffer for 10 minutes. Cover glasses were then incubated in immunolabeling buffer (PBS with 0.5% Triton X-100 and 0.1% NaN_3, pH 7.4) with 10% donkey serum (Jackson ImmunoResearch) to block non-specific binding. Cover glasses were incubated overnight at 4°C with monoclonal mouse anti-Cx36 (mCx36, MAB3045, 1:1000 dilution; Millipore, Billerica, MA) primary antibody in immunolabeling buffer with 10% donkey serum, followed by Cy5 conjugated donkey anti-mouse secondary antibody (1:500 dilution, Jackson ImmunoResearch) in immunolabeling buffer with 5% donkey serum for 3 hours. Cover glasses were then washed, mounted and transferred to a confocal microscope to capture images. HaloTag TMR was visualized with the TRITC filter set, and the Cx36 was visualized with the Cy5 filter set. Images of HeLa cells were digitally captured using a Zeiss LSM 510 Meta confocal microscope with a 63x, 1.4 NA Plan-Apochromat oil immersion objective using the PMT detectors and similar settings of pinhole, contrast, and brightness parameters. Images were exported unaltered in TIFF format with Zeiss LSM Image Browser.

Pulse-chase analysis

Transfected HeLa cell cover glasses were incubated in Ringer's medium containing 5 µM pulse labeling ligand Oregon Green (OG) for 15 minutes in a 24-well plate in a 37°C incubator.

Cover glasses were then washed to remove unbound ligand and incubated with Ringer's medium at 37°C. To analyze whether PKA activity altered Cx36 turnover rate, transfected HeLa cells were treated with Rp-8-cpt-cAMPS (5 μM) or Sp-8-cpt-cAMPS (5 μM) during the pulse-chase analysis. Rp or Sp was added to HeLa cells after 15 min of pulse label with OG, and was replaced every hour when necessary until the time for chase label. Cells were then labeled with tetramethylrhodamine (TMR) HaloTag ligand at various times (0.3, 1, 2, 3, 5, and 6 hours after pulse labeling) for 15 minutes. Some experiments with Cx43-Halo and Cx36-Halo constructs used transfected Hek293 cell cover glasses with an abbreviated set of chase times. All cover glasses were fixed with 4% paraformaldehyde and transferred to a confocal microscope for image capturing. HaloTag TMR was visualized with the TRITC filter set, and HaloTag OG was visualized with the FITC filter set.

Images were captured with Zeiss LSM 510 or LSM 780 confocal microscopes as series of confocal slices at 0.3 to 0.5 μm intervals. Acquisition parameters were initially set on control samples so that the brightest regions just reached saturation in a few pixels while the background just reached zero. Subsequent images were collected with the same settings. Post imaging processing was limited to making maximum intensity projections of stacks of images. Images were analyzed with the same settings using SimplePCI software (Hamamatsu, Sewickley, PA). Regions of interest (ROIs) were selected by setting an intensity threshold and applying a minimum size threshold. ROIs were defined as contiguous pixels with intensity threshold greater than 20% of the total intensity range and which covered a minimum area of 200 pixels. Each image was then manually scanned for individual ROIs that fit the criteria but were not part of the GJ plaques. These were manually removed from the analysis. Mean and total fluorescent intensity was measured in each channel for each ROI. 10 to 20 GJs were analyzed at each time

point in each experiment. At any given time point, the fraction of pulse label remaining was defined as the total pulse label divided by the total labeling (pulse + chase). The half-life of Cx36 was calculated by fitting an exponential function to the fraction of pulse label remaining over time.

FRAP experiments

FRAP experiments were performed using Zeiss LSM 780 and 880 confocal microscopes using 20x 0.8 NA Plan-Apochromat objectives and GaAsP detectors employing the FRAP routines in Zeiss Zen software. Immediately after HaloTag OG labeling and 15 minutes of wash period, coverslips were mounted in Ringer's medium and GJs imaged at a single focal plane at 0.5 to 2 sec intervals using a low laser intensity to ensure GJ stability. An ROI was selected away from edges of a GJ plaque and a series of high intensity laser sweeps was used to bleach the selected area. Immediately after bleaching, the sample was imaged at regular time intervals using the same low intensity as before the bleaching until the intensity of the bleached area had reached a plateau. Bleachings were repeated three more times after the intensity plateaued to study the effect of repeated exposure. An internal vesicle was selected as an ROI as a negative control and was bleached and imaged in the same manner as the ROI in the GJ plaque.

The droplet control was performed by suspending 5 µl of 1x working solution of the HaloTag OG ligand in 1ml mineral oil by vortexing. Drops of the emulsion on a cover slip were bleached and individual HaloTag OG ligand droplets were imaged in the same manner as were connexin GJs. More detailed method description can be found in Chapter Three.

Results

Result figures 2.5-2.8 have been previously published in the MS thesis, it is included in this dissertation to provide a batter foundation for the results following.

Validation of the functionality of Cx36-Halo construct

In order to confirm that the GJs we observed were formed by Cx36, we co-labeled the cover slips with Cx36 antibody. The GJs that showed HaloTag TMR labeling were positively labeled with Cx36 antibody (Figure 2.5), confirming that TMR labeling is efficient and sufficient in labeling Cx36 GJs in transfected HeLa cells.

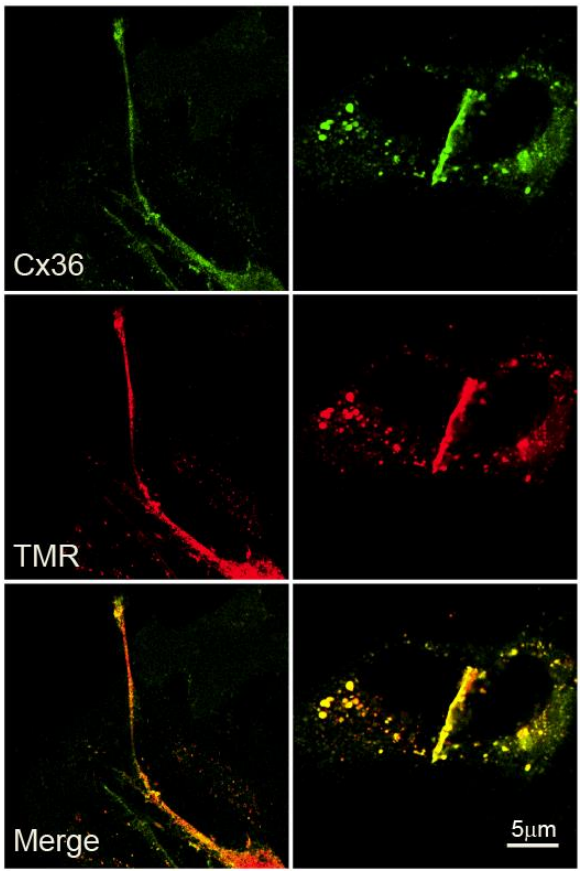

Figure 2.5. Fixed cell imaging of HeLa cells double labeled with Cx36 primary antibody and TMR ligand (Figure adapted from Helen Wang MS thesis).

In previous studies, we established that Cx36 coupling is regulated by PKA activity in HeLa cells (Ouyang et al. 2005). In order to determine whether introducing the HaloTag protein to Cx36 caused any functional changes in Cx36 regulation, we performed scrape-loading experiments using HeLa cells transiently transfected with the Cx36-Halo construct. We observed similar regulation as cells transiently transfected with wild-type Cx36 (Figure 2.6). 0 minute treatment with PKA inhibitor Rp-8-cpt-cAMPS (Rp) increased coupling significantly (Mixed effects model: Cx36-Halo, $p<0.001$; Cx36-WT, $p<0.001$; $n=3$ per condition for each form), while 10 minute treatment with PKA activator Sp-8-cpt-cAMPS (Sp) slightly reduced coupling (Cx36-Halo, $p<0.05$; Cx36-WT, $p<0.05$; $n=3$ per condition for each form). Background tracer coupling in HeLa cells transfected with HaloTag vector alone (Halo-EV) was slightly elevated by Rp treatment ($p<0.05$, $n=3$ per condition), but this effect was significantly smaller than the effect on wild-type Cx36 or Cx36-Halo ($p<0.001$ for both Cx36-Halo AND Cx36-WT; $n=3$ for each form).

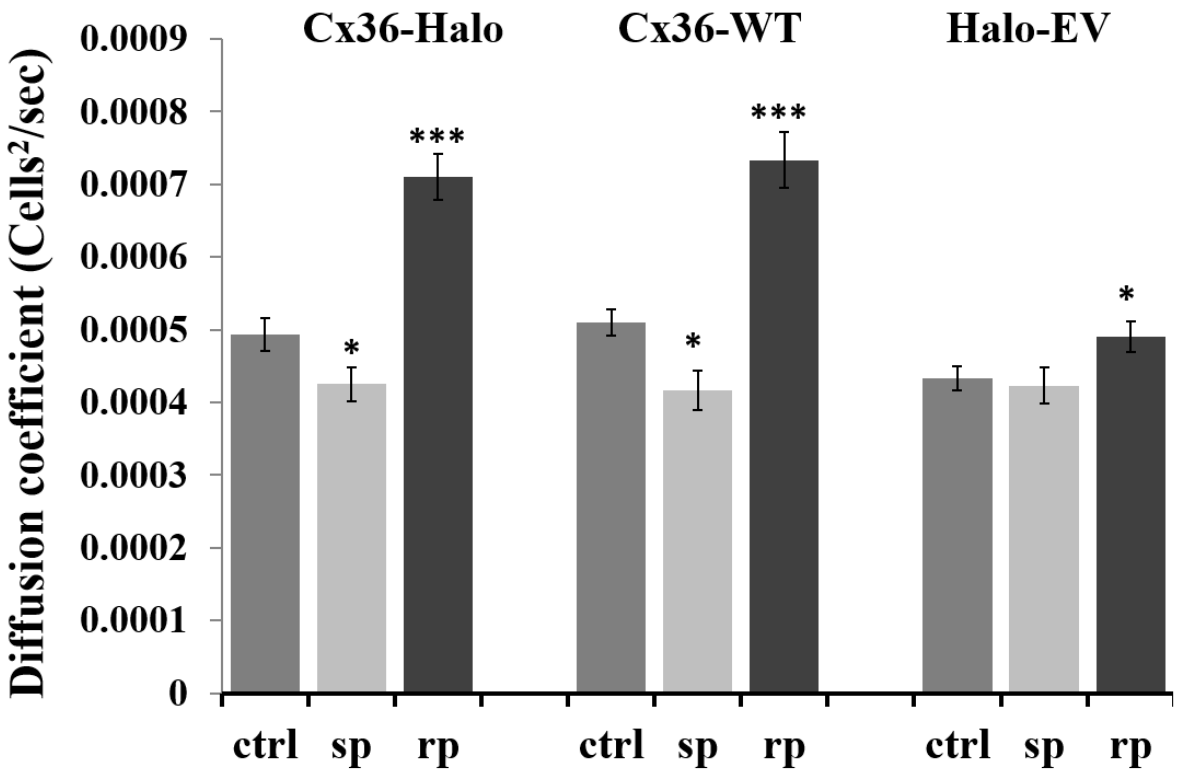

Figure 2.6. Tracer coupling measurements in HeLa cells transiently transfected with Cx36-Halo construct. Ctrl – control; Sp – 5 μM Sp-8-cpt-cAMPS (PKA activator); Rp – 5 μM Rp-8-cpt-cAMPS (PKA inhibitor). Data are means ± SEM, n=3 experiments per condition; * $p<0.05$, *** $p<0.001$.

Cx36-Halo has a half-life of 3.1 hours in HeLa cells

To study the turnover rate of Cx36 in HeLa cells, we performed pulse-chase studies using two different fluorescent ligands of HaloTag protein. Cover slips that were plated with Cx36-Halo transfected HeLa cells were labeled with HaloTag OG ligand at time 0 and followed by HaloTag TMR labeling at hour 0.3, 1, 2, 3, 4, and 6. At 0.3 hours, we observed that the majority of the GJ was labeled with OG (Figure 2.7). As the time progressed, the amount of TMR labeling increased in the GJ and the amount of OG labeling decreased.

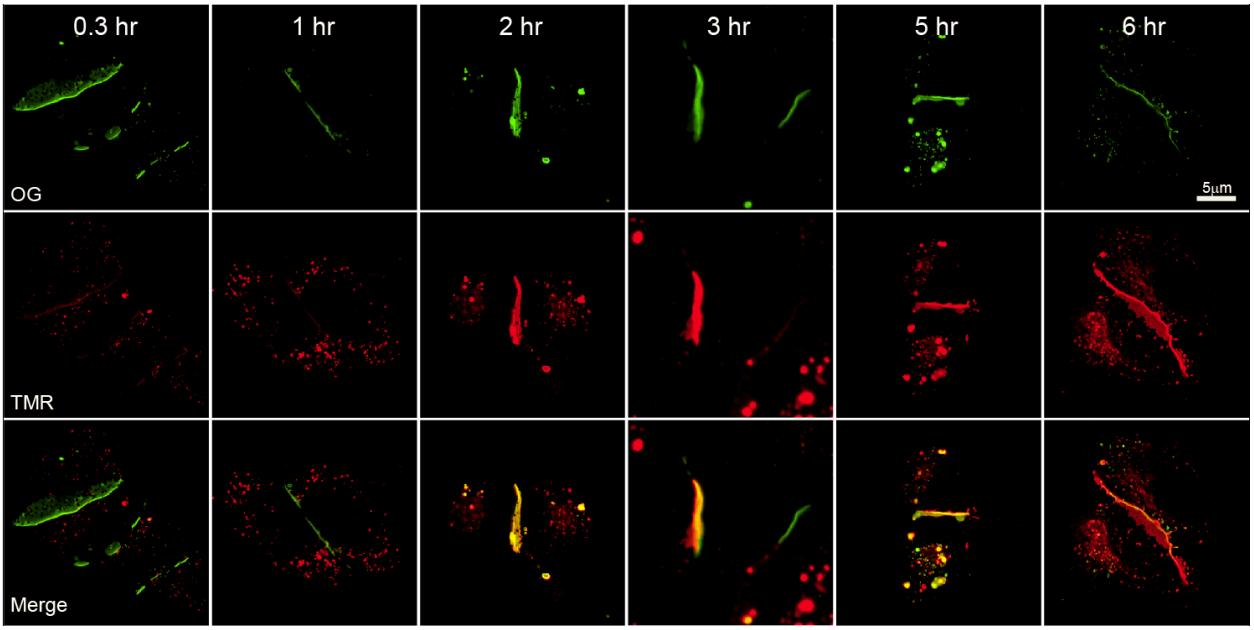

Figure 2.7. Pulse-chase analysis of Cx36 turnover rate. Confocal microscope images of Cx36-Halo in HeLa cells labeled with OG (pulse) and TMR (chase) at hour 0.3, 1, 2, 3, 5, and 6.

Figure 2.8 shows a plot of the fraction of old GJprotein in relationship with the total amount of labeled GJprotein present fit with an exponential decay curve. The calculated half-life for replacement of old protein was 3.1 hours, which is consistent with previous studies with other connexins (Herve et al., 2007; Flores et al., 2012).

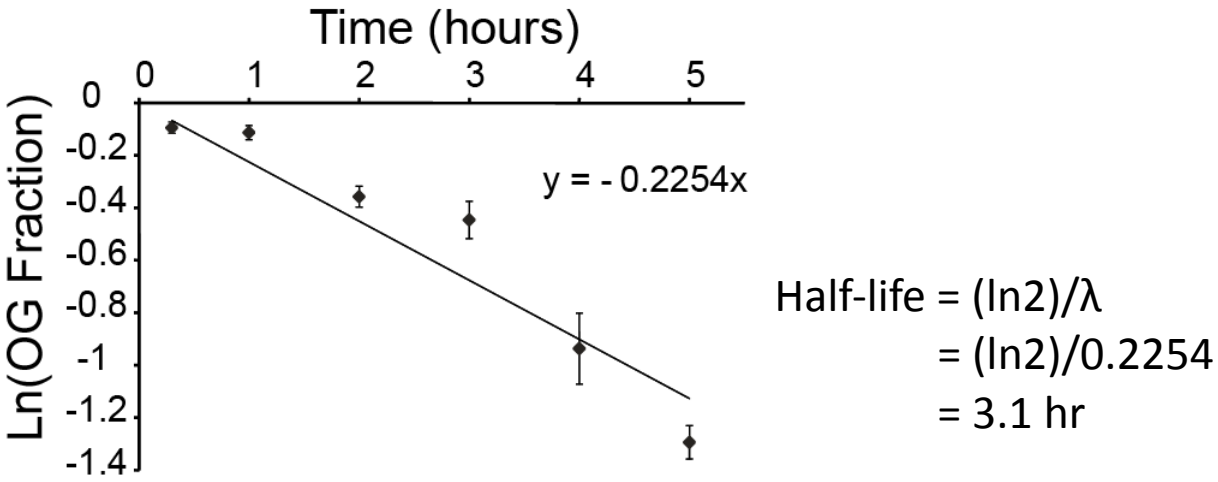

Figure 2.8. Calculation of Cx36 half-life in HeLa cells. n=10-20 GJs per time point

Cx36 is trafficked to the plasma membrane in vesicles, and removed as annular GJs.

It has been reported that new connexins are trafficked in vesicles as undocked hemichannels and removed as double membrane vesicles called annular junctions (Falk et al., 2009; Laird, 1996). In our confocal microscope images, we observed two different types of vesicles close to the GJs. These vesicles were present throughout all the time points.

The first type of vesicle was large in size and was usually hollow in the middle. These vesicles could contain either pulse (OG) or chase (TMR) ligand, or both (Figure 2.9A arrows). When close to pre-existing GJs, these vesicles were mostly labeled with pulse ligand. We found some OG labeled Cx36 budding off the pre-existing GJs near the ends (Figure 2.9A, open arrowhead) as well as in the middle of plaques (Figure 2.9A, asterisk).

The second type of vesicle was smaller in size, solid and often very numerous. These vesicles were mostly labeled with the chase ligand (TMR), indicating that they were recently synthesized. These small, new vesicles were often observed on the periphery of the pre-existing GJ plaques, either on the end (Figure 2.9Bi) or in the middle (Figure 2.9Bii). The small vesicles were often found adjacent to patches of chase-labeled GJ, suggesting that they were supplying newly synthesized GJ protein to existing plaques (Figure 2.9Bi and ii). This addition of vesicles to existing GJs was not obviously symmetric, meaning that a vesicle could be added to a GJ from either participating cell without concomitant addition of a vesicle from the other cell. This suggests that connexin hemichannels may be present in a GJ prior to docking with hemichannels from the opposing cell.

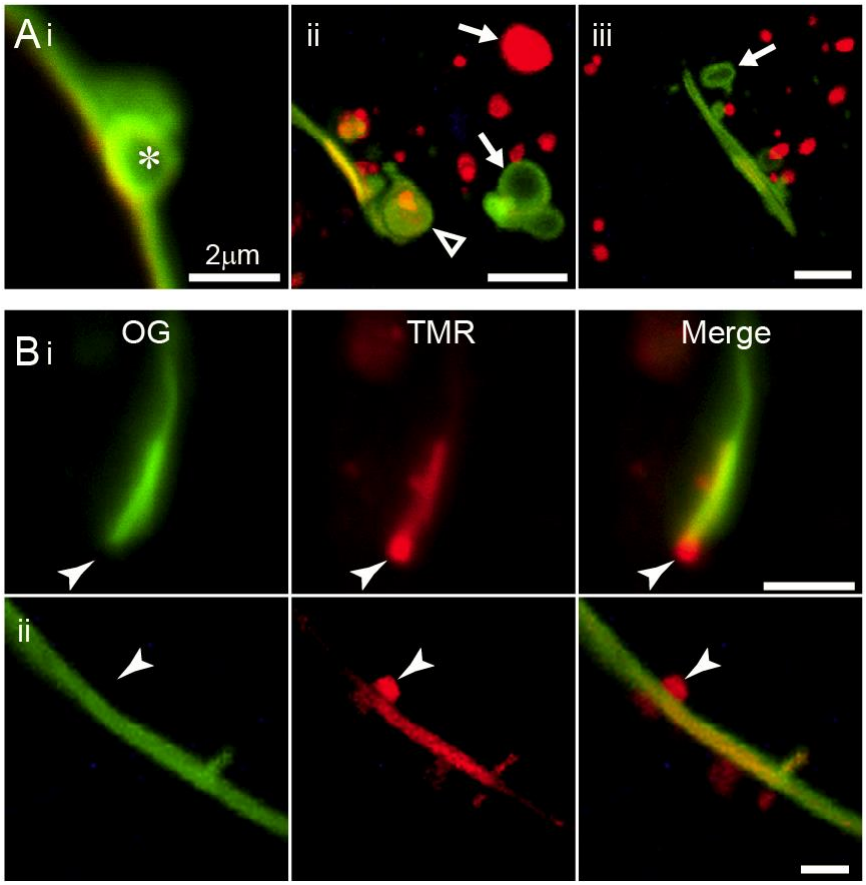

Figure 2.9. Removal and insertion vesicles of Cx36. (A) The removal of Cx36 from the GJ. Removal vesicles were usually a mixture of OG and TMR labeled. They often form circular vesicles. The vesicles can be removed from the edge (ii) as well as center (i) of a pre-existing GJ. (B) Insertion vesicles containing Cx36 trafficking into the GJ. Synthetic vesicles were mostly labeled with chase label. The insertion can happen at the edge (i) as well as the center (ii) of an existing GJ.

Dynamic trafficking of Cx36

In the pulse-chase experiment mentioned above, the TMR (chase) label was present in small vesicles throughout all time points, and was increasingly infused into the GJs (Figure 2.7). This suggests a progressive removal of the old GJprotein, which was labeled with OG, and replacement by new GJprotein, which became labeled with TMR. The TMR label at early time

points was patchy and at later time points was mixed throughout the whole GJ (Figure 2.10). The chase labeled connexin did not appear to be added only on the outer edges of existing plaques, as previously reported (Gaietta et al., 2002; Lauf et al., 2002).

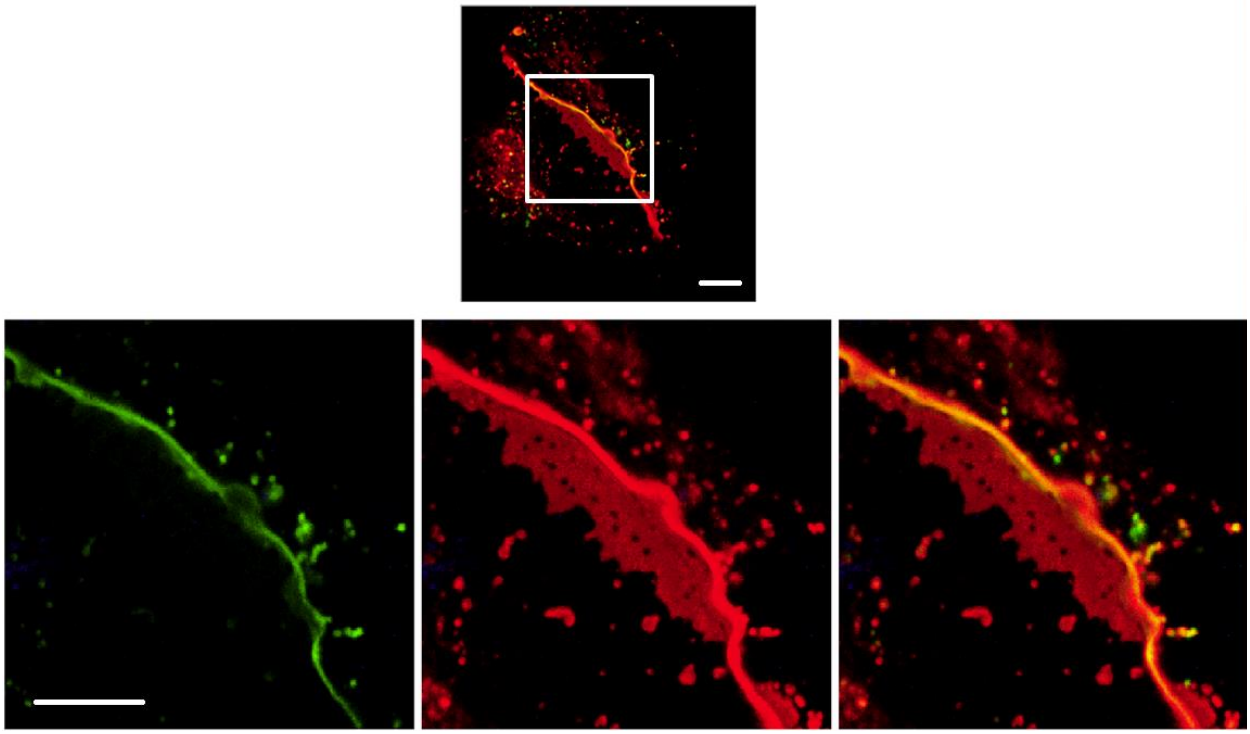

Figure 2.10. New GJ protein was mixed through the entire plaque; lower panels represent the split channels of the boxed region in the upper panel. Scale bars reflects 5µm.

Dynamics and mobility of Cx36 has remained elusive and the reason behind connexins' fast turnover rate is still a mystery. Several previous studies have examined the assembly and trafficking of Cx43 and found that new Cx43 material accreted to the outside edges of existing GJs and mixed very little with existing GJ channels (Gaietta et al., 2002; Lauf et al., 2002; Falk et al., 2009). This observation contradicts what we have observed in Figure 2.7. Movies taken with time-lapse fluorescent microscopy of Cx32-EGFP showed that Cx32 is highly dynamic, and small GJ plaques can fuse with each other or break apart at a fast rate, which is consistent to our

observation (Windoffer et al., 2000). In order to explain the differences in our observations and others, we explored the effects of the protein tag location, the cell line in which the fusion protein was expressed, and connexin type on the dynamics and mobility of the connexin protein. We also used FRAP experiments to investigate the mobility of Cx36 protein *in vivo*.

Mixing of old and new Cx36 does not depend on HaloTag position.

The observation that recently-synthesized Cx36 proteins spread throughout existing GJ plaques differs from observations with Cx43 (Gaietta et al., 2002; Lauf et al., 2002; Falk et al., 2009) on which the common framework of understanding of connexin trafficking and turnover are based. Is this a result of the position of the tag within the connexin protein, of the type of connexin studied, or of the tag itself and observation methods? To address these questions we developed additional HaloTag constructs of Cx36 with the tag inserted at the tip of the C-terminus, and of Cx43 with the tag positioned at the tip of the C-terminus or at either of two internal positions within the C-terminal domain (XcmI and EcoRI restriction sites). Cx43-HaloTag constructs did not form GJs when transfected into HeLa cells. However, all three Cx43 constructs tested formed GJs efficiently in HEK293 cells. We performed two types of experiments to determine whether these tagged connexins diffused through GJ plaques. First, we performed pulse-chase analysis of turnover with each of the constructs. Figure 2.11 shows labeling of Cx36-Halo-C-IN (Internal of C-terminus) and Cx36-Halo-C-END, respectively, at two hours chase time in HeLa cells. TMR chase label was observed throughout the entire GJ in both constructs.

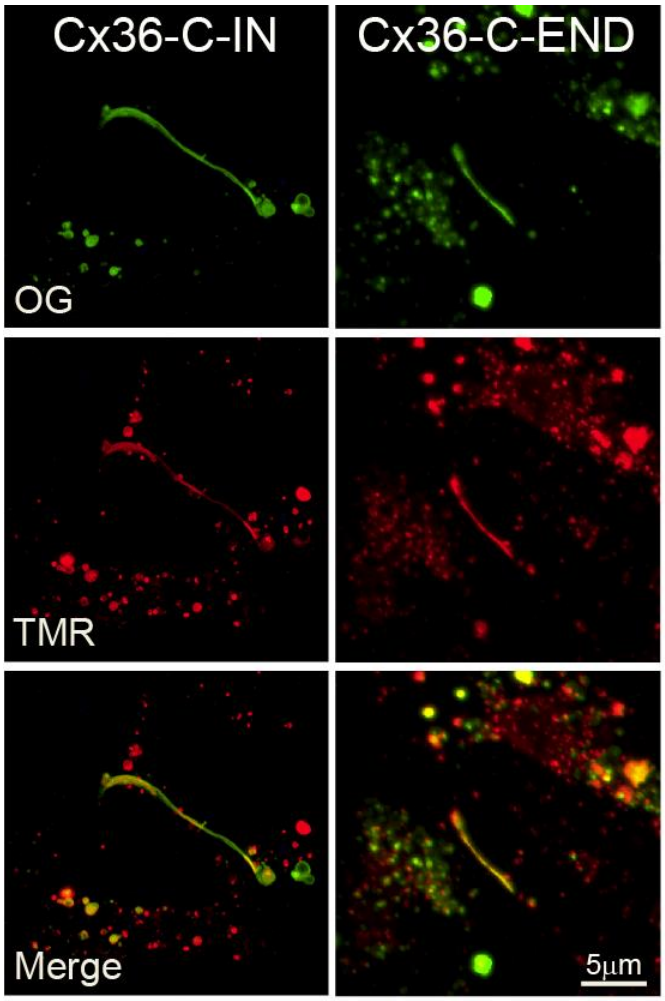

Figure 2.11. Pulse-Chase images of Cx36-C-IN and Cx36-C-END construct in HeLa cells. The Cx36-C-END construct showed chase ligand TMR spread throughout the entire GJ at the 2 hour mark, as did the Cx36-C-IN construct.

Cx43 also showed mixing of old and new connexins in GJs in Hek293 cells.

Figure 2.12A and B show labeling of Cx36-Halo-C-IN (Internal of C-terminus) and Cx36-Halo-C-END, respectively, at two hours chase time in Hek293 cells. For both constructs, the TMR chase label was present throughout the GJs. Figure 2.12C and D show labeling for one of the Cx43 internal constructs (Cx43-Halo-C-IN-XcmI) and Cx43-Halo-C-END, respectively, at two hours chase time. For both Cx43 constructs, the TMR chase label was present within the

existing GJ plaques. The Cx43 chase label was patchy in intensity, suggesting less mixing of the recently made connexin proteins with connexins present in the plaque.

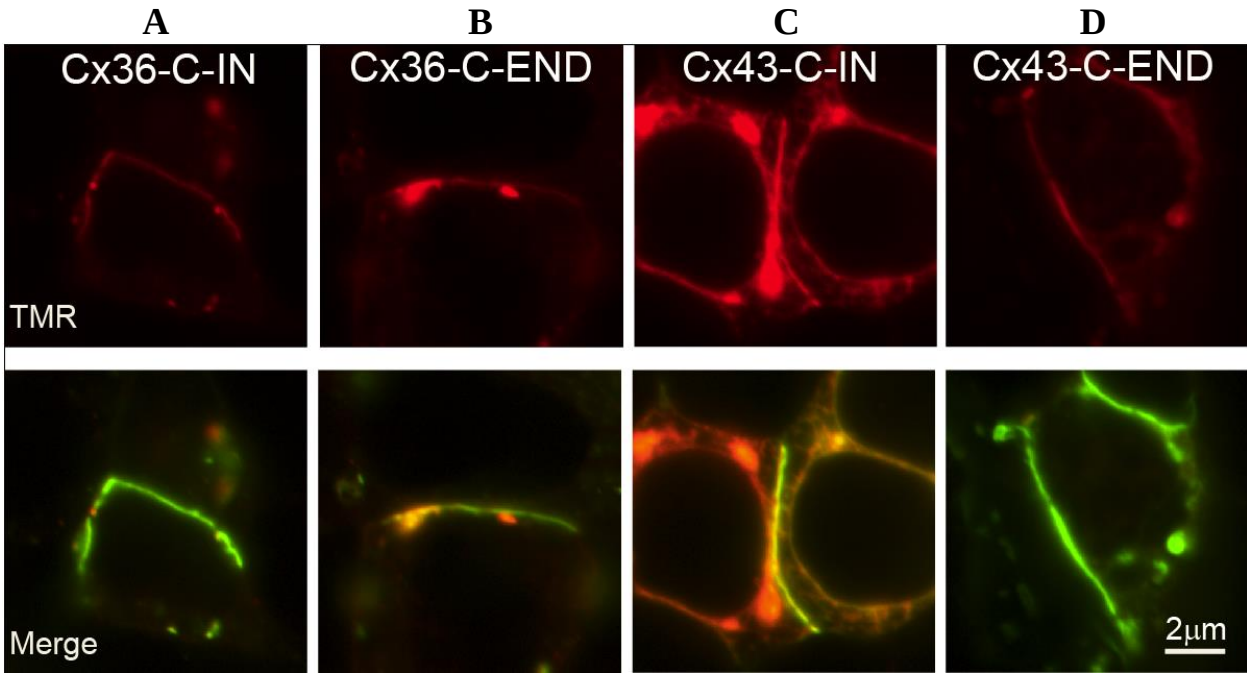

Figure 2.12. Pulse-chase images of Cx36-C-IN, Cx36-C-END, Cx43-C-IN and Cx43-C-END constructs in HEK293 cells. Cx36-C-IN and Cx36-C-END constructs showed lateral diffusion in HEK293 cells. Cx43-C-IN and Cx43-C-END constructs showed lateral diffusion (TMR chase label present throughout the GJ plaques, not confined to the outer edges) in HEK 293 cells contrary to previous reports.

Cx36 shows rapid lateral diffusion after local bleaching

As a second test of the ability of connexin proteins to diffuse laterally through GJ plaques, we performed live photobleaching studies of Cx36-Halo-C-IN in HeLa cells. Figure 2.13A shows a series of frames from a time sequence including one bleach of an OG-labeled Cx36 GJ (boxed region) and an OG-labeled internal vesicle (circular region). Bleaching and imaging were done using a confocal microscope with a 20x 0.8 NA objective and confocal zoom of 6. Under these conditions, the bleaching sweeps bleached more widely than the targeted band

of interest, and the bleached area quickly recovered label in the OG channel. Figure 2.13B shows the intensity profiles of both bleached regions of interest through the entire experiment comprising 4 sequential bleaches. Following each bleach, the OG label recovered to a new steady state level with a first order time course with a recovery half-time of 1.51 ± 0.22 sec (n=4 GJ, 2-6 bleaches per GJ). The post-bleach steady state was below the original baseline, reflecting both bleaching of the total pool of OG-labeled Cx36 and a portion of the OG-labeled Cx36 pool that was effectively immobile within the time course of the experiment. The mobile fraction of Cx36 ranged from 56% to 41% and decreased with each bleach (Figure 2.14).

Rapid recovery of photobleached connexin in GJ plaques has not been previously reported and we questioned whether this might be an artifact resulting from reversible bleaching of the OG fluorochrome by the bleaching sweeps. To test this, we photobleached aqueous droplets of the OG HaloTag ligand suspended in mineral oil using the same bleaching paradigm. Figure 2.13C and D shows that each bleach destroyed a fraction of the fluorochrome with no recovery. This lack of recovery was replicated at several different laser power settings and confocal zoom settings. Thus rapid recovery of OG-labeled Cx36 in the bleached area was not an artifact.

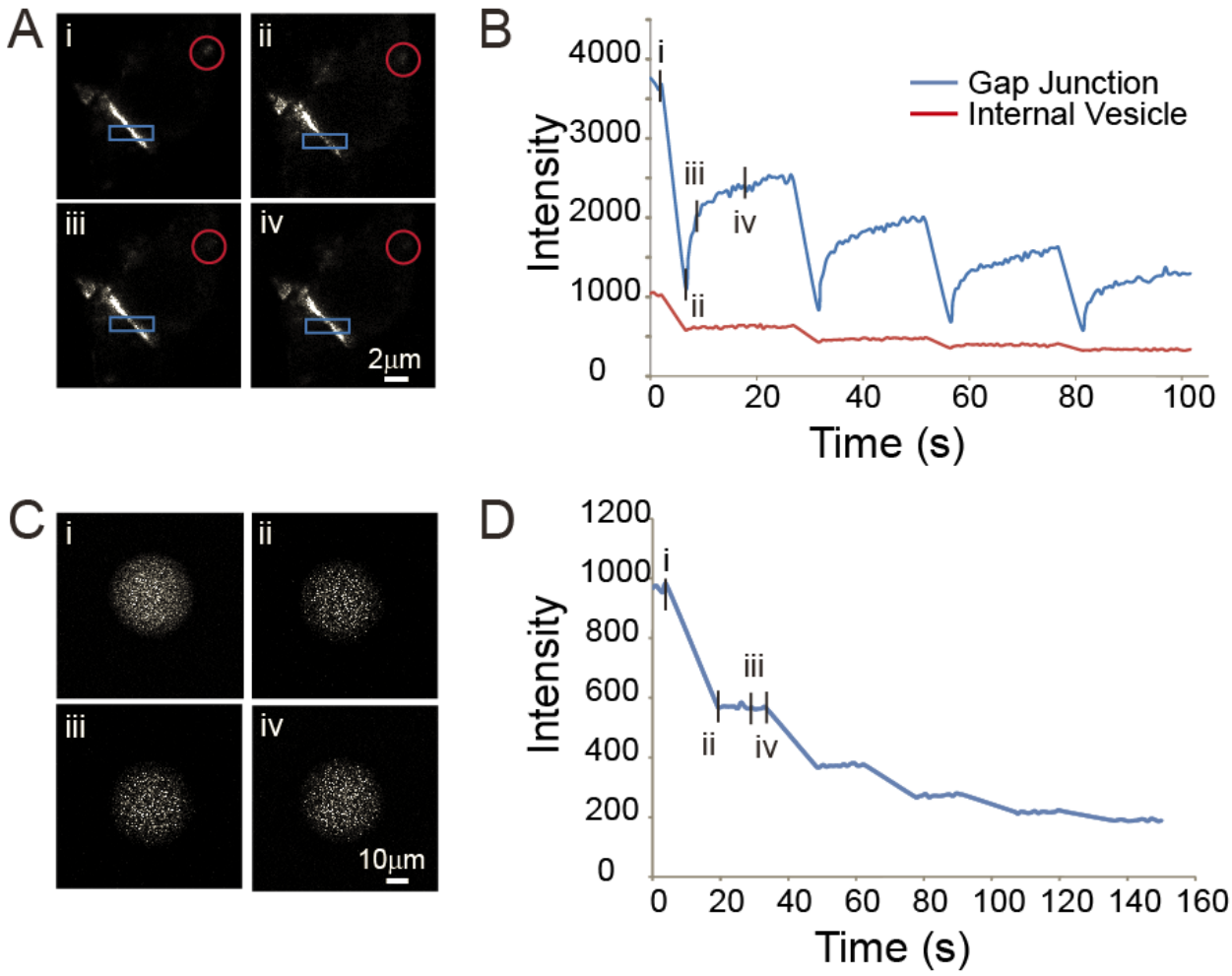

Figure 2.13. FRAP analysis of OG-labeled Cx36-Halo in HeLa cells. (A) Images of a GJ prior to bleach (i) and at 0.5, 1.5, and 10.4 sec post-bleach (ii-iv). Blue box is the bleached ROI and red circle is an intracellular vesicle bleached at the same time. (B) Intensity profiles of the bleached ROIs: GJ is blue line; vesicle is red line. GJ recovery half time was 1.9 sec. (C) FRAP of an OG ligand droplet using same bleaching parameters; images represent time points indicated in D. (D) Intensity profile of droplet bleach. Fluorochrome was not reactivated after bleaching.

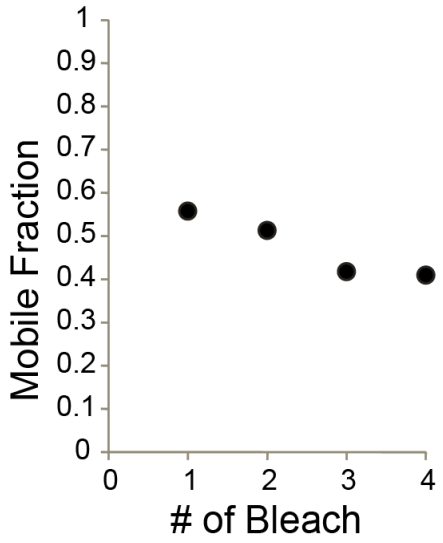

Figure 2.14: Mobile fraction of recovery decreases after each bleach with a range from 55-40%.

Finally, we also tested the ability of Cx43-Halo-Cinternal-XcmI to diffuse through existing GJ plaques. Photobleaching of OG-labeled C43 resulted in partial recovery of fluorescence in the bleached area with mobile fractions ranging from 78% to 46% (Figure 2.15). Thus some Cx43-Halo was mobile within the GJ.

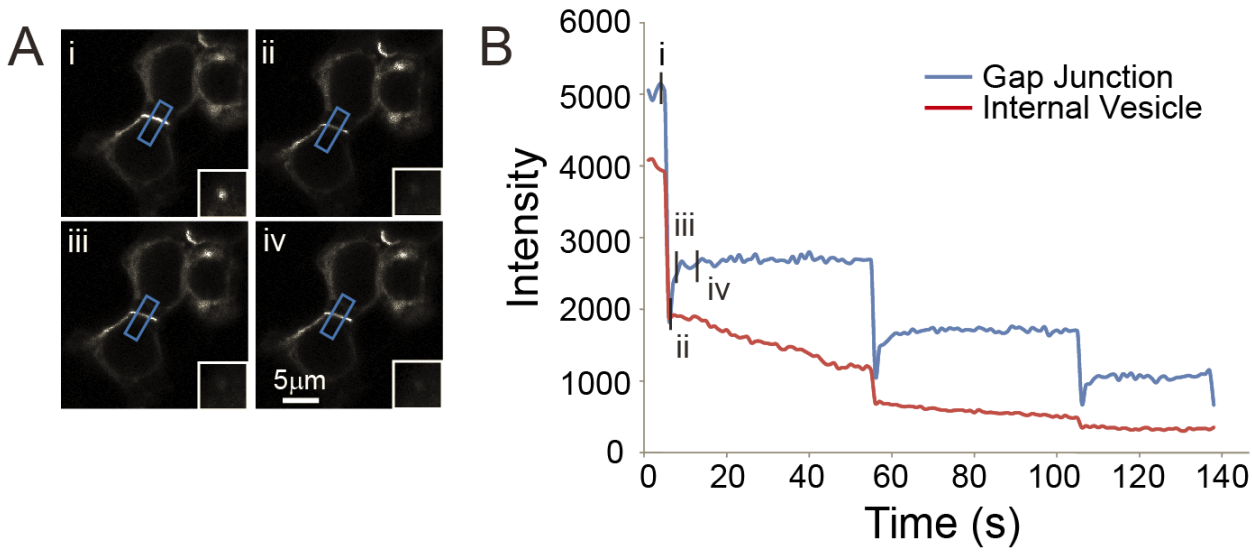

Figure 2.15. FRAP analysis of OG-labeled Cx43-Halo-C-IN in HEK293 cells. Images of a GJ prior to bleach (i) and at 0.5, 1.5, and 10.4 sec post-bleach (ii-iv). Blue box is the bleached ROI and inset panel of each image is an intracellular vesicle in the same frame bleached at the same time. (B) Intensity profiles of the bleached ROIs: GJ is blue line; vesicle is red line. (C) Mobile fraction of Cx43 following each bleach. Mobile fraction ranged from 78-46%.

Discussion

Validation of Connexin-HaloTag fusion constructs

To study the turnover rate of GJ protein, it is important to develop a means to label and track GJ protein efficiently and specifically. In this study, we employed the HaloTag technology to label Cx36 and Cx43. The HaloTag offers many advantages, including covalent labeling with non-toxic fluorescent ligands and monomeric structure (Encell et al., 2012). However, at 34 kDa, the HaloTag is about 25% larger than EGFP and almost as large as Cx36 itself. For reference, this tag is a little bit less than 2/3 the size of tdTomato. In spite of the large tag size, the protein produced by the Cx36-Halo construct successfully trafficked through the Golgi to the plasma membrane and formed GJs, even when bound to HaloTag ligands. Furthermore, the

Cx36-Halo GJs were functional and were regulated by PKA activity in the same manner as wild-type Cx36 GJs.

The position of the HaloTag within the connexin did result in minor differences in GJ formation that we did not assess quantitatively. Cx36 with an internal tag produced more GJs and fewer large internal vesicles than Cx36 with a C-terminal tag. Likewise, Cx43 with an internal tag at the XcmI site produced more GJs and fewer large internal vesicles than Cx43 with an internal tag at the EcoRI site or with a C-terminal tag. It should be noted that in our initial studies with HeLa cells, none of the Cx43 constructs formed GJs, although all did in later studies in Hek293 cells. Thus there may be aspects of the HaloTag that result in context-specific anomalies. Nonetheless, the labeling system was very effective for studying Cx36.

Cx36 vesicle trafficking mechanism

Previous studies have reported that connexons are incorporated into GJs as undocked hemichannels packaged in vesicles (Gaietta et al., 2002; Lauf et al., 2002), and removed as paired channels that form double membrane vesicles known as annular junctions (Laird, 1996; Gaietta et al., 2002; Lauf et al., 2002). These annular GJs subsequently are transported to lysosomes, where they are degraded (Laird, 1996; Piehl et al., 2007). Our microscopic evidence is consistent with this theory by showing two different classes of vesicles: small newly formed vesicles presumably for exocytosis and large ring shaped vesicles presumably resulting from endocytosis. A consistent observation in our imaging studies is that the small vesicles carrying newly-made Cx36 were often found attached to existing GJ plaques, either in the center of on the ends of the plaques, and patches of chase label could be seen in the GJ adjacent to the vesicles.

This strongly implies that these vesicles dock at existing GJs and their cargo diffuses into the GJ plaque. These findings agree with those of Shaw et al. (Shaw et al., 2007), who found that Cx43 cargo vesicles were targeted directly to adherens junctions adjacent to GJ plaques through microtubule plus-end tracking proteins.

Novel features of Connexin-HaloTag trafficking

Several previous studies have found that Cx43 present as undocked hemichannels in the plasma membrane accreted to the outside edges of existing GJs and mixed very little with existing GJ channels (Gaietta et al., 2002; Lauf et al., 2002; Falk et al., 2009). Our observations did not show such apparent accretion at the edges of GJs, but instead chase labeled Cx36 was found diffusely throughout the GJ plaques. Furthermore, our photobleaching studies showed that Cx36 was extraordinarily mobile within the GJ plaque, suggesting that we would not be able to detect accretion of new connexins on plaque edges.

It is not clear why these results differ so dramatically from those using other connexins with other tags. Our results with Cx43-HaloTag constructs showed some mixing throughout GJs, although to a lesser extent than Cx36; Cx43 also recovered partially from photobleaching. Thus while the properties of individual connexin types do differ, the presence of the HaloTag may impart greater mobility to connexins than does a fluorescent protein or tetracysteine tag. We should note that the fluorescently labeled HaloTag connexins are much brighter than fluorescent protein labeled connexins, so our observations of the chase label may have higher sensitivity. In addition, observations based on bleaching or photoconversion may suffer from inactivation of mobility, as we observed when using more focused bleaching light with higher power and higher numerical aperture (NA) objectives. The possible impact of phototoxicity on

fluorescent recovery will be discussed further in Chapter Three. Additional studies will be required to determine if the HaloTag specifically imparts higher mobility to connexins or other proteins.

Chapter Three:

Phototoxicity in FRAP experiments

Introduction

Live cell imaging and phototoxicity

Fluorescence based live cell imaging requires the living samples to be exposed under high intensities of focused illumination for a prolonged period of time. Phototoxicity is a common but often underestimated and overlooked issue that is associated with long-term exposure in imaging. Nature group compiled all papers published in Nature (Nature, Nature Cell Biology, Nature Immunology, Nature Methods, and Nature Neuroscience) in the period from January 1st, 2005 to November 3rd, 2013. Out of 4691 publications that conducted fluorescence study, only 1.4% discussed either phototoxicity or photodamage (5.1% occurrence Nature Methods, 0.9% in the rest combined) (Evanko, 2013).

A common misconception is to equate photobleaching with phototoxicity. Photobleaching is specific to fluorescence microscopy. It refers to the loss of fluorescent signal when a fluorophore is exposed to fluorescent illumination and excited into a state of inactiveness. It is an irreversible process and is common in imaging, even desired in applications like Fluorescence Recovery after Photobleaching (FRAP). Phototoxicity, on the other hand, can be a result of prolonged photobleaching. It refers to the interaction of light energy with cells and interference of cell metabolism in general (Diaspro et al., 2006). Phototoxicity can be a direct effect where reactive oxygen species (ROS) are generated by the energy transfer of an excited fluorophore in a triplet state to a molecule of oxygen and exciting it to a singlet state, a free-radical. This free-radical can interact with other molecules within the cell to generate downstream toxic effects (Tinevez et al., 2012). These indirect effects can include localized thermal influx generation, light induced ionizing, and unintended light-induced activation of membrane conductance. These toxic effects can lead to extreme phenotypes such as detachment

of cells from cover glasses, free radicals rupturing the cell membrane, collapsing chemical and ionic compartmentalization, leading to cell cycle arrest or cataclysmic cell death (Hoebe et al., 2007) (Tinevez et al., 2012).

Good quality live cell imaging requires a fine balance between exposure and resolution. To ensure good image quality, most microscopes we use for live cell imaging maximize spatial and temporal resolution by oversampling *x*, *y*, *z*, and *t*. It is not uncommon to acquire hundreds of images at each time point for a prolonged period of time. The extensive light exposure can cause an elevated "*photon-light budget*" (Arhel et al., 2006; Enninga et al., 2005; Amino et al., 2006; Tinevez et al., 2012).

FRAP and phototoxicity

FRAP is a powerful, microscopy-based method that allows us to study the molecular dynamics within a living cell. It can give us useful information on the dynamics and mobility of the specific protein of interest. In a FRAP experiment, high laser intensity is used to irreversibly bleach fluorescent molecules that are localized in the selected region of interest (ROI). Whether the fluorescent signal recovers in the ROI or not, or the recovery rate if it does, can provide us with details of about the dynamics of the protein of interest (Carisey et al., 2011).

There are two potential ways in which a bleached ROI can recover. The first is the diffusion of the fluorescently tagged protein from the unbleached region into the bleached region. This will be fast occurring process that requires the mobility of the protein of interest in the localized area. The second is through the continuous turnover of the protein of interest within the complex, allowing the bleached proteins to be replaced by newly synthesized proteins

that are trafficked into the ROI. This process will be a lot slower depending on the turnover rate of the protein of interest in the cell.

Several previous studies have found that Cx43 present as undocked hemichannels in the plasma membrane accreted to the outside edges of existing GJs and mixed very little with existing GJ channels (Gaietta et al., 2002; Lauf et al., 2002; Falk et al., 2009). Our observations did not support such apparent accretion at the edges of GJs, but instead chase labeled Cx36 was found diffusely throughout the GJ plaques. We performed FRAP experiments to study the mobility of Cx36 within the GJ plaques. Our photobleaching experiments showed that Cx36 was extraordinarily mobile within the GJ plaque. Our results with Cx43-HaloTag constructs showed some mixing throughout GJs, although to a lesser extent than Cx36; Cx43 also recovered partially from photobleaching. Rapid recovery of photobleached connexin in GJ plaques has not been previously reported and we questioned whether this might be an artifact resulting from reversible bleaching of the OG fluorochrome by the bleaching sweeps. To test this, we photobleached aqueous droplets of the OG HaloTag ligand suspended in mineral oil using the same bleaching paradigm. There was no recovery observed in the droplet tests. Thus rapid recovery of OG-labeled Cx36 in the bleached area was not an artifact.

There are several studies that have used FRAP to access connexin dynamics in the GJ plaques (Simek et al., 2009; Roh and Funderburgh, 2011), but phototoxicity was never raised as an issue. In live cell imaging, maintaining a light budget is an important aspect in limiting the production of ROS, hence reducing photobleaching, which can lead to phototoxicity. In FRAP, photobleaching is intentional. Excitation light dose, in the forms of laser power and light dwelling time, is increased significantly to bleach a fluorescent signal. Many protocols of FRAP call for a complete bleach emitted by the tagged protein (Carisey et al., 2011). Phototoxicity was

a major concern for live cell imaging where excitation light dose was minimized. It is reasonable to think that it might cause a bigger problem during FRAP experiment, where light power and bleach time is intentionally maximized.

In this study, we investigated a number of parameters in performing photobleaching during the FRAP experiment. Even though we observed rapid recovery in Cx36 GJ when using objective with lower numerical aperture (20x 0.8 NA) at low zoom, the recovery was not repeated when an objective with high numerical aperture (40x 1.2 NA) or a higher zoom was used. This could explain the differences in observation when it comes to protein dynamics and mobility in the system we study.

Methods and Material

FRAP experiments

FRAP experiments were performed using Zeiss LSM 780 and 880 confocal microscopes using 20x 0.8 NA Plan-Apochromat air or 40x 1.2 NA oil immersion objectives and GaAsP detectors employing the FRAP routines in Zeiss Zen software. Immediately after HaloTag OG labeling and 15 minutes of wash period, coverslips were mounted in Ringer's medium and GJs imaged at a single focal plane at 0.5 to 2 sec intervals using a low laser intensity to ensure GJ stability. An ROI was selected away from the end of a GJ plaque and a series of high intensity laser sweeps was used to bleach the selected area. Immediately after bleaching, the sample was imaged at regular time intervals using the same low intensity as before the bleaching until the intensity of the bleached area had reached a plateau. Bleachings were repeated three more times after the intensity plateaued to study the effect of repeated exposure. An internal vesicle was

selected as an ROI as a negative control and was bleached and imaged the same manner as the ROI in the GJ plaque. A scheme of the FRAP experiment is shown in figure 3.1.

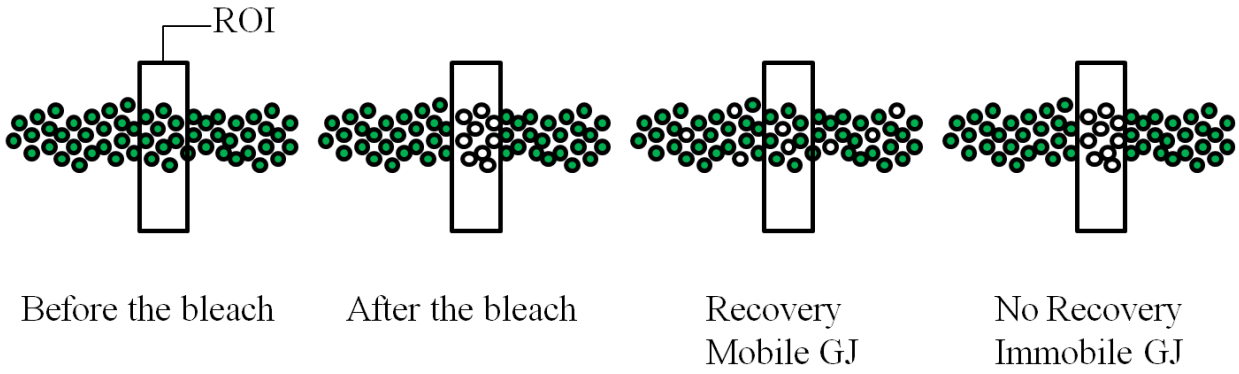

Figure 3.1: Scheme depicting the Photobleaching and fluorescence recovery of a region of interest (ROI) within a GJ. Before the bleaching, the connexin protein is labeled with HaloTag OG ligand. Immediately after the bleach event, the ligands in the ROI are irreversibly bleached. The model presents two scenarios following the bleaching. If the GJ proteins are mobile and can freely diffuse laterally, the tagged protein from the unbleached region will quickly move to the ROI as the bleached ones will move out. The whole GJ will reach equilibrium where the total fluorescent pool will reduce in signal strength. If the GJ proteins are immobile, the bleached area will remain bleached as the bleached fluorescent tag is unable to recover.

Aqueous Ligand droplet control

The droplet control was performed by suspending 5 µl of 1x working solution of the HaloTag OG ligand in 1ml mineral oil by vortexing. Drops of the emulsion on a cover slip were bleached and individual HaloTag OG ligand droplets were imaged in the same manner as were connexin GJs (Figure 3.2).

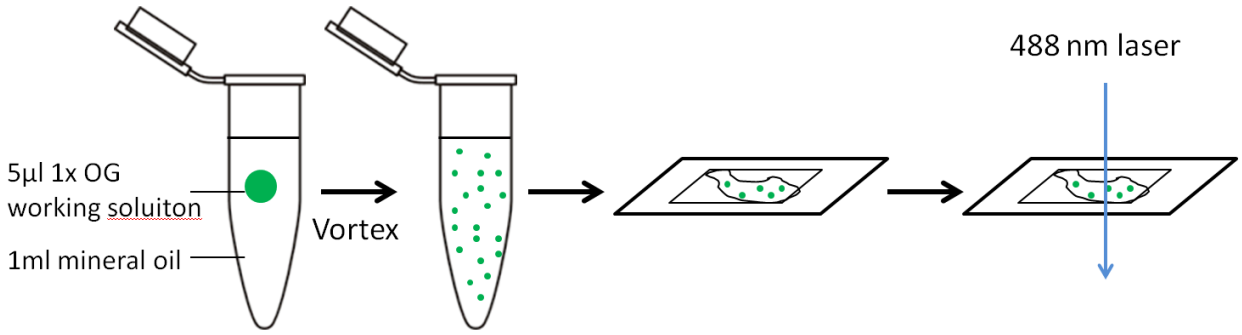

Figure 3.2: Scheme depicting the OG ligand droplet control.

Results

Focused laser power reduced or eliminated Cx36 recovery

During our study of Cx36 dynamics and mobility, we performed FRAP experiments under 20x objective at zoom 6 and observed very rapid recovery in the photobleached area (detailed results shown in Chapter Two, Figure 2.13). Rapid recovery of photobleached connexin in GJ plaques has not been previously reported and we questioned whether this might be an artifact resulting from reversible bleaching of the OG fluorochrome by the bleaching sweeps. To test this, we photobleached aqueous droplets of the OG HaloTag ligand suspended in mineral oil using the same bleaching paradigm and observed no recovery. The lack of recovery shown in the aqueous droplet test proved that the recovery we observed in Figure 2.13 was not an artifact of recovering fluorochrome, but the result of diffusion of GJ protein. However, when bleaching was done using confocal zoom greater than 6 with the 20x objective (Figure 3.3), or a 40x objective (Figure 3.4), recovery was greatly reduced (Figure 3.3A and B) or completely eliminated (Figure 3.4A and B). When performing the aqueous droplets test using 40x objective, we observed no recovery as well (Figure 3.4C and D), and this lack of recovery was replicated at several different laser power settings and confocal zoom settings. Unlike the

aqueous test we did under 20x objective in which the laser only destroyed a fraction of the fluorochrome with no recovery, the test we did under 40x destroyed most of the fluorochrome in just one bleach.

We presume that the failures to recover under certain imaging conditions are the result of light-induced damage to the connexin proteins or membrane lipids. This may also be responsible for our observation that, even under bleaching conditions that allow recovery, the mobile fraction of Cx36-Halo decreased with each subsequent bleach in the region of interest (Figure 2.14).

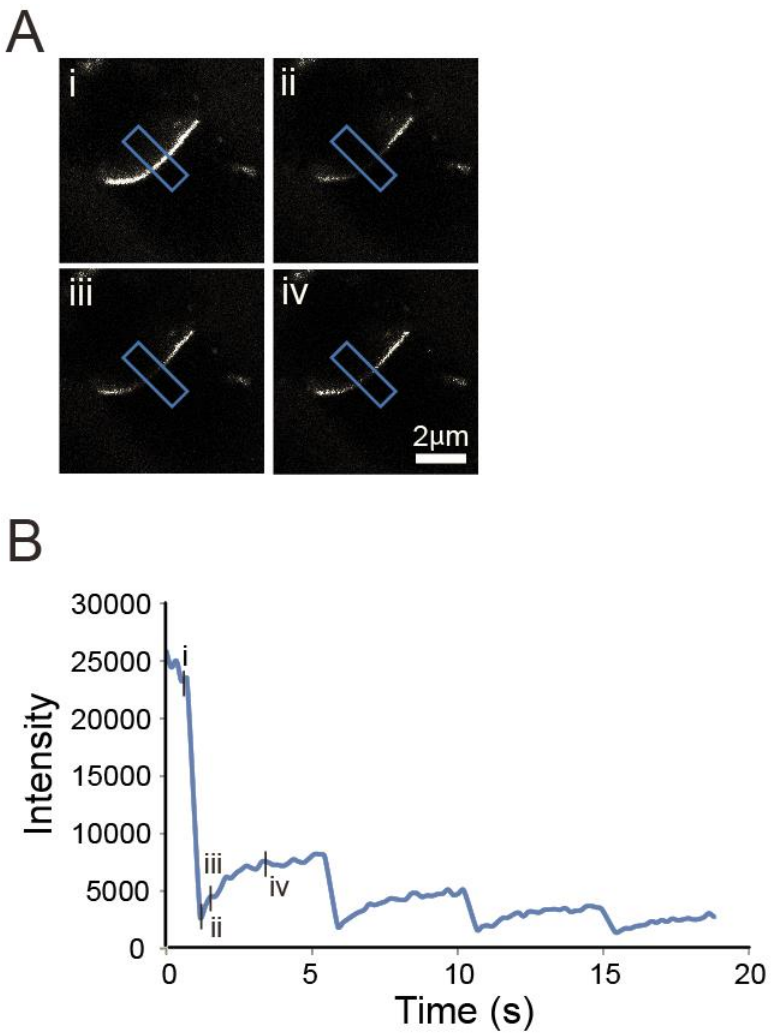

Figure 3.3. FRAP analysis of OG-labeled Cx36-Halo in HeLa cells under 20x objective at high zoom (zoom 12). (A) Images of a GJ prior to bleach (i) and at 0.45, 0.8, and 1.5 sec post-bleach (ii-iv). Blue box is the bleached ROI. (B) Intensity profiles of the bleached ROIs. Recovery of Cx36 was greatly reduced.

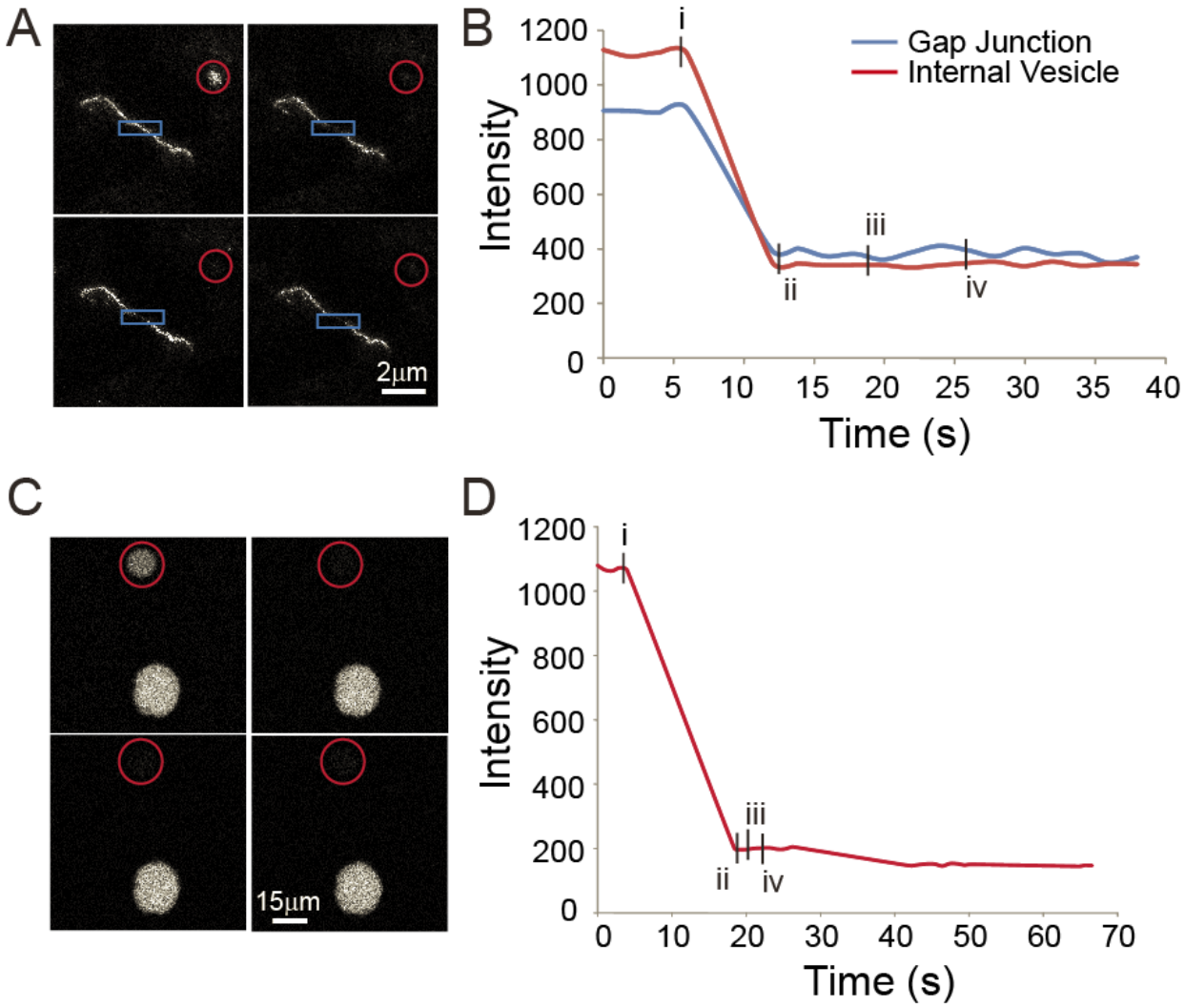

Figure 3.4. FRAP analysis of OG-labeled Cx36-Halo in HeLa cells with higher light throughput objective (40x oil). (A) Images of a GJ prior to bleach (i) and at 0.5, 2.5, and 20.8 sec post-bleach (ii-iv). Blue box is the bleached ROI and red circle is an intracellular vesicle bleached at the same time. (B) Intensity profiles of the bleached ROIs: GJ is blue line; vesicle is red line. Cx36 showed no recovery. (C) FRAP of an OG ligand droplet using same bleaching parameters; images represent time points indicated in A. (D) Intensity profile of droplet bleach. Fluorochrome was not reactivated after bleaching.

We compiled all the bleaching parameters that we have tested when performing FRAP experiments, either on Cx36 GJ or HaloTag OG ligand aqueous droplet test, and the results are shown in table 3.1.

Object	Objective	Laser %	Zoom	Recovery
Cx36	**20x**	**100%**	**<6**	**YES**
	20x	100%	>6	Limited
	40x oil	100%	Any	No
Droplet Ctrl	20x	50%	Any	No
	20x	100%	Any	No
	40x oil	50%	Any	No
	40x oil	100%	Any	No

Table 3.1. Summary of recovery of Cx36 GJ and HaloTag OG ligand droplet control under different bleaching conditions.

Discussion

To reduce phototoxicity, the key is to reduce the generation of ROS resulting from prolonged light exposure. There are several parameters that can influence the light budget. The most common parameters that we manipulate are the amount of excitation light dose and the rate at which the light dose is delivered. Scientists have being actively seeking ways to minimize the excitation light dose by reducing the exposure time or light intensity. However, the amount of light dose is directly related to image quality. Reducing either exposure time or light intensity can result in weakening fluorescence signals and reduction in signal to noise ratio. Image quality will suffer as a result.

The delivery rate of excitation light dose matters for phototoxicity as well. There are natural ROS scavengers present in the cell, such as glutathione, ascorbate, and tocopherol. They allow cells to cope with a certain amount of photodamage with no long term impact on cell health (Dixit and Cyr, 2003; De Vos et al., 2009). When we deliver photons at a lower rate for a given light dose, we allow the ROS scavengers to regenerate and cope with the generation of ROS (Tinevez et al., 2012). There are commercialized ROS scavengers that can be added as

imaging media supplements. However, those scavengers could deplete the cells of all oxygen supply and suppress ATP dependent machinery in the cell, and result in impaired cell function, especially functions relying on the hydrolysis of ATP.

FRAP experiments are very useful when studying the dynamics of the protein of interest in a living system. However, when performing FRAP experiments, all the measures mentioned above were out of the window since we are maximizing laser power and increasing bleach sweeping time to achieve complete bleach of the fluorochrome. In our study, we discovered that Cx36 recovered at a very rapid rate when laser power is more diffused over a wider area, but showed no recovery when the laser power was more focused. In the experiments where recovery was observed, the fluorochrome was never fully bleached. Every bleach only destroyed a fraction of the fluorochrome, and the same recovery behavior repeated after each bleach for as long as the bleaches were repeated or the entire pool of fluorochrome was bleached beyond visualization. This partial bleach was confirmed when we performed the HaloTag OG ligand aqueous droplets. When a small aqueous droplet of the OG ligand was bleached under 20x objective, only a fraction of the fluorochrome was destroyed, but no recovery was observed, confirming that the rapid recovery of OG-labeled Cx36 in the bleached area was not an artifact. When the laser power was more focused, at a higher zoom under 20x objective, or under 40x objective, all fluorochrome within the ROI was destroyed in one bleach. Recovery was no longer observed. Again this full bleach of fluorochrome was confirmed by the aqueous droplets test under 40x objective with no recovery.

We suspect that the failures to recover when laser power is more focused are the result of light-induced damage to the GJ or connexin proteins. Similar to high laser power imaging over a long period of time, bleaching part of a GJ with 100% laser power can lead to an increased

generation of ROS that cause a tremendous amount of stress. When the laser power was more focused, the amount of light on unit area of GJ increased, and ROS scavengers may not have sufficient capacity to remove ROS and restore cells to normal function. The delivery and trafficking system for Cx36 GJ, which will be discussed in detail in Chapter Four, is very delicate. In Chapter Four, we will discuss the role of actin filament in Cx36 GJ mobility. Actin filaments work in association with Myosin, which hydrolyze ATP (Pollard and Borisy, 2003). ATP is the product of the oxygen-dependent citric acid cycle. It is possible that under focused laser power, the delivery machinery was disrupted by the overproduction of oxygen free radicals and Cx36 lost its mobility within the GJ plaques.

Chapter Four:

Dynamics and Mobility of Cx36 – Role of Actin Filaments in Cx36 Trafficking and Mobility

Introduction

Dynamic trafficking of GJ proteins

GJ channels are tightly packed double membrane protein structures. Each individual GJ plaque can contain thousands of channels and extend several micrometers in diameter. An important event of the assembly of GJ is the oligomerization of individual connexin proteins in connexons. The process of oligomerization occurs after the connexin proteins exit from the endoplasmic reticulum (ER) and into the Golgi apparatus and trans-Golgi network (TGN) (Johnson et al. 2002). The connexons are then inserted into the plasma membrane, align and interact with connexons from the adjacent cells. GJ proteins have abnormally high turnover rate, ranging mostly from 1.5-3.5 hours, with the exception of Cx50 in lenses (Table 1.1) (Herve et al. 2007). The translocation of connexins from intracellular space to the plasma membrane are key to keep up with the fast pace of turnover, and thus key to maintain cell-to-cell communication. How these multi-unit structures are assembled and inserted in the GJ plaques at such a fast rate have remained elusive.

Actin and vesicle trafficking

Transport of membrane proteins in general from intracellular space to the plasma membrane is likely to involve tubulovesicular networks (Nakata et al., 1998; Lippincott-Schwartz et al., 1998). The TGN is defined as the sorting facility for synthesized proteins. Cytoskeleton machinery has been shown to play an important part in protein trafficking. Both the microtubule and actin cytoskeleton have essential contribution to intracellular vesicle trafficking. Protein transportation at Golgi and TGN utilizes both microtubule and actin

associated motor proteins (Caviston and Holzbaur, 2006; Palmer et al., 2005). They are important not only for transportation of vesicles, but also for the integrity of the morphology of the Golgi complex (Egea et al., 2006; Allan et al., 2002). There have been extensive studies on the role of microtubules in trafficking (Thyberg and Moskalewski, 1999; Musch, 2004; Vaughan and Dean, 2006; Palmer et al., 2005). The actin cytoskeleton is highly dynamic and highly regulated by an abundance of actin-binding proteins and upstream signaling pathways that modulate actin polymerization and depolymerization. This polymerization and depolymerization process generates forces that manipulate membranes in the process of vesicle biogenesis and propel vesicles through the cytoplasm to reach their destination, facilitating many cellular functions based on membrane dynamics, such as endocytosis, exocytosis, and vesicular trafficking at the Golgi (Hanley, 2014). Actin filaments have been attracting more attention as their roles in vesicle trafficking have been studied. The role of actin filaments has been tested in the transport of vesicles from Golgi to plasma membrane (Hirschberg et al., 1998; Cao et al., 2005), as well as their removal to early and late endosomes in association with microtubules (Apodaca, 2001; Brown and Song, 2001; Mundy et al., 2002).

There are several studies that have investigated the role of cytoskeleton and GJ assembly, and the results have varied from case to case. Some reports show that interrupting cytoskeleton depresses some aspect of GJ assembly. George et al. showed that trafficking of Cx32 and 43 to plasma membrane was suppressed by a small extent when microtubule was interrupted (George et al., 1999). Wang and Rose showed that the assembly of Cx43 into GJ plaques requires actin filaments and clustering of Cx43 at cell-cell contact is prevented by Cytochalasin B and D treatment (Wang and Rose, 1995). Other reports, however, have shown that interrupting cytoskeleton does not alter GJ assembly and formation at all (Ito et al., 1974; Shen et al., 1986;

Kidder et al., 1987; Feldman et al., 1997). In our live-cell imaging using the Bessel Beam Plane Illumination Microscope, we noticed very fine finger-like Cx36 filadendrites extending from the GJ plaques. These filadendrites are thin extension of the GJs from the center of the GJ plaques. They change their morphology at a fast pace, and constantly break off and fuse back with the GJ plaques or with each other. Double label with actin filaments showed that these thin filadendrites co-localize with actin perfectly and inhibiting the elongation of actin filaments eliminates the presence of these filadendrites. We hypothesize that these filadendrites that move rapidly are important in Cx36 GJ morphology, and that interrupting actin filaments will disturb the integrity of GJ plaques and their functions. To confirm the hypothesis, we treated Cx36-Halo transfected HeLa cells with two actin disrupting drugs, Cytochalasin D and Latrunculin A, and observed the resulted effects on Cx36 GJ plaques.

Methods and Material

Labeling, immunostaining and imaging

For fixed cell imaging, transfected HeLa cell cover glasses were incubated in Ringer's medium containing 5μM HaloTag TMR fluorescent ligand for 15 minutes. Cover glasses were then washed to remove unbound ligand and fixed with 4% paraformaldehyde. For actin filament labeling, fixed cover glasses were rinsed with PBST (0.5% Triton) and incubated in PBST containing phalloidin 488 for 30 min before being washed again and mounted. Cover glasses were then imaged with a confocal microscope. HaloTag TMR was visualized with the TRITC filter set; HaloTag OG and 488 phalloidin were visualized with the FITC filter set.

For pulse-chase labeling, HeLa cell cover glasses were incubated in Ringer's medium containing 5µM HaloTag OG fluorescent ligand for 15 minutes, washed and transferred to fresh Ringer's medium containing 5µM HaloTag fluorescent ligand for 15 minutes. Cover glasses were then washed to removed unbound ligand and fixed with 4% paraformaldehyde. Fixed cover glasses were rinsed with PBST (0.5% Triton) and incubated in PBST containing phalloidin 647 for 30 min before being washed again and mounted. Cover glasses were imaged with a confocal microscope, and 647 phalloidin was visualized with the Cy5 filter set.

For live cell imaging, transfected HeLa cell cover glasses were incubated in Ringer's medium containing 5µM HaloTag fluorescent ligand for 15 minutes. Cover glasses were then washed to remove unbound ligand and immediately imaged under Bessel Beam Plane Illumination Microscope from HHMI Janelia Farm Research Campus in the laboratory of Dr. Eric Betzig. Cells were imaged at 37˚C in DMEM with HEPES containing no phenol red. Images were taken at 10s intervals. Deconvolution of all images was performed in Amira version 5.3 (Visage Imaging) using an iterative maximum-likehood image restoration algorithm (Gao et al., 2014).

Drug Treatments

For disrupting Golgi apparatus

To analyze the transport of Cx36 from ER to the plasma membrane, transfected HeLa cells were treated with Brefeldin A (2 µg/ml in Ringer's medium with 0.1% DMSO), which disassembles the Golgi apparatus, during the pulse-chase analysis. BFA was added to the cells after 15 minutes of pulse label OG incubation and washing, and was left in the wells before the

chase label TMR was added. Cells were incubated in TMR for 15 minutes. In the control experiments, cover glasses were treated with DMSO (0.1%) and the treatment was identical to that of BFA.

For disrupting of actin filaments

To analyze the effect of disrupting actin filaments on GJ formation and integrity, transfected HeLa cells were incubated in DMEM containing Cytochalasin D (0.2μM), which induces actin depolymerization, or Latrunculin A (0.2μM), which inhibits actin polymerization, for two hours prior to TMR labeling.

Tile Analysis

To calculate the fraction of GJ expressed at cell-cell contact, we took 25 tiles (5x5) of neighboring images, and stitched them together in Zeiss Zen software to yield a 1063μm by 1063μm area (Figure 4.1A). Total number of GJ and total number of HeLa cell pairs expressing Cx36-Halo were counted manually. We encountered four different kinds of expression (Figure 4.1B). The fraction of HeLa cell pairs expressing Cx36-Halo that harbored a cell-cell GJ is the ratio of total number of GJ expressed over the number of cell pairs expressing Cx36-Halo. Figure 4.1B1, 2, and 3 all show cell pairs expressing Cx36-Halo and harboring Cx36 GJs, whether the GJ is in plaque sheet form or small punctate form. Figure 4.1B4 shows a pair of Cx36-Halo positive cells with no GJ present at the cell-cell contact.

A.

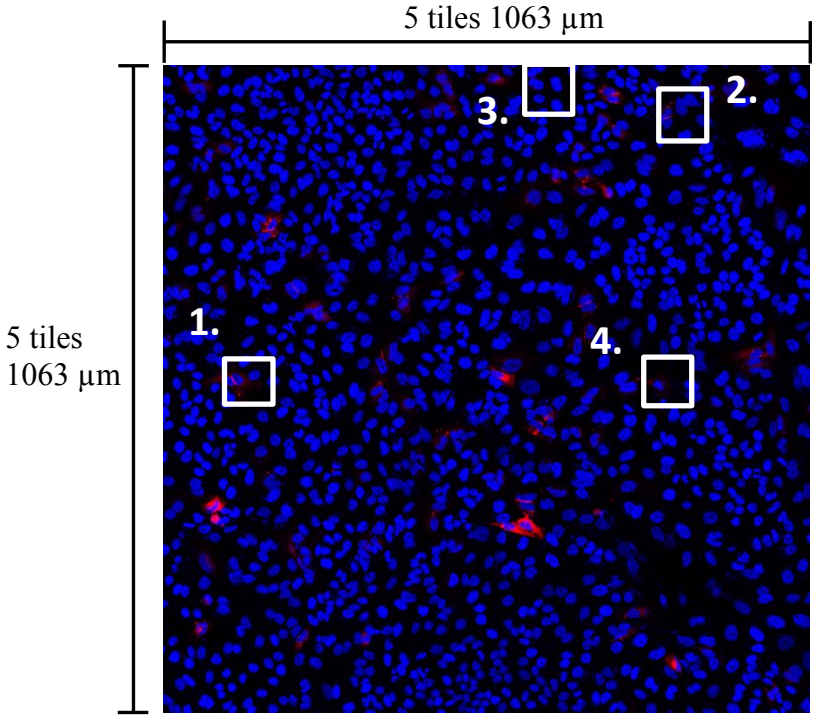

B.

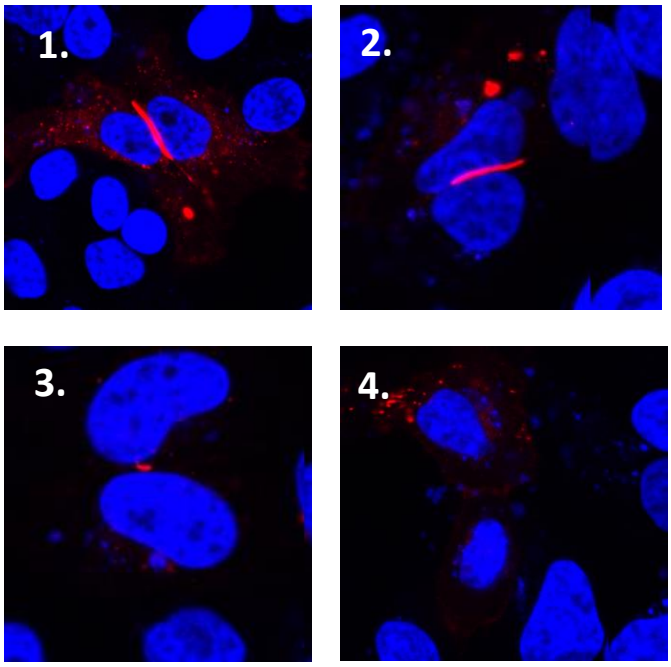

Figure 4.1: Tile Analysis. We captured 25 neighboring images and stitched them together to form a 1063 µm by 1063 µm area (A). The number of Cx36-HaloTag expressing pairs and the number of GJ present are counted manually. (B) 1-3 showed pairs of neighboring cells harboring Cx36 GJ plaques, either large or small. 4 shows a pair of neighboring cells expressing Cx36-Halo but not harboring Cx36 GJ.

Results

Cx36 GJ assembly requires the Golgi apparatus

With the exception of Cx26 (Zhang et al., 1996), it is generally considered that connexins are modified in the ER (Zhang et al., 1996; Ahmad et al., 1999b), transported to the Golgi, assembled in the trans-Golgi network (Musil and Goodenough, 1993; Koval et al., 1997), and finally inserted into the plasma membrane (Laird, 1996; Thomas et al., 2005). To determine if the trafficking of Cx36 to the plasma membrane involves this pathway, we performed the pulse chase analysis with treatment of Brefeldin A (BFA), which disassembles the Golgi apparatus. The original GJs were labeled with OG, and chased with TMR. We saw that at time 0.3 hours, all the GJs were labeled with OG, with a minimal amount of TMR labeling (Figure 4.2). As time progressed, the amount of TMR labeling did not increase in the GJs. In the BFA treated cells, in which GJs were less abundant and contained very little chase label, we found that newly made Cx36 was added to the large internal vesicles throughout the chase period.

Most of the TMR label was present in small vesicles and some large vesicles; almost none integrated into the GJs, and OG remained the predominant label through the 5^{th} hour (Figure 4.2) even through the intensity of the label decreased with time. The fraction of OG present in the GJs showed no significant change from hour 0 to 5 (One-way ANOVA: hour 0.3 86.7 ± 7.4%, hour 5 91.2 ± 6.5%; n=5 GJs per time point; p=0.33), while the change of fraction of OG was significant when BFA was not added (One-way ANOVA: hour 0.3 91.6 ± 5.7%, hour 5 31.4 ± 6.2%; n=10-20 GJs per time point; $p<0.0001$). We conclude that the Golgi was essential for Cx36 GJ assembly.

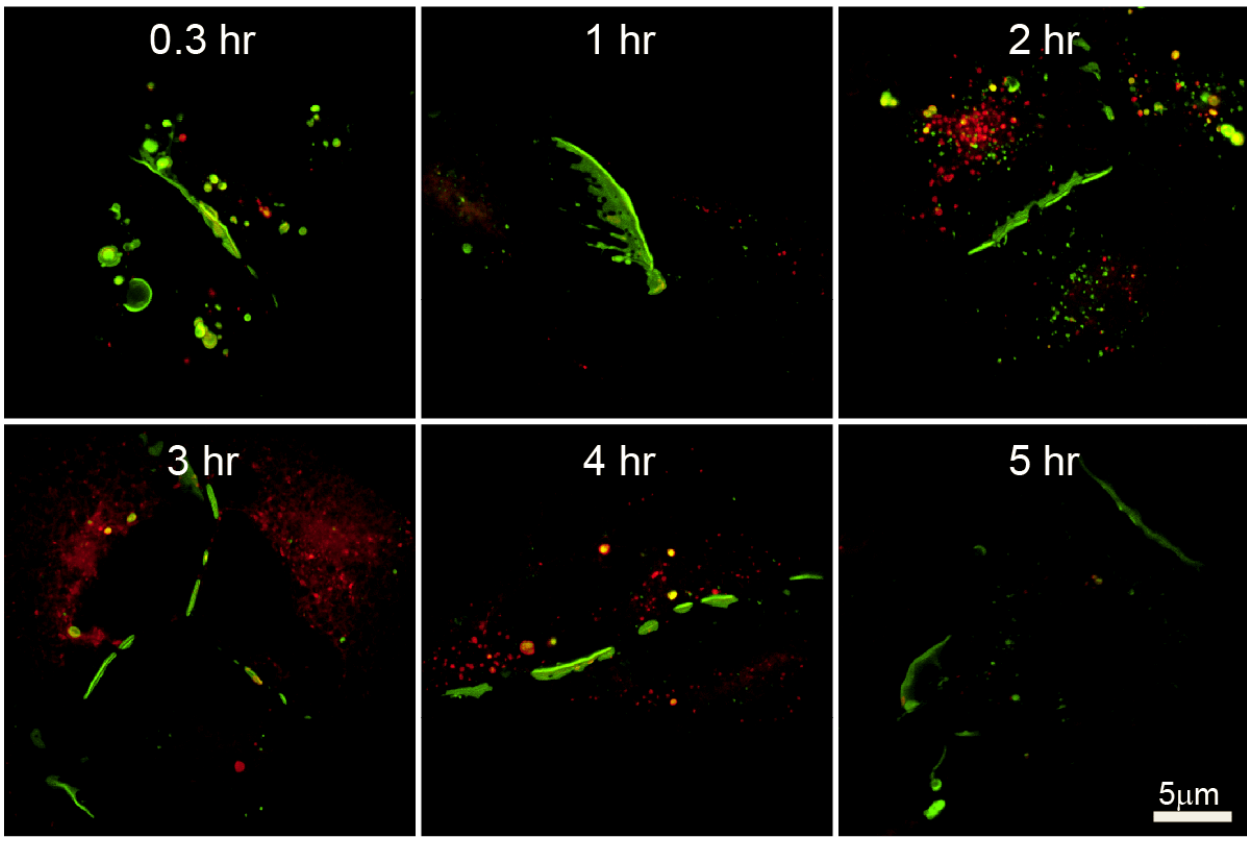

Figure 4.2. Pulse-chase analysis of Cx36-Halo in HeLa cells with Brefeldin A treatment throughout the chase period. Pulse (OG; green) and chase (TMR; red) ligands are the same as in figure 3. Treatment with BFA prevented insertion of newly made Cx36 into GJs. By 5 hr, GJs were very rare and difficult to find. Images are confocal stacks 2.5 µm in thickness. Scale bar applies to all images.

Thick actin bundles connect edges of all GJs. Vesicles were associated with actin filaments leading to the GJ.

To study the association between Cx36 GJ and actin, we performed a pulse-chase experiment with Phalloidin 647 labeling for the actin filaments. We found that thick actin bundles connect edges of all GJ. When there are two GJ at the same cell-to-cell contact, actin bundles connect them together (Figure 4.3).

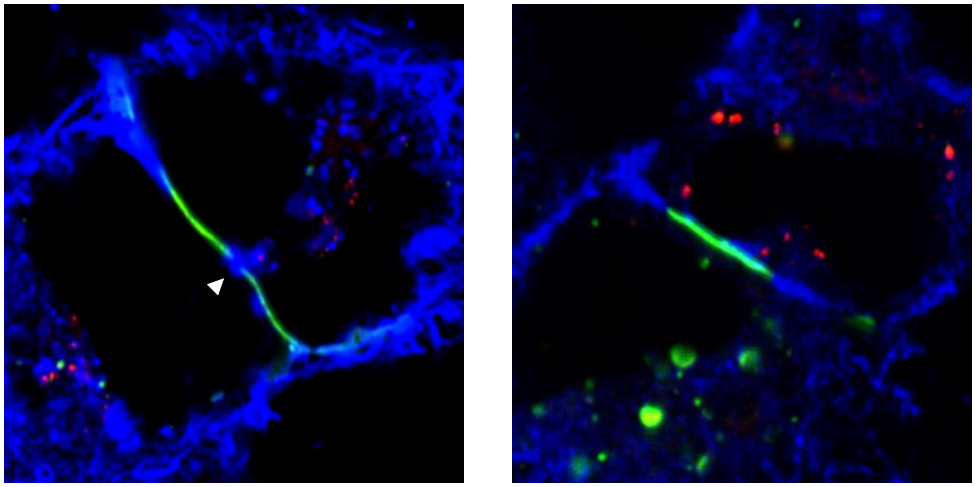

Figure 4.3: Thick actin bundles (blue phalloidin labeling) connected all edges of GJ plaques (OG labeling), indicated by arrowhead, but actin filaments were rare within any plaque.

We found actin filaments associated closely with GJ plaques, and with all the vesicles surrounding the GJ. Figure 4.4A1 and B1 show the association between actin material and removal vesicles labeled with OG. In A1, the vesicles (arrowheads) just left the GJ plaque. In B1, the removal vesicle (arrowhead) is just budding of the surface of the GJ plaque. Figure 4.4A2 and B2 show the association between actin material and insertion vesicles. In A2, we can see that there is a gap between the TMR labeled GJ, and a thin actin filament is leading an insertion vesicle directly to where the gap is located (Figure 4.4) (arrow). Phalloidin 647 bleached very quickly and impaired the quality of actin filament imaging. The association between actin filaments and insertion vesicles is discussed further below.

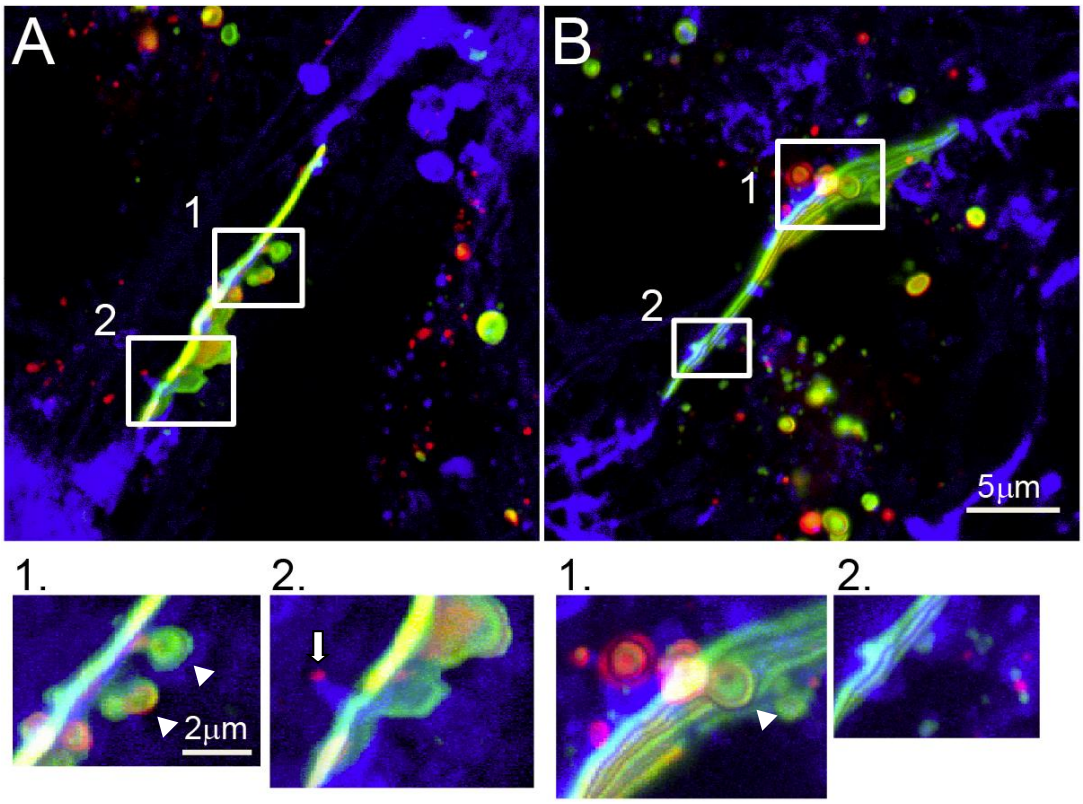

Figure 4.4. Cx36 vesicles associate with actin filaments. (A-B) Insertion and removal of Cx36 into and out of the GJ. Both insertion (A2, B2) and removal (A1, B1) vesicles were associated with actin filaments leading to the GJ.

Live-cell imaging showed pulse-labeled finger-like filadendrites extending from the edges of the plaques, and the morphology of these filadendrites changed at a fast pace.

To further study the dynamics of Cx36 and trafficking mechanism of Cx36 in live HeLa cells we collaborated with Dr. Eric Betzig (HHMI Janelia Farm Research Campus) and performed live cell imaging using Bessel Beam Plane Illumination Microscope. In the live imaging, many GJs showed substantial numbers of finger-like filadendrites extending from both the edges (Figure 4.5A) and the center (Figure 4.5B) of the plaques. The filadendrites extending from the edge are the continuation of the GJ plaques themselves; they are about the same thickness as the GJ plaque. These filadendrites extending from the edges were observed in GJs made of Cx32-EGFP (Windoffer et al., 2000). The ones extending from the center, however, are

much thinner than the actual GJ plaques, and consist solely of pulse OG labeled Cx36. Their morphology was constantly rearranged by breaking off and fusing back with the plaques (Figure 4.5 asterisks).

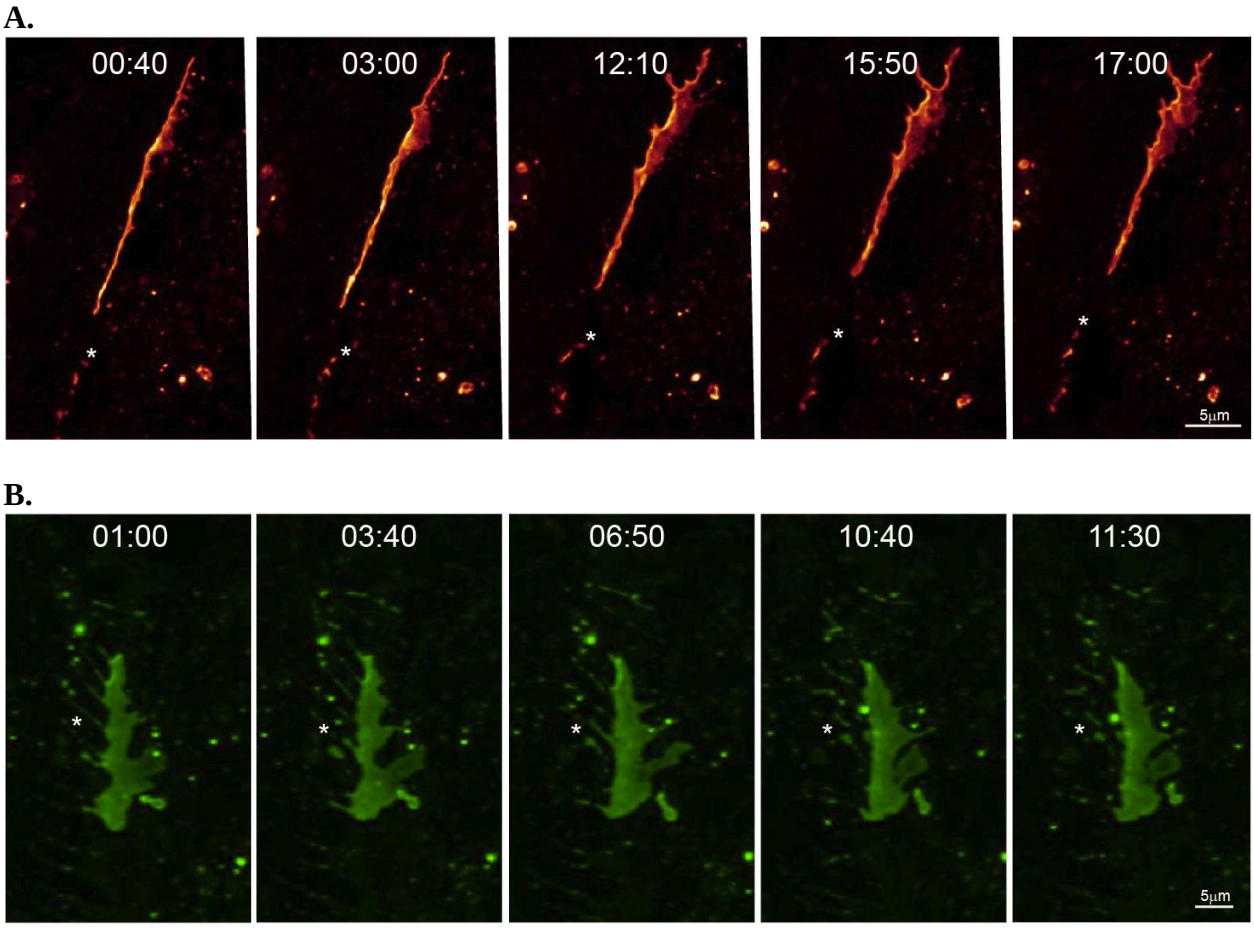

Figure 4.5. Live cell imaging with Bessel Beam Plane Illumination Microscope revealed filadendrites (asterisks) extending from the ends (A) and the edges (B) of the GJ plaques. The filadendrites changed shape rapidly, including breaking off from the plaque and fusing with each other or back to the plaque. Time stamps are in minutes and seconds. Both panel A and B showed OG labeling.

The presence of these filadendrites was confirmed by fixed cell imaging. We observed these finger-like structures extending from both the center and the edge of the GJ plaques (Figure 4.6).

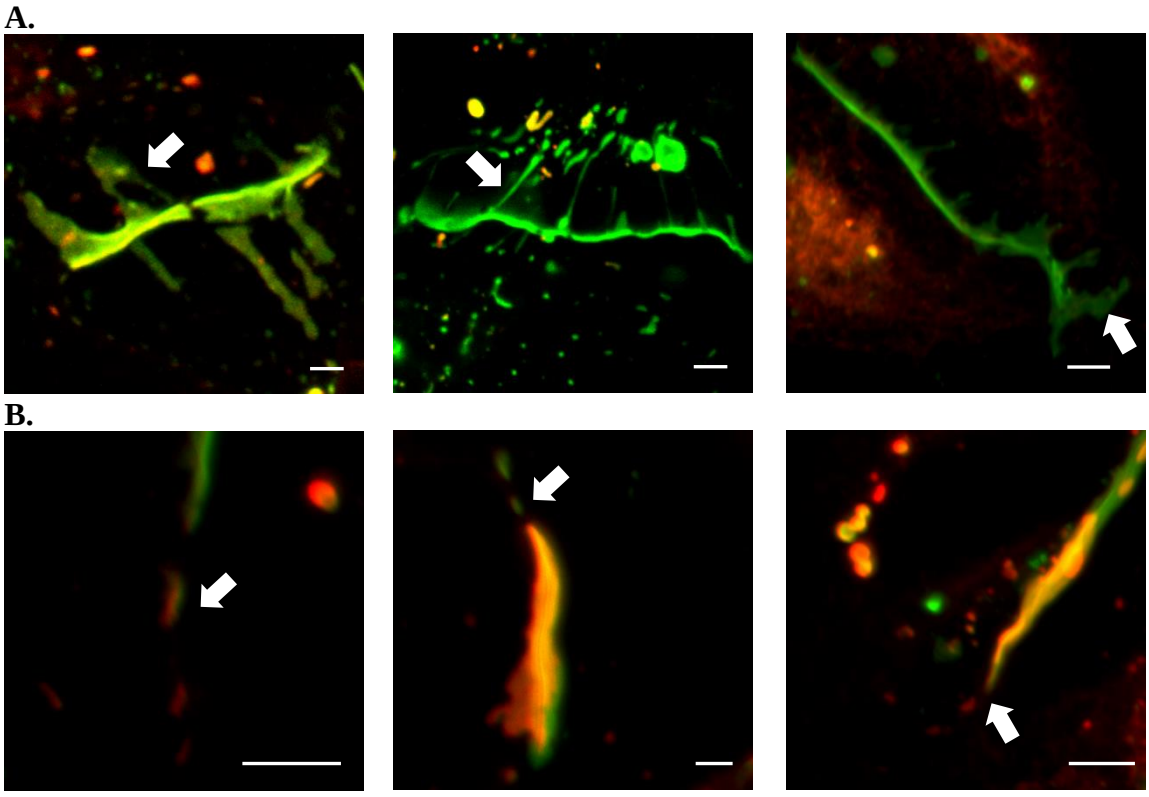

Figure 4.6. Fixed cell imaging confirmed the presence of both types of filadendrites (white arrows). The filadendrites extending out of the edges of GJ were mostly labeled with pulse (OG) ligand. Green showed Cx36-Halo pulse label (OG), and Red showed Cx36-Halo chase label (TMR). Scale bars represent 2µm.

The filadendrites were associated with actin filaments.

The observed filadendrites showed great mobility, and its fast dynamics determined the shape and arrangement of Cx36 GJ. This suggested that the presence of these filadendrites is important in GJ dynamics. To confirm the association of the filadendrites with the actin cytoskeleton, we doubled labeled Cx36-Halo-C-IN transfected HeLa cells with HaloTag TMR ligand and phalloidin 488, which labels the actin cytoskeleton. We observed perfect co-localization between Cx36 filadendrites and thin filaments of actin. The co-localization was not

limited to the filadendrites coming out of GJ plaques, but the thin GJ filaments connecting two adjacent cells where thick GJ plaque was not present as well (Figure 4.7 arrows).

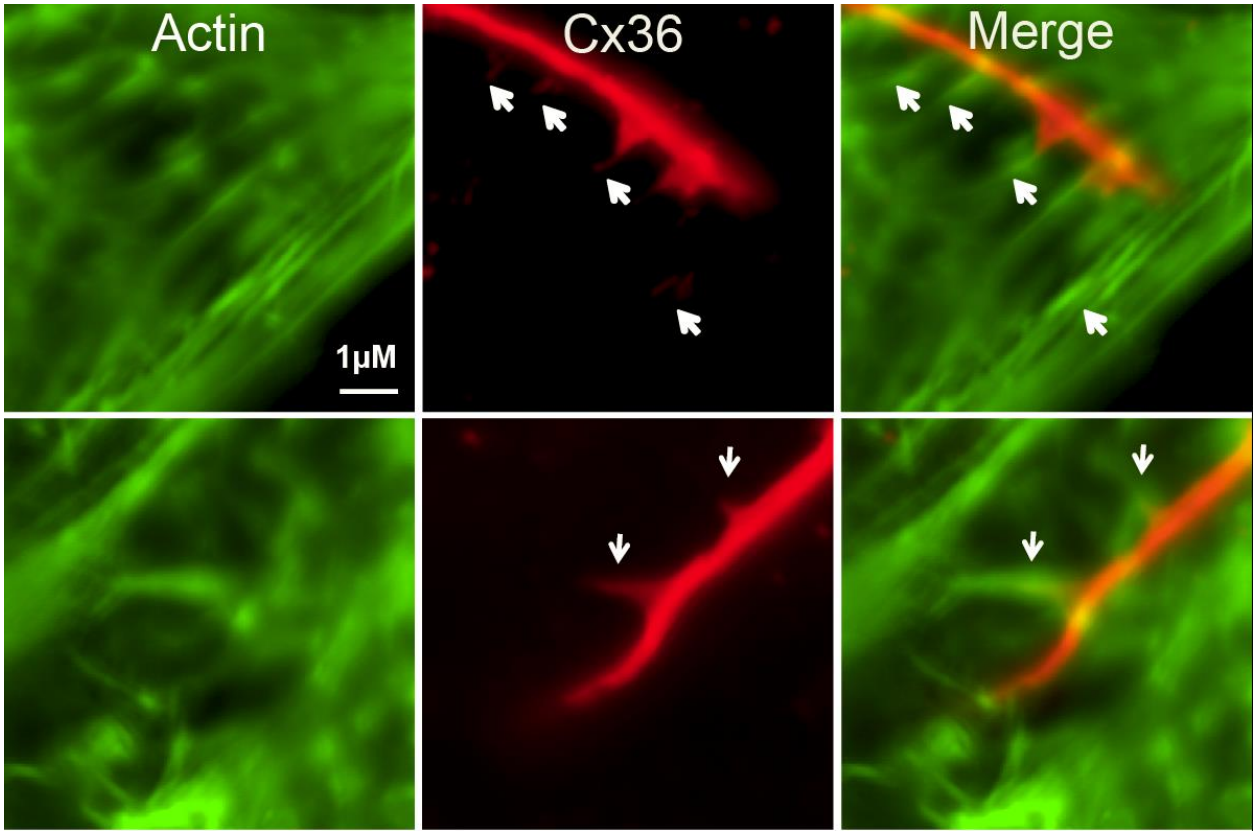

Figure 4.7: Double labeling of GJ (red-TMR) and actin (green-phalloidin) showed colocalization (white arrows), suggesting the filadendrites were associated with actin filaments.

Disrupting actin filaments compromised GJ integrity and eliminated the presence of filadendrites.

To further study the role of actin filaments in GJ assembly, we treated Cx36-Halo-C-IN transfected HeLa cells with two actin-disrupting drugs: Cytochalasin D and Latrunculin A. Cytochalasin D is a mycotoxin that binds to F-actin polymer and induces actin depolymerization (May et al., 1998; Wakatsuki et al., 2001). Latrunculin A is a marine toxin that forms 1:1

complexes with actin monomers in order to inhibit actin polymerization (Coue et al., 1987; Spector et al., 1989; Wakatsuki et al., 2001). Fixed cell imaging revealed that in the control (no drugs added) condition, actin bundles connected GJ plaques (Figure 4.8 left panel). Thin and long actin filaments ran parallel to the GJ plaques, and thin short actin filaments ran perpendicular to the plaques. Small insertion vesicles were always found associated with thin actin filaments. In Cytochalasin D treated cells, the actin cytoskeleton was completely disrupted and broken down (Figure 4.8 middle panel). We no longer saw thick actin bundles connecting two pieces of GJs in the same cell-to-cell contact. Thin actin filaments were difficult to find and there was no association between insertion vesicles and actin labels. In Latrunculin A treated cells, thin actin filaments were reduced but not broken down (Figure 4.8 right panel).

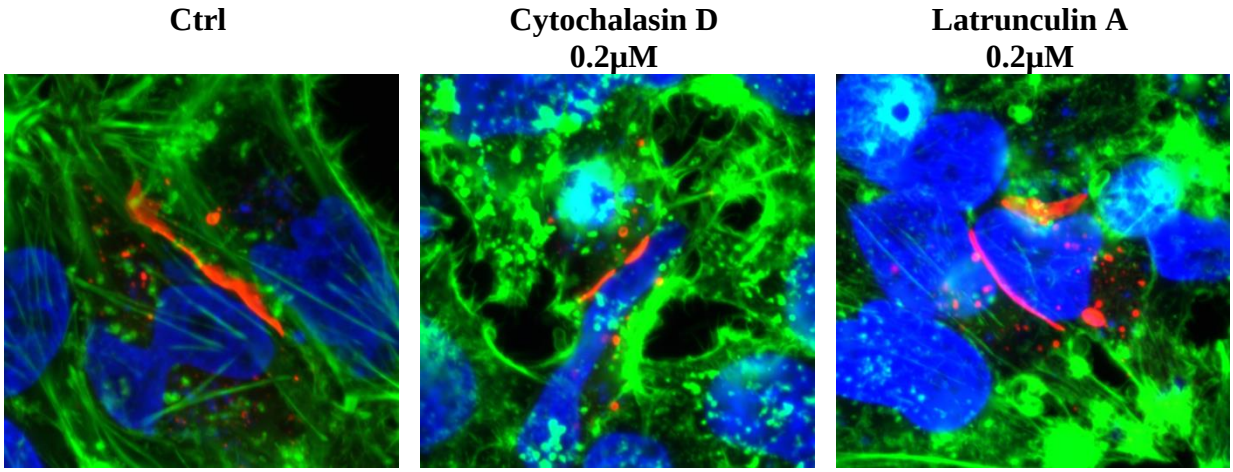

Figure 4.8. Effects of Cytochalasin D and Latrunculin A treatments on Cx36 GJs. Treatment of Cytochalasin D for 2 hrs prior to labeling disrupted actin filaments (green phalloidin) and broke down GJ (Red). Treatment of Latrunculin A reduced actin filaments, but did not break down GJ.

Fixed cell imaging of Cytochalasin D treatment revealed fragmented GJ plaques. To answer the question of whether actin filaments play an important role in supporting GJ structure, we measured the length (Figure 4.9A) and area (Figure 4.9B) of every GJ present on a cover

glass to obtain the median length and area. We compared the median length and area across the control, Cytochalasin D treated, and Latrunculin A treated cells in 6 cover glasses. Cytochalasin D, which disrupts actin filaments, significantly reduced the length and area of GJs present by breaking down existing GJs (Student t-test: length Cy-D, $p<0.01$; area Cy-D, $p<0.001$; n=6 cover slips per condition). Latrunculin A, which prevents elongation of new actin filaments but does not affect existing actin filaments, did not alter the length or area of GJ present (Length: Ctrl, 27.1±2.5μm, La-A, 22.2±2.0 μm; Area: Ctrl, 36.4±2.9 μm^2; La-A, 31.5±4.5 μm^2; n=6 cover slips per condition). This observation suggested that actin filaments are crucial in stabilizing the GJ plaques. GJ plaques can exists as long as actin filaments remain. When actin filaments depolymerize, GJ plaques break down.

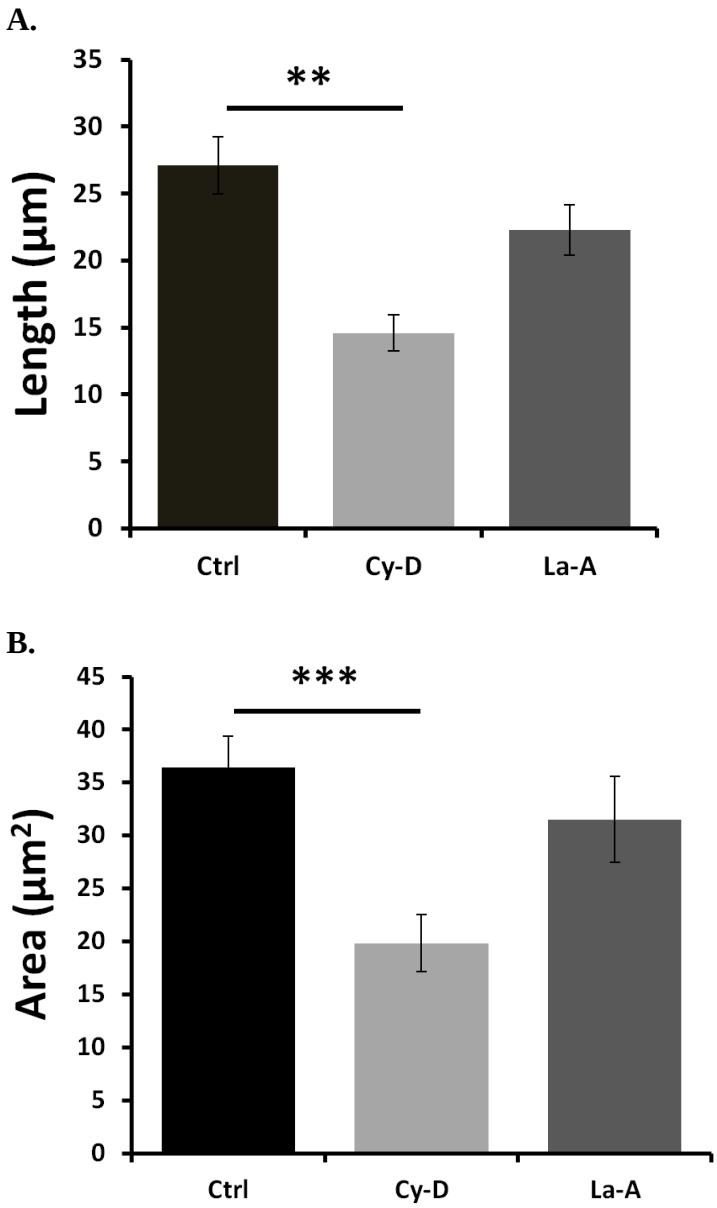

Figure 4.9: Length (A) and area (B) of GJ measured in control and drug treated Cx36-Halo-C-IN transfected HeLa cells. Medians of 7-38 GJ measured in each experiment were used for comparison. Ctrl – control; Cy-D – Cytochalasin D; La-A – Latrunculin A. ** $P<0.01$, *** $P<0.001$, n=6.

To confirm that the presence of actin filaments is essential for the existence of GJ plaques, we used tile analysis to calculate the fraction of HeLa cell pairs expressing Cx36-Halo that harbored GJs at cell-to-cell contact. Cytochalasin D significantly reduced the ratio of

neighboring cells expressing GJs (Student t-test: Cy-D, $p<0.05$; n=5 analyzed area per condition). Latrunculin A did not alter the ratio significantly (Figure 4.10) (Ctrl, 37.8±2.2%, La-A, 30.2±3.7%; n=5 analyzed area per condition). This shows that actin plays an important role in stabilizing GJ and breaking down existing actin filaments disrupted the integrity of GJ plaques.

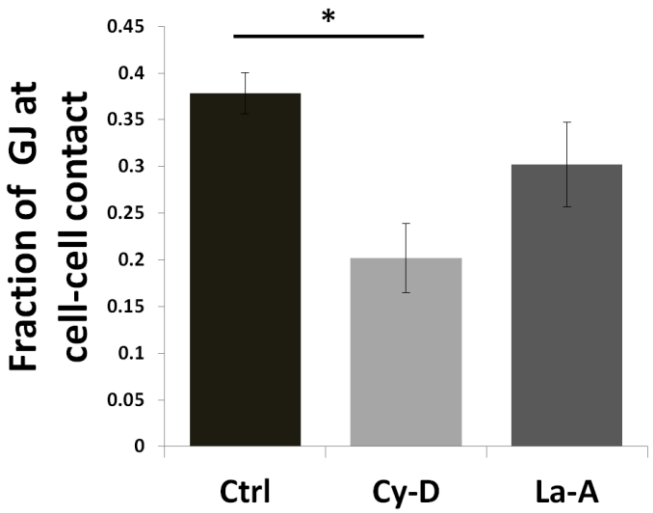

Figure 4.10: Fraction of HeLa cells pairs expressing Cx36-Halo that harbored a cell-cell GJ. Ctrl – control; Cy-D – Cytochalasin D; La-A – Latrunculin A. * $P<0.05$, n=5

Disrupting actin filaments eliminates the thin Cx36 filadendrites

Thin Cx36 filadendrites co-localize perfectly with actin filaments, revealing close association between the two. We studied the effects of actin filament disruption on the presence of filadendrites. Six cover slips of Cx36-Halo expressing HeLa cells were imaged for control, Cytochalasin D treated, or Latrunculin A treated conditions. Every GJ was imaged on either the whole cover glass or a designated area of the cover glass. We then calculated the fraction of GJ expressing thin Cx36 filadendrites. Interestingly, not only Cytochalasin D treated cells, but Latrunculin A treated cells showed a significant reduction in the presence of filadendrites

compared to the untreated cells (Student t-test: Cy-D, $p<0.001$, La-A, $p<0.001$; n=6 cover slips per condition). In the Cytochalasin D treated cells, the presence of the filadendrites was almost completely eliminated (Figure 4.11). These data indicate that the extension of the finger-like structure is not only dependent on the presence of actin filaments, but also the active elongation of actin filaments.

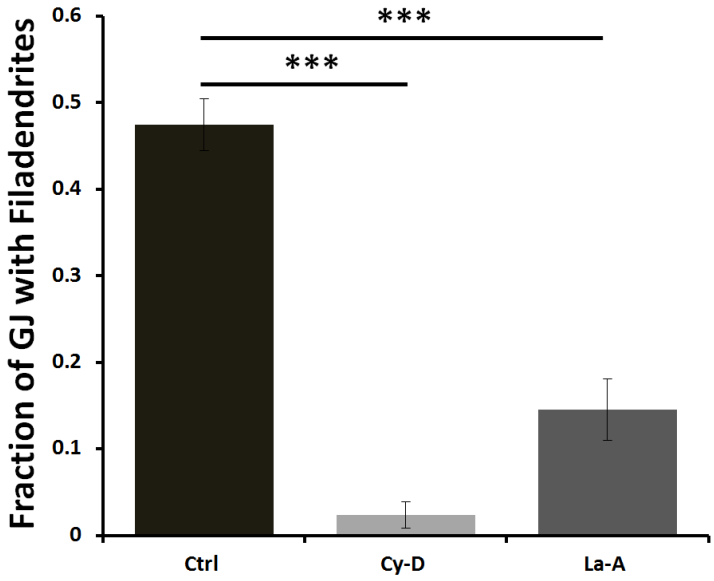

Figure 4.11: Fraction of GJ that had one or more filadendrites. Ctrl – control; Cy-D – Cytochalasin D; La-A – Latrunculin A. Data are means ± SEM, *** $P<0.001$, n=6.

Disruption of actin filaments does not significantly affect new GJ material insertion.

Double labels of Cx36-Halo transfected HeLa cells with HaloTag TMR ligand and phalloidin 488 revealed close association between small insertion vesicles and thin actin filaments. To study whether disrupting actin filament affects new GJ material insertion into the GJ plaques, we performed pulse-chase analysis with the presence of Latrunculin A because Latrunculin A treatment did not significantly affect the number and integrity of GJ plaques, but decreased the presence of thin Cx36 filadendrites. TMR chase label was added two hours after

OG pulse label. Percentage increase in TMR label was calculated by the difference in percentage of TMR label over total label between hour 2 and hour 0 divided by the percentage of TMR label over total label at hour 0. Treatment of Latrunculin A did not significantly decrease the percentage increase in TMR label (Figure 4.12) (Student t-test: Ctrl, 103±13.2%; La-A, 60.4±25.8%; n=4 experiment per condition, each experiment has 7-14 GJs). Pulse-chase analysis with treatment of Cytochalasin D was not performed because the total number of GJ plaques present was limited and the integrity was the GJ remaining was severely affected.

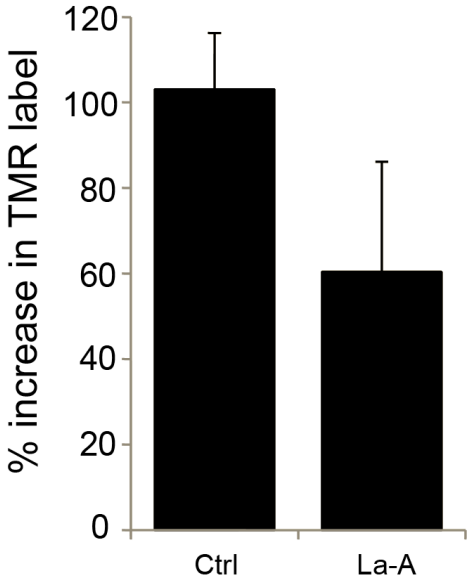

Figure 4.12. Percentage increase in TMR label from hour 0 to hour 2. Ctrl – control; La-A – Latrunculin A. Data are means ± SEM, n=4. Each experiment has 7-14 GJs.

Discussion

Golgi apparatus is involved in Cx36 trafficking to the GJ plaques

Previous studies have reported that connexons are incorporated into GJs as undocked hemichannels packaged in vesicles (Gaietta et al., 2002; Lauf et al., 2002) where the oligomerization occurs. Old GJ proteins are removed as paired channels that form double

membrane vesicles known as annular junctions (Laird, 1996; Gaietta et al., 2002; Lauf et al., 2002). The annular GJs subsequently are transported to lysosomes, where they are degraded (Laird, 1996; Piehl et al., 2007). In the BFA treated cells, newly synthesized Cx36 did not integrate into GJs. This suggests that the packaging and transportation of Cx36 involves the traditional ER-Golgi-TGN-plasma membrane pathway in order to form GJ plaques at cell-cell contact. However, the un-inserted newly synthesized Cx36 still formed large hollow vesicles that morphologically resembled annular junctions. These are unlikely to be the conventional annular junctions since the newly synthesized Cx36 never reached the plasma membrane and docked with hemichannels from the adjacent cells. Kumar and Gilula (Kumar and Gilula, 1992) showed that when connnexins are over-expressed, double-membraned GJ-like sheets form within the intracellular compartment. Many of the TMR labeled Cx36 annular junctions in our system are probably artifacts of over-expression of Cx36 in HeLa cells. These annular junctions are transported to lysosomes subsequently where the GJ proteins are degraded (Laird, 1996; Thomas et al., 2002).

Actin filaments are essential for GJ integrity

Studies have shown that actin filaments play an important role in the transport of vesicles from Golgi to plasma membrane (Hirschberg et al., 1998; Cao et al., 2005), as well as their removal to early and late endosome in association with microtubules (Apodaca, 2001; Brown and Song, 2001; Mundy et al., 2002). However, details of how actin filaments affect the integrity of Cx36 GJ plaques have never been revealed. In our studies, we used drug treatment (Latrunculin A and Cytochalasin D) to disrupt actin cytoskeleton and studied their effects on GJ plaques. We utilized the difference in mechanisms in which the two drugs affect actin cytoskeleton to

differentiate the effects caused by the presence of actin filaments or the elongation process of actin. Latrunculin A does not break down existing actin filaments, like Cytochalasin D, and only prevents the elongation of actin filaments by preventing polymerization of actin monomers (Coue et al., 1987; Spector et al., 1989; Wakatsuki et al., 2001). In our studies, we found that actin filaments can stabilize GJ plaques. Without the presence of actin cytoskeleton, the GJ plaques disintegrate into smaller and shorter pieces and eventually can no longer exist. We did find association and co-relation between actin filaments and Cx36 insertion vesicles. It is possible that the filadendrites extend from the GJ plaques to fuse with small insertion vesicles. Blocking actin filament elongation, which we found to reduce filadendrites (Figure 4.11), did not significantly reduce the ability for new GJ material to be inserted into the plaques.

More potential effects of actin filaments on Cx36 GJ assembly and functional regulation will be discussed in the next chapter.

Chapter Five:

Factors influencing Cx36 Plasticity

Part of the study in this chapter was published in my Dissertation of Master's Degree.

Introduction

GJ coupling is regulated by PKA activity

Cx36 GJ coupling is regulated by protein kinase A activity. In early scrape loading experiments using HeLa cells stably transfected with wild-type Cx36, treatment of PKA activator Sp-8-cpt-cAMPS (Sp) decreased Cx36 coupling, while treatment of PKA inhibitor Rp-8-cpt-cAMPS (Rp) increased coupling (Ouyang et al., 2005) (Figure 5.1A-D). Scrape loading experiments using transiently transfected HeLa cells (unpublished data from O'Brien lab) show similar results in the Rp treated condition, but failed to reduce coupling while treated with Sp, possibly due to activation of phosphatases by the transfection reagent (Figure 5.1E). In the transiently transfected HeLa cells, the control and Sp conditions gave a baseline coupling that was comparable to that in non-transfected HeLa cells. This baseline coupling of HeLa cells may be explained by a recent publication by Marandykina et al. Marandykina lab showed that Cx36 GJ coupling in HeLa transfectants can be inhibited by the presence of endogenous arachidonic acid, which stabilizes a closed conformation state of the channel that leads to low fraction of functional channels. Transfection reagent could be activating a phospholipase pathway, or lipids in the transfection reagent could be causing uncoupling directly (Marandykina et al., 2013). In tracer coupling experiments done in both non-transfected and empty vector transfected cells, there is still coupling observed when treated with PKA activator, probably due to the background coupling by other connexins.

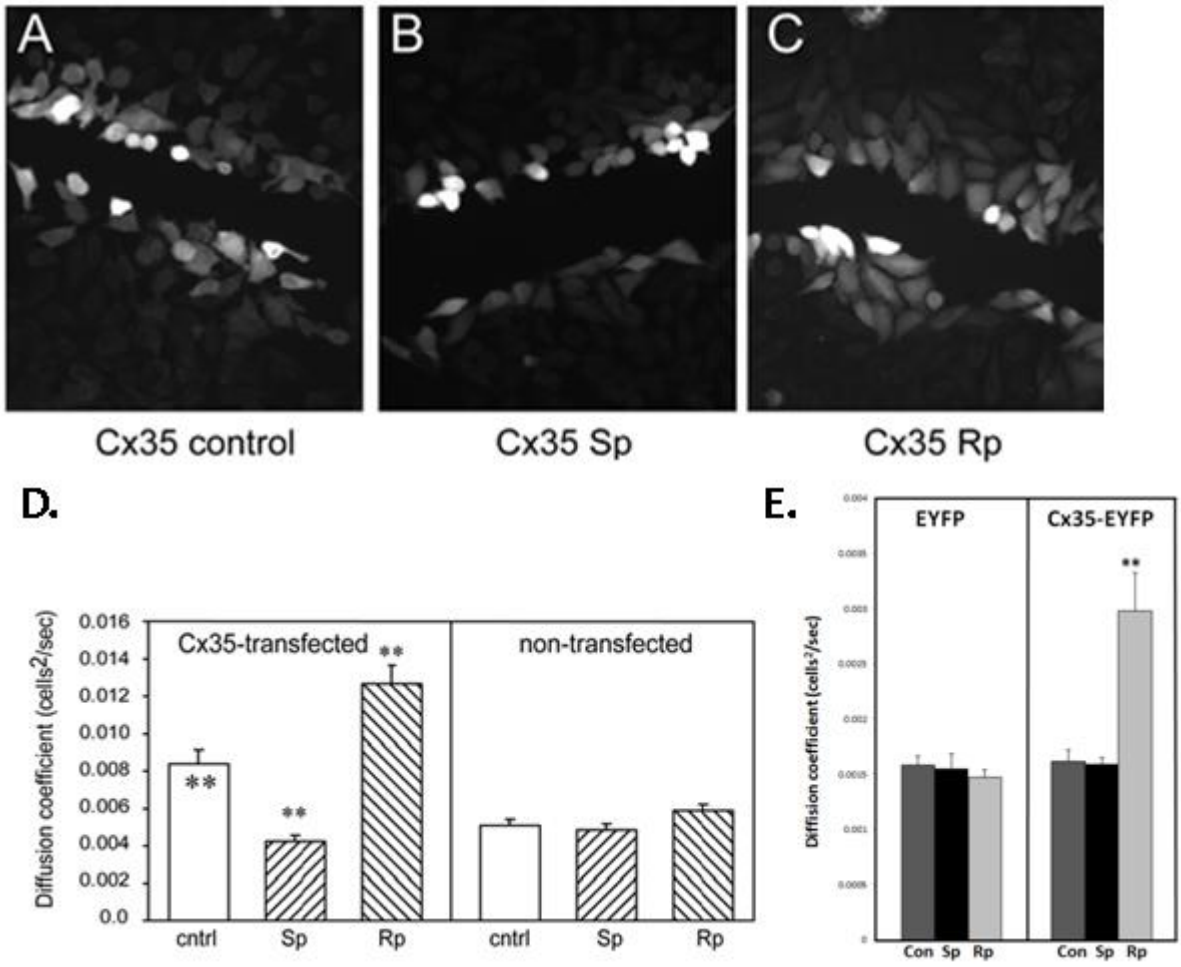

Figure 5.1: Effects of PKA activation and inhibition on tracer coupling in Cx35-HeLa cells measured by scrape-loading. (A-D) from Ouyang et al., 2005 (Originally published in Molecular Brain Research) (Images reproduced with permission from Elsevier). (E) Unpublished data from O'Brien Lab (performed by Cheryl M. Mitchell, analyzed and compiled by Helen Wang).

Cx36 is regulated by PKA at two major regulatory sites, Ser110 in the intracellular loop and Ser293 (S276 in Cx35) in the C-terminus (Figure 5.2A). Phosphorylation of these two sites is critical for the regulation of coupling mentioned in the figure above (Ouyang et al., 2005; Kothmann et al., 2007). The intracellular loop also harbors a calmodulin kinase binding site (Alev et al., 2008). Ser315, located towards the end of the C-terminus, has long been an important candidate in possibly assembling a protein complex that contributes to the

phosphorylation states of the regulatory sites (Figure 5.2B). Ser315 is phosphorylated by CamKII (Alev et al., 2008), and Ouyang et al. showed that mutation at Ser315 (S298 in Perch Cx35) inverts the coupling mechanism when measured by tracer coupling in HeLa cells (Ouyang et al., 2005).

A.

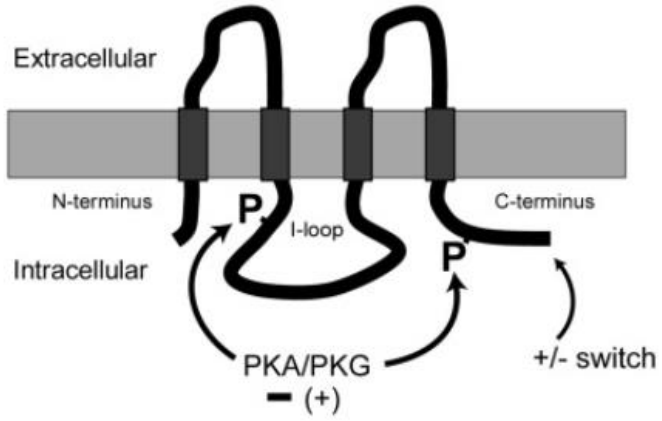

B.

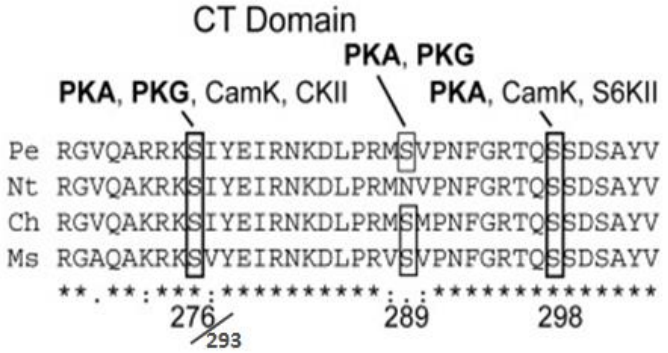

Figure 5.2. Important regulatory sites in Cx36. A) Ribbon structure of Cx36 showing phosphorylation sites Ser110 and Ser293. B) Cx36 C-terminus structure showing regulatory phosphorylation sites. From Kothmann et al., 2007 (Originally published in Visual Neuroscience) (Images reproduced with permission from Cambridge University Press).

Cx35/36 C-terminal mutations invert regulation

The C-terminus of Cx35 is essential for its interaction with scaffolding proteins. One study has shown that the interaction of the Cx35 C-terminus and PDZ domain containing protein zonula occludens-1 (ZO-1) could be important in the regulation of electrical synapses (Flores et al., 2008). Previous studies from O'Brien lab attempted to decipher the role of the Cx35 C-terminus in Cx35 coupling regulation by using Cx35 mutants. Results showed that a C-terminal truncation would completely invert the regulation pattern of Cx35 by PKA. Treatment of PKA activator Sp would increase coupling, and PKA inhibitor Rp would decrease coupling. It was hypothesized that Cx35 C-terminus is important in recruiting scaffolding proteins that bind regulatory phosphatases or kinases. Interestingly, mutation of one regulatory serine (S298) alone can result in the inverted regulation pattern as well. It is possible that the phosphorylation of S298 can cause conformation change in Cx36 C-terminus, making it more accessible to a scaffolding protein. However, by keeping S298 intact and truncating the very end of the C-terminus (PDZ domain interaction site) of Cx35 did not change the regulation pattern back to that from the wild-type, showing that both S298 and PDZ domain interaction are regulating Cx35/36 GJ coupling (Figure 5.3).

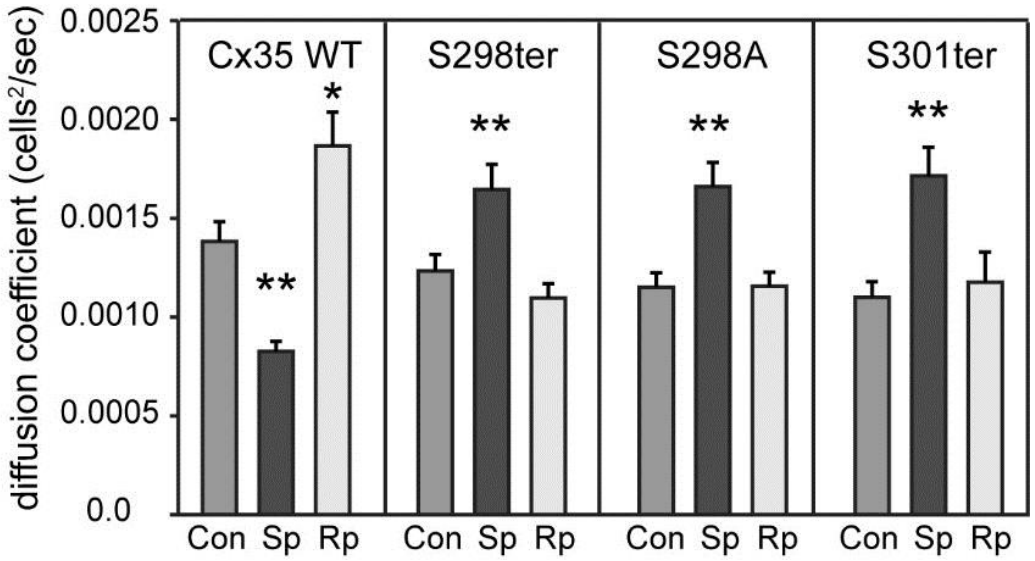

Figure 5.3. Tracer coupling measurements in HeLa cells stably transfected with Cx35 or mutants S298ter, S298A, and S301ter. Con – control; Sp – 20 μM Sp-8-cpt-cAMPS (PKA activator); Rp – 20 μM Rp-8-cpt-cAMPS (PKA inhibitor). Data are means + SEM, n = 25 to 35; * $P<0.05$, ** $P<0.01$ (unpublished data from O'Brien lab).

Nagy lab showed that a number of PDZ domain containing proteins, including ZO-1, ZO-2, ZO-3 and MUPP1, bind directly to the tip of the C-terminal of Cx36 (Li et al., 2004; Li et al., 2009b; Li et al., 2012). Phosphorylation of Ser315 and PDZ proteins interaction with the Cx36 C-terminal tip could both contribute to regulation of assembly of a protein complex, that disruption of Cx36 C-terminal could lead to inverted regulation and coupling (Ouyang et al., 2005).

Factors influencing turnover rate

Although our reported half-life of Cx36 in HeLa cells is consistent with the studies of other connexins in cell cultures and whole organs (Herve et al., 2007), as well as the electrophysiology data of Cx36 half-life in Mauthner cells reported by the Pereda group (Flores

et al., 2012), there are still considerable factors that may influence the measurement of half-lives. Turnover rate of plasma membrane proteins have been reported to be very different in different cell types. It is believed that the turnover rate of a certain protein can be cell type specific instead of protein specific. For example, Cx32 showed a half-life of 4-6 hours in rat hepatocytes (Traub and Wong, 1983), but only 2.5-3 hours in mouse embryo hepatocytes (Traub et al., 1987), suggesting that Cx32 GJs turn over faster in embryo cells. When turnover rate studies are carried out in primary cultures of cells, cells may contain intact GJs from their previous neighbors before cell division and isolation, and these GJs are removed and internalized at a very rapid rate (Herve et al., 2007). In these conditions, connexin turnover rate might be faster in cell cultures than intact tissues. However, pulse-chase analysis showed that Cx43 had similar half-life in metabolically labeled rat heart (Beardslee et al., 1998) and cultured myocytes (Laird et al., 1991; Darrow et al., 1995; Laing et al., 1998). In some cases, connexins in primary cell culture even showed a slower turnover rate, e.g. a reported half-life for Cx45 of 4.2 hours in HeLa cells (Hertlein et al., 1998) but only 2.9 hours in rat cardiac myocytes (Darrow et al., 1995).

The half-life of Cx36 is too long to contribute substantially to short-term changes in coupling of neurons driven by transmitters such as dopamine, which alters plasticity in minutes. In this study, we want to see whether changing the short term plasticity by altering PKA activity can influence long term plasticity in terms of turnover rate of Cx36. The dynamic movements of Cx36 filadendrites are too fast to directly influence long term plasticity like Cx36 half-life, but they could be associated with short term plasticity that is regulated by neurotransmitter. We also analyzed how the disruption of actin filaments affects Cx36 regulation by PKA.

We have found a few regulatory processes that might influence Cx36 plasticity. Short term plasticity, like GJ coupling, is regulated PKA. Cx36 CT plays an important role in PKA

regulated plasticity. Long term plasticity, like Cx36 turnover, is likely to be regulated by the insertion and removal of connexin vesicles and is influenced by a number of factors mentioned above. In this chapter, we want to determine out that whether the factors regulating Cx36 plasticity are inter-connected, i.e. whether changing Cx36 coupling affects connexin half-life. We also investigated further the role of Cx36 CT.

Methods and Material

Tracer coupling

Transfected HeLa cell cover glasses were maintained in oxygenated Ringer's medium at 35^{o}C. The medium was supplemented with 0.05% Neurobiotin and cells were scraped with a 25-gauge needle. Incubation with Neurobiotin was continued for 10 minutes to allow loading and diffusion. Cells were then washed twice with 0.1 M phosphate buffer to remove excess Neurobiotin and fixed with 4% paraformaldehyde (Electron Microscopy Sciences, Hatfield, PA) in 0.1 M phosphate buffer. When used, the PKA activator Rp or inhibitor Sp was added to the oxygenated incubation medium 10 minutes before the scrape for pre-incubation and replaced with fresh drug upon Neurobiotin addition. Drugs were present throughout the 10 minute tracer diffusion period. To analyze the effect of disrupting actin filaments on GJ coupling, transfected HeLa cells were incubated in oxygenated Ringer's medium containing Cytochalasin D (0.2µM) or Latrunculin A (0.2µM) at 35^{o}C for 45 minutes prior to PKA activator or inhibitor treatment. Cytochalasin D and Latrunculin A were present during the 10 minute incubation with Rp and Sp, as well as the 10 minute tracer diffusion period.

Following fixation, cells were probed with streptavidin-Cy3 (Jackson ImmunoResearch, West Grove, PA) and photographed on a Zeiss (Thornwood, NY) fluorescence microscope (Axiovert 200 with 40x, 0.5 NA Hoffman Modulation Contrast objective) with a Hamamatsu C4742-95 digital camera using HCImage software (Hamamatsu, Sewickley, PA). Five images were taken of different patches of loaded cells for each experiment and treated as replicates in the data analysis.

The diffusion coefficient of Neurobiotin through the coupled network of HeLa cells was determined from fluorescence intensity data using a compartmental diffusion model (Zimmerman and Rose, 1985). Fluorescence intensities of coupled cells were used to calculate diffusion coefficients based upon a linear 25-compartment diffusion model as described in Chapter Two.

Results

Blocking of Cx35 CT does not invert regulation

Truncation of Cx35 CT resulted in inverted regulation of Cx35 coupling by PKA. In order to see whether blocking the PDZ domain interaction site alone is sufficient to invert regulation, we created Cx35-EGFP fusion protein where EGFP was inserted at the very end of Cx35 C-terminus. In this construct, the C-terminus was unavailable for PDZ domain interaction, but did not invert Cx36 coupling regulation (Figure 5.4). A single mutation at S298A, however, inverted regulation as shown in figure 5.3.

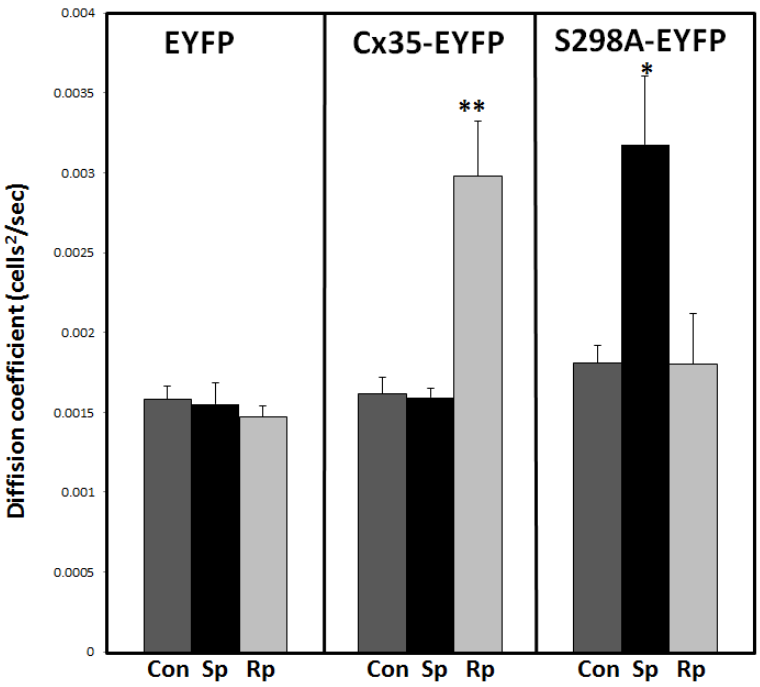

Figure 5.4. Tracer coupling measurements in HeLa cells transiently transfected with EYFP, Cx35-EYFP, and Cx35 S298A-EYFP. Con – control; Sp – 20 μM Sp-8-cpt-cAMPS (PKA activator); Rp – 20 μM Rp-8-cpt-cAMPS (PKA inhibitor). Data are means + SEM, n = 3; * $P<0.05$, ** $P<0.01$. (Performed by Cheryl M. Mitchell, analyzed and compiled by Helen Wang)

Interrupting actin filament elongation inverted regulation

Actin filaments associate with thin Cx36 filaments that constantly broke off and fused back with Cx36 GJ plaques at a rapid pace. The fast movement may contribute to the high level of short term plasticity. To study the effect of actin filament on Cx36 plasticity regulated by PKA activity, we performed scrape loading experiment with drugs that affect actin filaments. Cytochalasin D binds to F-actin polymers and causes loss of GJ at cell-cell contacts. Latrunculin A binds to actin monomers and prevents polymerization and filament elongation.

Disrupting actin filaments by Cytochalasin D and Latrunculin A both inverted Cx35 coupling regulation by PKA (Figure 5.5).

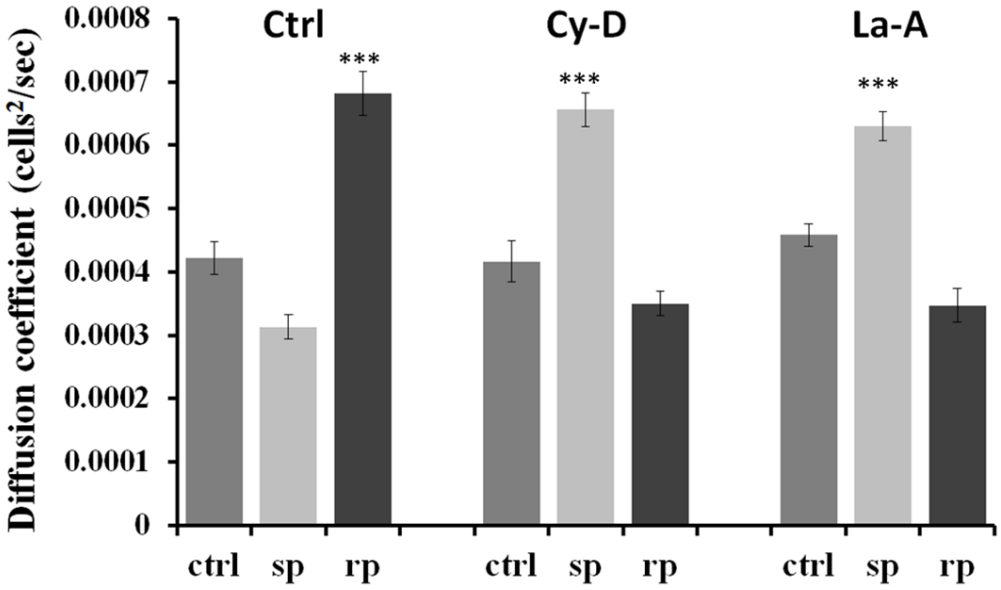

Figure 5.5. Tracer coupling measurements with drug treatments to interrupt actin filaments in HeLa cells transiently transfected with Cx36-Halo. Ctrl – control; Cy-D – 0.2μM Cytochalasin D; La-A – 0.2μM Latrunculin A; Sp – 5 μM Sp-8-cpt-cAMPS (PKA activator); Rp – 5 μM Rp-8-cpt-cAMPS (PKA inhibitor). Data are means + SEM, n = 3; *** P<0.001.

Half-life of Cx36 is not affected by its phosphorylation states

To determine whether the turnover rate of Cx36 was affected by PKA activity, we performed pulse-chase analyses in the presence of the PKA inhibitor Rp or the PKA activator Sp, which had significantly altered tracer coupling in 20 minutes. There were no significant differences in the half-life of Cx36 with either treatment (Figure 5.6), showing that the long term plasticity of Cx36 was not affected by changing in short term plasticity.

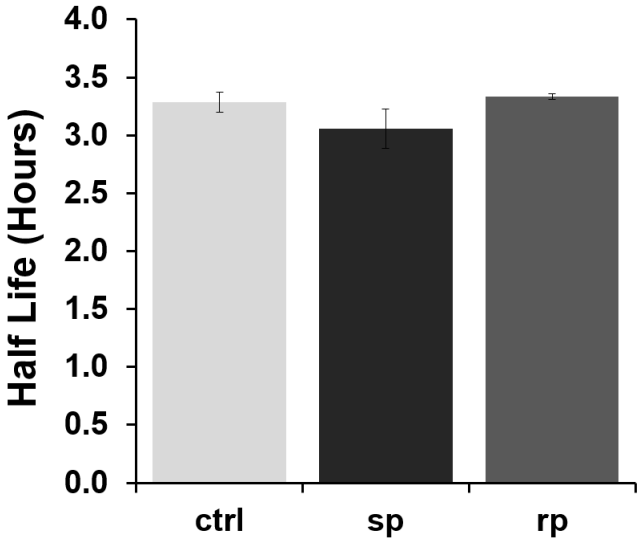

Figure 5.6: Half-lives of Cx36 GJ plaques were not altered by the treatment with 5 μM Sp-8-cpt-cAMPS or Rp-8-cpt-cAMPS throughout the chase period. N=3 experiments with 10-20 GJs per time point in each. Data are means ± SEM.

Discussion

Contribution of Cx36 turnover to electrical synaptic plasticity

Electrical synapses display a great deal of functional plasticity, being subject to alterations in coupling strength due to biophysical properties of the coupled cells, activity-dependent modification of the synapses, and modification driven by neurotransmitters (Pereda et al., 2013; O'Brien, 2014). The mechanisms responsible for these forms of plasticity are of great interest. In previous studies, profound dopamine-driven short-term plasticity of coupling in Cx36 GJs on AII amacrine cell dendrites in the rabbit retina was found to be directly correlated with phosphorylation of regulatory sites on Cx36, with no changes in number or size of the GJs (Kothmann et al., 2009). Similarly, Li et al. (Li et al., 2013) also showed a direct relation of dramatic changes in photoreceptor coupling during light or dark adaptation in the mouse retina to

Cx36 phosphorylation while the number of Cx36 plaques per unit area in the photoreceptor synaptic layer was not affected. However, Katti et al. (Katti et al., 2013) found that Cx36 protein level was regulated by diurnal and circadian rhythms in mouse retina. The level of Cx36 transcript peaked in the late night and immunolabeling showed higher Cx36 expression level in the night than in the day in the photoreceptor synaptic layer. This suggests that Cx36 GJs in the photoreceptor layer may contain more Cx36 protein at night than during the day, reflecting the fluctuation in Cx36 protein synthesis rate and potentially contributing to the elevated coupling at night.

In all electrical synapses, the continuous insertion and removal of connexons through turnover has the potential to alter electrical synaptic strength. In studies of goldfish Mauthner cell mixed synapses, Flores et al. (Flores et al., 2012) found that introduction of synthetic peptides that disrupt endocytosis or formation of SNARE complexes enhanced or reduced, respectively, electrical coupling. Glutamatergic transmission was altered in parallel as well. Peptides that mimicked the C-terminus of Cx36, interfering with Cx36 interactions with scaffolding proteins, also reduced electrical coupling. These experiments indicate that steady state maintenance of GJs through turnover is important for maintenance of electrical coupling. They further demonstrate that the C-terminus of Cx36 is important in stabilizing the GJs.

Our studies in HeLa cells indicate that turnover of Cx36 and functional plasticity driven by changes in connexin phosphorylation occur on different time scales. This is likely also to be the case in neurons, in which short-term changes in coupling of neurons driven by transmitters such as dopamine, which take minutes to achieve, do not appear to be accompanied by a change in Cx36 abundance. However, it is certainly reasonable to expect regulation of insertion and removal/degradation rates to contribute to changes in coupling strength in longer time frames

such as through a circadian cycle. Changes in Cx36 expression and neuronal coupling occur on an hours to weeks time scale during the course of central nervous system development and following a variety of types of injury. These changes are regulated by neurotransmitters and involve both transcriptional and post-transcriptional mechanisms (Belousov and Fontes, 2013). Factors that control turnover must be important in establishing the steady-state level of Cx36 expression, and it is apparent that these can be modified under certain circumstances.

Actin filaments could be the anchors for regulatory subunits that influence PKA activity and Cx36 GJ coupling.

Cx36 coupling is regulated by PKA activities. Treatment of PKA inhibitor Rp or the PKA activator Sp had significantly altered tracer coupling in 20 minutes, while changing the PKA activities does not alter the half-life of Cx36 in HeLa cells. Since the two regulatory processes occur on different time scales, mostly likely they are independent of each other. However, the fast pace of changes in Cx36 morphology, demonstrated by the fast recovery rate when photobleached (Chapter Two) and the fast movements of the finger-like filadendrites (Chapter Four) suggested that Cx36 trafficking could still play an important role in short term plasticity. By disrupting actin filaments, which associate closely with the filadendrites of Cx36 GJ plaques, we completely reversed how PKA activity regulates Cx36 coupling. The only time that we have observed this reversed regulation was when Cx36 C-terminus was truncated or a regulatory serine (S298) was mutated. Cx36 interacts with PDZ family proteins, which can act as scaffolds that recruit integral membrane, cytoskeletal, and signaling proteins to the vicinity of the plasma membrane (Flores et al., 2008). Given the similarity in regulation, it is possible that

actin filaments are anchors that provided a platform for Cx36 C-terminus and regulatory protein interaction. This possibility will be further discussion in Chapter Six.

Chapter Six:

Future Directions

Part of the study in this chapter was published in my Thesis of Master's Degree.

Part of this study was done using Perch Cx35. Cx35 and Cx36 are used interchangeably in this chapter.

Rationale and Hypothesis - Proteins associated with Cx35/36

Cx36 GJs play an important role in both photoreceptor and AII amacrine cells in the retina (Lee et al., 2003) (Kothmann et al., 2009) (O'Brien et al., 2012) (Li et al., 2013). The signaling mechanisms that control plasticity, however, are different in the two neural networks. While both mechanisms are regulated by cAMP and PKA activity, they yield precisely the opposite response to cAMP signaling. A major difference between the two networks is the presence of protein phosphatase 2A (PP2A) in the signaling pathway within AII amacrine cells. In AII amacrine cells, activation of D1 dopamine receptors activate adenylyl cyclase, which catalyzes the transformation of ATP to cyclic AMP. Cyclic AMP binds to and activates protein kinase A, which activates PP2A. PP2A dephosphorylates the regulatory serines (S110 and S276) on Cx36, and causes decreased coupling.

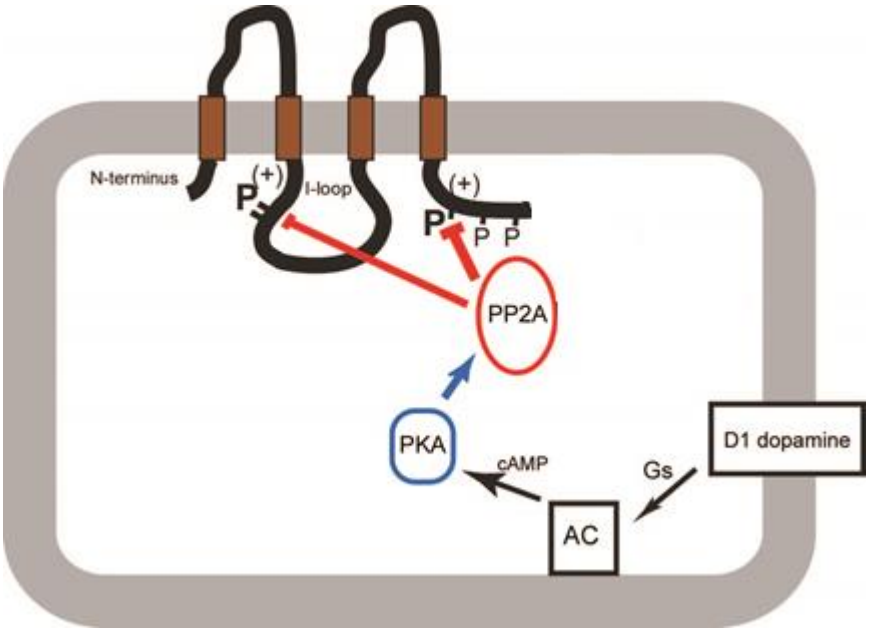

Figure 6.1. Model of regulations control Cx35/36 coupling by cAMP and PKA in AII amacrine cells (Adapted from unpublished illustration by John O'Brien, PhD).

The C-terminus of Cx35/36 is essential to protein interactions (Helbig et al., 2010). It has long been hypothesized that connexins interact with regulatory proteins through signaling complexes containing scaffolding proteins (Flores et al., 2008). To explore protein binding interactions that may be involved in the C-terminal interaction that regulates Cx35 coupling, we did a protein microarray study in collaboration with Mark Bedford (MD Anderson Cancer center). We used synthetic peptides corresponding to the C-terminus of Cx35 and probed an array of functional protein domains that are involved in "reading" protein phosphorylation events or binding to PDZ target sites. We identified several PDZ domains bound directly to the C-terminus of Cx36 (outlined in blue and highlighted in blue in the array list). These proteins include PDZ domains from NHERF2, Mupp1, PDZK1, and nNos, and the interactions ware reduced when S298 of Cx36, an important regulatory site near the end of C-terminus, was phosphorylated (Figure 6.2). Pull-down assays with lysates of bacteria expressing GST fusions with the PDZ-containing portions of these proteins showed that each binds the C-terminus of Cx36 (Figure 6.3). The reduction in protein-protein interaction when S298 was phosphorylated was confirmed in the pull-down assay as well (Figure 6.3).

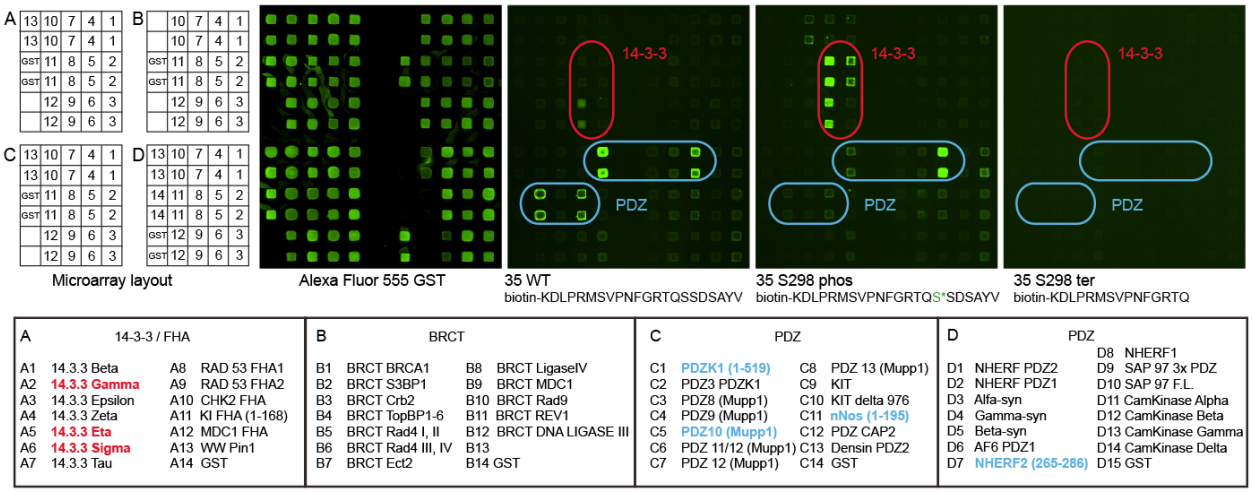

A	14-3-3 / FHA		
A1	14.3.3 Beta	A8	RAD 53 FHA1
A2	14.3.3 Gamma	A9	RAD 53 FHA2
A3	14.3.3 Epsilon	A10	CHK2 FHA
A4	14.3.3 Zeta	A11	KI FHA (1-168)
A5	14.3.3 Eta	A12	MDC1 FHA
A6	14.3.3 Sigma	A13	WW Pin1
A7	14.3.3 Tau	A14	GST

B	BRCT		
B1	BRCT BRCA1	B8	BRCT LigaseIV
B2	BRCT S3BP1	B9	BRCT MDC1
B3	BRCT Crb2	B10	BRCT Rad9
B4	BRCT TopBP1-6	B11	BRCT REV1
B5	BRCT Rad4 I, II	B12	BRCT DNA LIGASE III
B6	BRCT Rad4 III, IV	B13	
B7	BRCT Ect2	B14	GST

C	PDZ		
C1	PDZK1 (1-519)	C8	PDZ 13 (Mupp1)
C2	PDZ3 PDZK1	C9	KIT
C3	PDZ8 (Mupp1)	C10	KIT delta 976
C4	PDZ9 (Mupp1)	C11	nNos (1-195)
C5	PDZ10 (Mupp1)	C12	PDZ CAP2
C6	PDZ 11/12 (Mupp1)	C13	Densin PDZ2
C7	PDZ 12 (Mupp1)	C14	GST

D	PDZ		
		D8	NHERF1
D1	NHERF PDZ2	D9	SAP 97 3x PDZ
D2	NHERF PDZ1	D10	SAP 97 F.L.
D3	Alfa-syn	D11	CamKinase Alpha
D4	Gamma-syn	D12	CamKinase Beta
D5	Beta-syn	D13	CamKinase Gamma
D6	AF6 PDZ1	D14	CamKinase Delta
D7	NHERF2 (265-286)	D15	GST

Figure 6.2: Protein domain microarray probed with Cx35 C-terminal peptides. The array was probed with biotinylated peptides conjugated to Cy3-streptavidin; a control array was probed with an Alexa 555 anti-GST antibody. The peptide probe sequence is listed below each image; phospho-Ser298 is highlighted in green. Positive hits on the array are outlined, with 14-3-3's circled in red and PDZ's circled in blue. The positives are similarly color coded in the array list. (performed and compiled by Alexsandra Espejo and Dr. Mark Bedford from the Bedford Lab in MD Anderson Cancer Center, and Dr. John O'Brien)

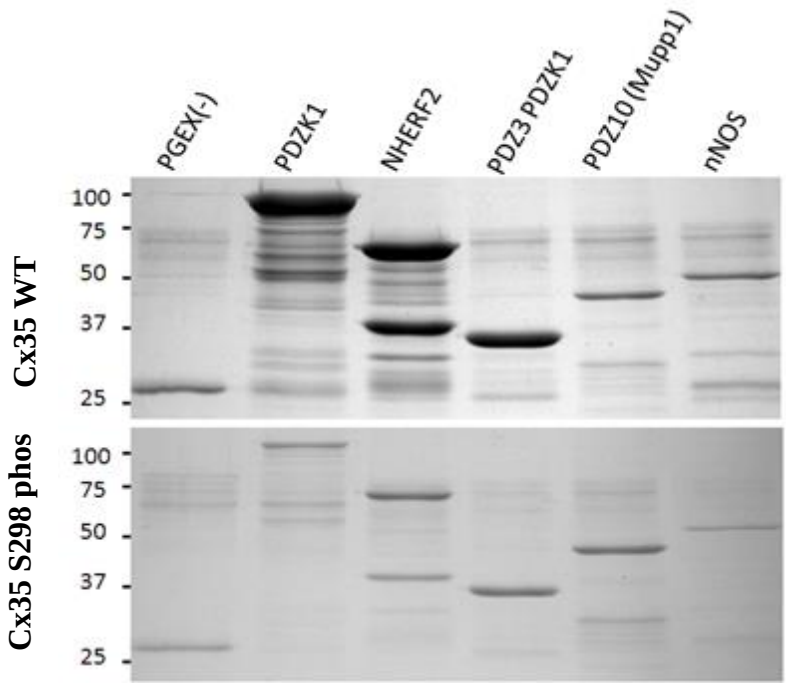

Figure 6.3. Pull-down assays using Cx35 CT peptides, both wild-type and Phospho-S298, against five PDZ proteins with positive hits from the protein microarray. Protein samples were detected with Coomassie Brilliant Blue stain.

NHERF2 and PDZK1 are important regulators of ion channels in chemical synapses (Paquet et al., 2006) (Magalhaes et al., 2012). Both proteins can bind to AKAPs (A-kinase anchoring proteins) and mediate cAMP and PKA regulated regulations of ion transport functions (Singh et al., 2009). We find both proteins expressed in the retina. NHERF2 is expressed in Muller glial cells with little overlap with Cx36, and PDZK1 is diffusely present in the inner plexiform layer (IPL). MUPP 1 has been found to co-localize with Cx36 and can potentially interact with Cx36 in the retina (Li et al., 2012). Neuronal NOS is a signaling protein with a single PDZ domain that anchors many different targets and impacts a wide range of activities including neurotransmission and neurotoxicity (Wang et al., 1999).

In addition to these PDZ proteins, we also studied the interaction between Cx36 and 14-3-3 proteins. Three isoforms of 14-3-3 proteins were found to bind (red outlines and highlighted

in red in the array list). Truncation of Cx36 C-terminus at S298 completely abolished these interactions. Phosphorylation of S298 increased the interaction between Cx36 CT and three isoforms of 14-3-3 proteins. Pull-down assays with lysates of bacteria expressing GST fusions with these 14-3-3 proteins showed that each binds the C-terminus of Cx36 (Figure 6.4) and the increase in protein-protein interaction when S298 was phosphorylated was confirmed in the pull-down assay as well (Figure 6.4).

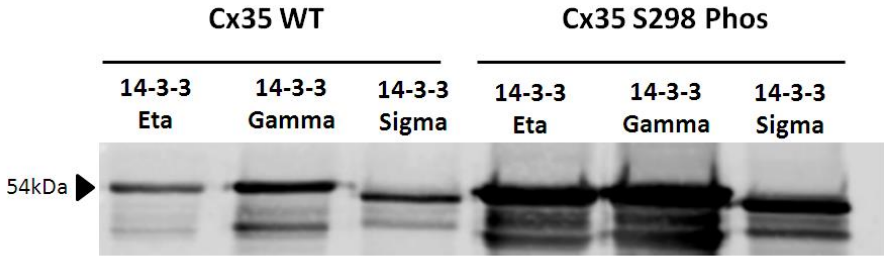

Figure 6.4. Pull-down assays using Cx35 CT peptides, both wild-type and Phospho-S298, against three purified GST-14-3-3 proteins with positive hits from the protein microarray. Protein samples were detected with western blot.

14-3-3 proteins are small phosphoserine/phosphothreonine binding proteins that bind to specific phosphorylated sites and have central roles in regulating hundreds of phosphorylation-dependent cellular processes (van Heusden, 2005). They can form dimers and often act as a bridge between two sides of the same molecules or connection between two different molecules (Gardino et al., 2006). There has not been much study done on the potential interaction between Cx36 and 14-3-3 proteins. Only one connexin is known to interact with 14-3-3 proteins and the functions of such interaction are unclear (Park et al., 2006; Park et al., 2007).

To study the role of PDZ proteins and 14-3-3 proteins in Cx36 GJ coupling, functional studies can be done using biochemical and cell biological methods. We can manipulate 14-3-3

protein expression level in HeLa cells transfected with Cx36. Expression of endogenous 14-3-3 proteins that are known to bind to Cx36 can be knocked down with siRNA. We can also overexpress the three 14-3-3 protein isoforms by transiently transfecting an expression plasmid into the Cx36 stably transfected cell line. Scrape loading experiments can be performed with the HeLa cells with knocked-down or overexpressed three 14-3-3 protein isoforms. If 14-3-3 proteins indeed play an important role in Cx36 GJ coupling, an overexpression should significantly increase Cx36 GJ coupling, and 14-3-3 protein knockdown should significantly decrease coupling. The same experiments can be performed with the identified PDZ proteins to study the effect of knocked-down or overexpressed PDZ proteins on Cx36 GJ coupling.

We can also use the Cx36-HaloTag construct we created to perform pull-down assay. Since HaloTags form an irreversible covalent bond with their ligand, we can utilize HaloTag magnetic resin to pull down proteins that interact with Cx36 CT. We have attempted the pull-down assay in past studies and it has presented some issues. The most obvious problem is the size of inserted HaloTag could affect Cx36 CT binding with interacting proteins and HaloTag ligand at the same time. We can try using different titrations of Cx36-HaloTag fusion protein and Cx36 WT protein to find a balance where the whole connexin can be pulled down by the subunit expressing Cx36-Halo, while the WT subunit can still pull-down 14-3-3 or PDZ proteins. Theoretically, the composition of Cx36 GJ should not discriminate Cx36-Halo from Cx36 WT in assembly.

Cx35/36 C-terminus is important in protein-protein interaction. These interactions may play an important role in Cx36 GJ plasticity. In Chapter Five, we showed that truncation of Cx36 C-terminus from S298, mutation of S298, and truncation of C-terminus from S301 can all invert the regulation pattern of Cx36 by PKA activity (Figure 5.3). 14-3-3 proteins interact with

phosphorylation sites, and S298 is a potential target for 14-3-3 proteins. It is possible that 14-3-3 proteins are responsible for anchoring the scaffolding proteins that recruit PP2A. Without the active phosphorylation site, PP2A cannot be recruited to dephosphorylate Cx35 at S110 and S276, and result in change in regulation pattern. Blocking the tip of the Cx36 CT by occupying it with EYFP does not invert such regulation (Figure 5.4). The tip of the Cx36 CT contains the PDZ binding domain, meaning if PDZ proteins play a role in regulation of Cx36 coupling, they are not enough to cause the inversion in regulation alone.

We have observed this inversion in regulation in Chapter Four, when actin filaments were disrupted. When Cx36-Halo transfected HeLa cells were treated with Cytochalasin D and Latrunculin A, Cx36 GJ coupling showed reversed pattern of regulation by PKA. It has been shown that Cx36CT interact with PDZ protein ZO-1, and ZO-1 was thought to link connexin GJ to actin cytoskeleton (Flores et al., 2008). It is possible that actin filaments dock the regulatory proteins including PP2A or PDZ proteins to the vicinity of plasma membrane, where GJs are located. When actin filaments are disrupted, PP2A are no longer close to the phosphorylation sites of Cx36 and are no longer available to dephosphorylate Cx36, causing the inversion of regulation. It has also been identified that Cx36 CT domain is involved in the assembly and trafficking to the electrical synapse (Helbig et al., 2010). We hypothesize that PDZ proteins, 14-3-3 proteins, and actin filaments all work in conjunction at Cx35/36 CT to regulate Cx36 coupling. Figure 6.5 shows a proposed model of Cx35/36 C-terminal assembly complex.

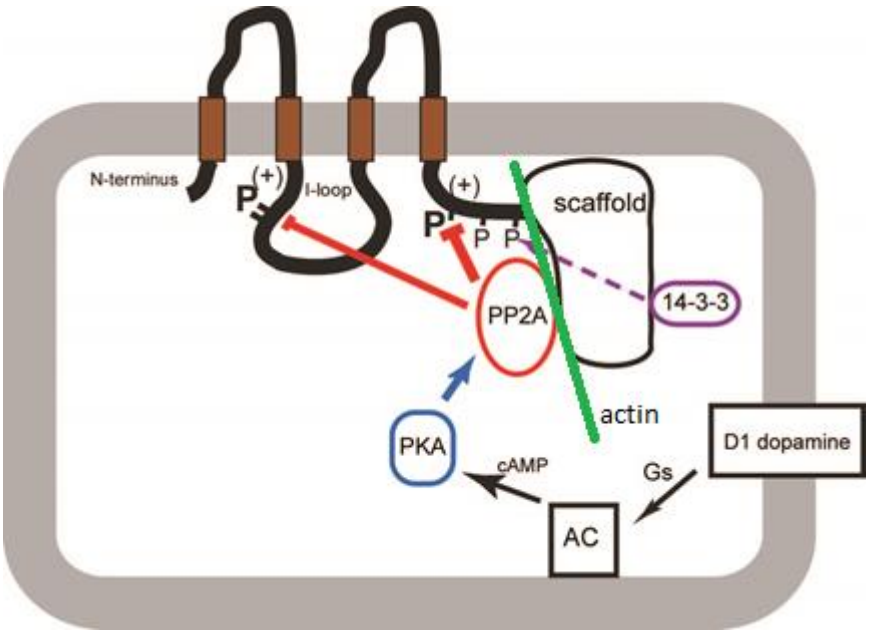

Figure 6.5. Proposed model of Cx35/36 C-terminal assembly complex that may control Cx35/36 coupling in AII amacrine cells. We propose that Cx35/36 C-terminus is important in binding to a scaffolding protein that assembles other regulatory proteins, including PP2A that regulate the phosphorylation and de-phosphorylation of Cx35/36. Evidence suggests that phosphorylation of S298 and 14-3-3 binding is important for this complex formation (Adapted from unpublished illustration by John O'Brien, PhD).

In order to study the involvement of actin filaments in Cx36 GJ plasticity, we need to confirm the interaction between actin filaments and Cx36 CT. We can transiently transfect HeLa cells with Cx36-S298-ter, and double label Cx36 with phalloidin. We hypothesize that actin filaments will lose their association with Cx36 without the presence of CT. We should no longer see actin bundles connecting edges of GJ plaques, or small insertion vesicles associated with thin actin filaments. We will also perform FRAP experiment with the presence Cytochalasin D, which binds to actin monomer and disrupt existing actin filaments. One theory is that Cx36 recovery is active and drives along the thin actin filaments, resulting in the fast mobility and recovery of Cx36. In this theory, disruption of actin filament should abolish the recovery of Cx36 we observed after photobleaching. However, it is also possible that the mobility of Cx36

within the plaques is passive and due to a pool of Cx36 that is not anchored by the actin filaments and scaffolding protein to hold them in place. In this theory, disrupting the actin filaments should result in higher mobility of Cx36. When we perform the FRAP experiments again with the presence of Cytochalasin D, mobile fraction would be significantly higher compared to untreated condition.

Methods and Material (results shown above)

Protein Microarray

Purified protein domain-GST fusion proteins were spotted on Whatman FAST slides. The microarray was probed with a biotinylated 22 amino acid wild-type C-terminal peptide and with the same sequence phosphorylated at Ser298 or truncated at Ser298. The biotinylated peptides were pre-conjugated to Cy3-streptavidin; a control array was probed with an Alexa 555 anti-GST antibody.

Pull-down assays

Wild-type and S298Phos C-terminal peptides attached to streptavidin magnetic beads were incubated with purified or crude GST-fusion proteins. Protein samples attached to the beads were resolved on polyacrylamide gels, and detected with Coomasie Brilliant Blue stain or western blot. For western blot, samples were transferred to nitrocellulose or PVDF membranes. Blots were probed with the antibody of choice. Fluorochrome-conjugated secondary antibodies

are applied at 1:5,000 dilution in TBST, and labeled bands are detected by fluorescence with a Typhoon multi-imager with 16-bit dynamic range.

Chapter Seven:

Summary, Discussion and Impacts

Information is passed down in the nervous system through synapses, both chemical synapses and electrical synapses. Both types of synapses have demonstrated a great range of plasticity. Factors influencing chemical synaptic plasticity have been studied extensively. Turnover rate of receptors and ion channels have been found to impact the plasticity of chemical synapses. Electrical synapses (GJ) however, have been a neglected counterpart, though they are present throughout our nervous system and play an important role in direct transfer of ions and small molecules. The O'Brien lab has devoted years to deciphering the contributors of Cx36 GJ plasticity. Cx36 is the most abundant neuronal GJ protein in the central nervous system, and has shown a great range of plasticity. Retina has been a great system to study Cx36 GJ coupling where Cx36 are responsible for the coupling between photoreceptors and AII amacrine cells. Past members of the O'Brien lab showed that phosphorylation states of Cx36 at regulatory serines are important in regulating Cx36 coupling. Changes in the phosphorylation state of Cx36 are regulated by PKA activity and it occurs on a relative short time scale in minutes. Recent studies have shown involvement of connexin turnover in regulating cell-cell communication and can potentially regulate electrical synaptic plasticity.

In my previous studies, we have created a new fusion protein, Cx36-HaloTag, to study the turnover rate of Cx36 in HeLa cells. HaloTag can form irreversible covalent bond with its ligand and allow the discrimination of new GJ material from the old one. By performing pulse-chase analysis, we calculated the half-life of Cx36 in HeLa cells to be 3.1 hours. This opened up a new type of plasticity on a much longer time scale. The turnover rate is too slow to take part in the plasticity regulated by phosphorylation of Cx36, which takes place in minutes, but it can still contribute to long-term plasticity.

To study the mechanism of Cx36 turnover, we focused on the Cx36 trafficking mechanism. In our pulse-chase labeling, we observed new GJ material diffused throughout the entire GJ plaques. This observation contradicted the well-established trafficking mechanism that has been reported for Cx43, where new Cx43 material accreted to the outside edges of existing GJ and mixed very little with existing GJ channel. These observations of Cx43 trafficking mechanism are what the common framework of understanding of connexin trafficking and turnover are based on. We performed two types of experiments to confirm whether these tagged connexins diffuse through GJ plaques. First, we created different fusion proteins of Cx36-HaloTag and Cx43-HaloTag with HaloTag inserted into both the internal portion and the very end of the CT tip, and transfected the different fusion protein into different cell lines, HeLa cells and HEK293 cells. Cx43-HaloTag constructs did not form GJs when transfected into HeLa cells but formed GJs efficiently in HEK293 cells. We performed pulse-chase analysis of turnover with each of the constructs and TMR chase label was present within the existing GJ plaques in each different construct respectively. The Cx43 chase label was patchy in intensity, suggesting less mixing of the recently made connexin proteins with connexins present in the plaque. As a second test of the ability of connexin proteins to diffuse laterally through GJ plaques, we performed live photobleaching studies of Cx36-Halo-C-IN in HeLa cells. The bleached areas in Cx36 GJ plaque were able to recover with a half-life of 1.5 seconds. The post-bleach steady state was below the original baseline, reflecting both bleaching of the total pool of OG-labeled Cx36 and a portion of the OG-labeled Cx36 pool that was effectively immobile within the time course of the experiment. These two experiments confirmed that Cx36 proteins were able to diffuse freely in a GJ plaque, and the diffusion occurs at a very fast pace.

Rapid recovery of photobleached connexins in GJ plaques has not been previously reported and it is going to be an uphill battle to change the public's view on the trafficking mechanism of connexins. We considered the three possible explanations for the observed recovery. First, the recovery could be the result of a temporary inactivation and fast reactivation of the fluorochrome. This possibility was eliminated by performing the aqueous droplet test as a negative control. Under the same experimental conditions, the Oregon Green working solution droplets did not recovery after photobleaching. Second possibility was that new GJ material replenished at a fast speed to replenish the bleached area. This possibility was unlikely given that the calculated half-life of Cx36 was 3.1 hours, and the half-life of the recovery was 1.5 seconds. These observations and results led us to believe that the third possibility, that GJ protein were free to diffuse within the plaques, was the reason behind the fast recovery we observed. We also noticed that when bleaching was done using confocal zoom greater than 6 with the 20x objective or a 40x objective, recovery was greatly reduced or completely eliminated. This led us to believe that the intensity of the bleaching laser can affect GJ's ability to recover and can potential explain the discrepancy between our observation and others that were reported in Cx43. In all the previously reported FRAP experiments done on Cx36, it is a common practice to confine the laser power to a thin band so the bleaching occurs in a very refined area with clear edge. It was also absolutely essential to bleach the fluorescent signal within the ROI. However, our results have shown that using higher zoom or high laser power might not be the proper way to approach this problem. Phototoxicity has been an issue that was overlooked or underestimated. Some studies have done live-cell imaging for long periods of time and have pointed out that the total amount of light intensity and the rate where light was being delivered can contribute to phototoxicity. Measures have been taken in many live-cell

imaging studies to reduce phototoxicity. However, in FRAP experiments, where photobleaching is an intended effect, it is hard to imagine that maximizing photobleaching would not cause a certain level of phototoxicity. Phototoxicity is the fast generation of ROS to the point where the cells cannot regenerate ROS scavengers and recover fast enough. It can cause downstream toxic effects that affect cellular function, and cause cell death. No studies on connexin mobility using FRAP as an analytical method have discussed the possibility that photobleaching may cause inactivation of mobility. In our study, we used low NA objective and low zoom to minimize the intensity of laser power. Using these conditions, the bleaching sweeps bleached more widely than the targeted band of interest, and it bleached only a fraction of the fluorochrome. In standard FRAP protocol, these conditions would be considered unacceptable. However, we were able to observe fast recovery of Cx36 into the bleached area which no one else was able to achieve in the past. Even under our bleaching condition that allowed recovery, we still found the mobile fraction of Cx36-Halo to decrease with each subsequent bleach in the ROI, showing that these gentle bleaching conditions are still impairing trafficking mechanism of Cx36, just to a lesser extent. In order to confirm that this recovery was not an artifact resulting from reversible bleaching of the OG fluorochrome by the bleaching sweeps, we photobleached aqueous droplets of the OG HaloTag ligand suspended in mineral oil using the same bleaching paradigm and observed no recovery in any of the laser power setting and confocal zoom setting that we tested. This confirmed that the rapid recovery of OG-labeled Cx36 in the bleached area was not an artifact, but a result of lateral diffusion.

When studying trafficking mechanism of Cx36 in live-cell imaging, we noticed thin-finger like filadendrites extending from both the center and the edges of the GJ plaques. The ones extended from the edges of the GJ plaques were reported before in Cx32-EGFP live

imaging. They were extensions of the plaques themselves and constantly broke off and fused back with the plaques. The thin finger-like filadendrites that extended from the center of the GJ plaques, however, were novel features. Our study showed that these filadendrites co-localized with fine actin filaments. Actin filaments have been proposed to be a major player in maintaining cell integrity and assisting vesicles trafficking. We found that thick actin bundles connected edges of all GJ plaques, and thin actin filaments associated with insertion vesicles. When actin filaments were disrupted by Cytochalasin D, GJ broke down and could no longer exist after two hours of treatment. When actin elongation was prohibited, the presence of the thin Cx36 filadendrites was greatly reduced as well. We do not know exactly how these thin connexin filadendrites play into the plasticity of Cx36 GJ, but the possibilities are endless. One possibility is that connexin filadendrites extend along actin filaments on the plasma membrane. They fetch insertion vesicles that reach the actin filament, fuse with the connexin filadendrites, and are added to the GJ plaques. However, when we disrupt actin elongation when performing pulse-chase analysis, we failed to see a significant reduction in the percentage increase in chase TMR label after two hours. This could be because of other mechanisms involved in new GJ material addition. There have been reports and speculations of different mechanisms how new connexons are added to the GJ plaques. Shaw et al. (Shaw et al., 2007) found that Cx43 cargo vesicles were targeted directly to adherens junctions adjacent to GJ plaques through microtubule plus-end tracking proteins. Lauf et al. (Lauf et al., 2002) and Gaietta et al. (Gaietta et al., 2002) found that Cx43 present as undocked hemichannels in the plasma membrane accreted to the outside edges of existing GJs and mixed very little with existing GJ channels. It is possible that connexons are added to the GJ plaques in different ways. As a result, inhibiting one mechanism would not yield a full inhibition of connexin addition. Another possibility is that the extension

of Cx36 filadendrites is a way for the GJ plaques to rearrange themselves. No new material was added to the GJ plaques from the breaking off and fusing back of the filadendrites. Instead, existing GJ material is shuffled from one part of the plaque to another. This theory would be consistent with the observation that all the thin connexin filadendrites were labeled with pulse OG label. GJ plaques are usually highly redundant. Each individual GJ plaque can contain thousands of channels and extend several micrometers in diameters. However, usually only less than 1% of all the GJ channels are active and open for conduction at the same time (Bukauskas and Verselis, 2004). The reason behind this high redundancy and the necessity for connexin to have a high turnover rate was unknown. It is possible that after old GJ material is removed as annular junction and removed into lysosomes, GJ plaques use the filadendrites as a rearranging mechanism to ensure the proper and even distribution of active GJ channels within a big GJ plaque. The connexin filadendrites are novel features that have never been documented or explored. Our observations can open new doors in the studying of Cx36 trafficking, turnover and plasticity.

There is so much to be studied about Cx36 and so little that we have already known. With all the pieces of the puzzle that we have obtained that are part of the big picture, electrical synaptic plasticity, we tried to investigate if they were inter-connected and influencing each other. We found that changing phosphorylation states of Cx36 by regulating PKA activity does not affect the half-life of Cx36 in HeLa cells, which means that short term plasticity of Cx36 does not lead to long term changes in Cx36 turnover. We also found that inhibiting actin polymerization inverted regulation of Cx36 coupling by PKA activity. This was a very exciting discovery for us. The only other situations when we observed such inversion in coupling regulation was when the CT of Cx36 was truncated, or when serine S298 in the CT was mutated.

We referred to the inversion as the "C-terminal switch". The fact that disrupting actin elongation caused the same switch told us that actin might associate specifically with the CT of Cx36 in regulating coupling. We have hypothesized that CT of Cx36 is important for the assembly of scaffolding proteins that harbors regulatory proteins like PP2A. It has been hypothesized that actin plays an indirect role in GJ assembly by working with cadherins, calcium dependent adhesion proteins (Takeichi, 1990; Johnson et al., 2002). It is reasonable to hypothesize that actin filaments can play an important role in anchoring the CT of Cx36 and recruiting Cx36 associated proteins to the vicinity of Cx36 CT and the plasma membrane. Potential targets for such regulatory proteins include PP2A, PDZ proteins and 14-3-3 proteins.

In conclusion, our study has created new fusion proteins with HaloTag and revealed dynamics and trafficking mechanisms of Cx36 that have never been reported before. We also found key players that contribute in Cx36 plasticity on several different time scales. There is still much to learn about electrical synaptic plasticity, and we are excited about the potentials this study has presented.

Bibliography

Ahmad S, Evans WH (2002) Post-translational integration and oligomerization of connexin 26 in plasma membranes and evidence of formation of membrane pores: implications for the assembly of gap junctions. The Biochemical journal 365:693-699.

Ahmad S, Diez JA, George CH, Evans WH (1999a) Synthesis and assembly of connexins in vitro into homomeric and heteromeric functional gap junction hemichannels. The Biochemical journal 339 (Pt 2):247-253.

Ahmad S, Diez JA, George CH, Evans WH (1999b) Synthesis and assembly of connexins in vitro into homomeric and heteromeric functional gap junction hemichannels. The Biochemical journal 339:247-253.

Alev C, Urschel S, Sonntag S, Zoidl G, Fort AG, Hoher T, Matsubara M, Willecke K, Spray DC, Dermietzel R (2008) The neuronal connexin36 interacts with and is phosphorylated by CaMKII in a way similar to CaMKII interaction with glutamate receptors. Proceedings of the National Academy of Sciences of the United States of America 105:20964-20969.

Allan VJ, Thompson HM, McNiven MA (2002) Motoring around the Golgi. Nature cell biology 4:E236-242.

Amino R, Thiberge S, Martin B, Celli S, Shorte S, Frischknecht F, Menard R (2006) Quantitative imaging of Plasmodium transmission from mosquito to mammal. Nature medicine 12:220-224.

Apodaca G (2001) Endocytic traffic in polarized epithelial cells: role of the actin and microtubule cytoskeleton. Traffic 2:149-159.

Arhel NJ, Souquere-Besse S, Charneau P (2006) Wild-type and central DNA flap defective HIV-1 lentiviral vector genomes: intracellular visualization at ultrastructural resolution levels. Retrovirology 3:38.

Beardslee MA, Laing JG, Beyer EC, Saffitz JE (1998) Rapid turnover of connexin43 in the adult rat heart. Circulation research 83:629-635.

Belluardo N, Mudo G, Trovato-Salinaro A, Le Gurun S, Charollais A, Serre-Beinier V, Amato G, Haefliger JA, Meda P, Condorelli DF (2000) Expression of connexin36 in the adult and developing rat brain. Brain research 865:121-138.

Belousov AB, Fontes JD (2013) Neuronal gap junctions: making and breaking connections during development and injury. Trends in neurosciences 36:227-236.

Berthoud VM, Bassnett S, Beyer EC (1999) Cultured chicken embryo lens cells resemble differentiating fiber cells in vivo and contain two kinetic pools of connexin56. Experimental eye research 68:475-484.

Blatow M, Rozov A, Katona I, Hormuzdi SG, Meyer AH, Whittington MA, Caputi A, Monyer H (2003) A novel network of multipolar bursting interneurons generates theta frequency oscillations in neocortex. Neuron 38:805-817.

Bloomfield SA, Volgyi B (2009) The diverse functional roles and regulation of neuronal gap junctions in the retina. Nat Rev Neurosci 10:495-506.

Breidert S, Jacob R, Ngezahayo A, Kolb HA, Naim HY (2005) Trafficking pathways of Cx49-GFP in living mammalian cells. Biological chemistry 386:155-160.

Brown BK, Song W (2001) The actin cytoskeleton is required for the trafficking of the B cell antigen receptor to the late endosomes. Traffic 2:414-427.

Bukauskas FF, Verselis VK (2004) Gap junction channel gating. Biochimica et biophysica acta 1662:42-60.

Bukauskas FF, Elfgang C, Willecke K, Weingart R (1995) Heterotypic gap junction channels (connexin26-connexin32) violate the paradigm of unitary conductance. Pflugers Archiv : European journal of physiology 429:870-872.

Cao H, Weller S, Orth JD, Chen J, Huang B, Chen JL, Stamnes M, McNiven MA (2005) Actin and Arf1-dependent recruitment of a cortactin-dynamin complex to the Golgi regulates post-Golgi transport. Nature cell biology 7:483-492.

Carisey A, Stroud M, Tsang R, Ballestrem C (2011) Fluorescence recovery after photobleaching. Methods in molecular biology 769:387-402.

Caviston JP, Holzbaur EL (2006) Microtubule motors at the intersection of trafficking and transport. Trends in cell biology 16:530-537.

Christie JM, Bark C, Hormuzdi SG, Helbig I, Monyer H, Westbrook GL (2005) Connexin36 mediates spike synchrony in olfactory bulb glomeruli. Neuron 46:761-772.

Conn PJ, Pin JP (1997) Pharmacology and functions of metabotropic glutamate receptors. Annual review of pharmacology and toxicology 37:205-237.

Connolly CN, Wafford KA (2004) The Cys-loop superfamily of ligand-gated ion channels: the impact of receptor structure on function. Biochemical Society transactions 32:529-534.

Coue M, Brenner SL, Spector I, Korn ED (1987) Inhibition of actin polymerization by latrunculin A. FEBS letters 213:316-318.

Darrow BJ, Laing JG, Lampe PD, Saffitz JE, Beyer EC (1995) Expression of multiple connexins in cultured neonatal rat ventricular myocytes. Circulation research 76:381-387.

De Vos WH, Hoebe RA, Joss GH, Haffmans W, Baatout S, Van Oostveldt P, Manders EM (2009) Controlled light exposure microscopy reveals dynamic telomere microterritories throughout the cell cycle. Cytometry Part A : the journal of the International Society for Analytical Cytology 75:428-439.

De Zeeuw CI, Chorev E, Devor A, Manor Y, Van Der Giessen RS, De Jeu MT, Hoogenraad CC, Bijman J, Ruigrok TJ, French P, Jaarsma D, Kistler WM, Meier C, Petrasch-Parwez E, Dermietzel R, Sohl G, Gueldenagel M, Willecke K, Yarom Y (2003) Deformation of network connectivity in the inferior olive of connexin 36-deficient mice is compensated by morphological and electrophysiological changes at the single neuron level. The Journal of neuroscience : the official journal of the Society for Neuroscience 23:4700-4711.

Deans MR, Gibson JR, Sellitto C, Connors BW, Paul DL (2001) Synchronous activity of inhibitory networks in neocortex requires electrical synapses containing connexin36. Neuron 31:477-485.

Deans MR, Volgyi B, Goodenough DA, Bloomfield SA, Paul DL (2002) Connexin36 is essential for transmission of rod-mediated visual signals in the mammalian retina. Neuron 36:703-712.

Diaspro A, Testa I, Faretta M, Magrassi R, Barozzi S, Parazzoli D, Vicidomini G (2006) 3D localized photoactivation of pa-GFP in living cells using two-photon interactions. Conference proceedings : Annual International Conference of the IEEE Engineering in Medicine and Biology Society IEEE Engineering in Medicine and Biology Society Annual Conference 1:389-391.

Diestel S, Eckert R, Hulser D, Traub O (2004) Exchange of serine residues 263 and 266 reduces the function of mouse gap junction protein connexin31 and exhibits a dominant-negative effect on the wild-type protein in HeLa cells. Experimental cell research 294:446-457.

Dixit R, Cyr R (2003) Cell damage and reactive oxygen species production induced by fluorescence microscopy: effect on mitosis and guidelines for non-invasive fluorescence microscopy. The Plant journal : for cell and molecular biology 36:280-290.

Egea G, Lazaro-Dieguez F, Vilella M (2006) Actin dynamics at the Golgi complex in mammalian cells. Current opinion in cell biology 18:168-178.

Encell LP et al. (2012) Development of a dehalogenase-based protein fusion tag capable of rapid, selective and covalent attachment to customizable ligands. Current chemical genomics 6:55-71.

Enninga J, Mounier J, Sansonetti P, Tran Van Nhieu G (2005) Secretion of type III effectors into host cells in real time. Nature methods 2:959-965.

Evans WH, Ahmad S, Diez J, George CH, Kendall JM, Martin PE (1999) Trafficking pathways leading to the formation of gap junctions. Novartis Foundation symposium 219:44-54; discussion 54-49.

Falk MM, Gilula NB (1998) Connexin membrane protein biosynthesis is influenced by polypeptide positioning within the translocon and signal peptidase access. The Journal of biological chemistry 273:7856-7864.

Falk MM, Kumar NM, Gilula NB (1994) Membrane insertion of gap junction connexins: polytopic channel forming membrane proteins. The Journal of cell biology 127:343-355.

Falk MM, Buehler LK, Kumar NM, Gilula NB (1997) Cell-free synthesis and assembly of connexins into functional gap junction membrane channels. The EMBO journal 16:2703-2716.

Falk MM, Baker SM, Gumpert AM, Segretain D, Buckheit RW, 3rd (2009) Gap junction turnover is achieved by the internalization of small endocytic double-membrane vesicles. Mol Biol Cell 20:3342-3352.

Fallon RF, Goodenough DA (1981) Five-hour half-life of mouse liver gap-junction protein. The Journal of cell biology 90:521-526.

Feldman PA, Kim J, Laird DW (1997) Loss of gap junction plaques and inhibition of intercellular communication in ilimaquinone-treated BICR-M1Rk and NRK cells. The Journal of membrane biology 155:275-287.

Fernandes R, Girao H, Pereira P (2004) High glucose down-regulates intercellular communication in retinal endothelial cells by enhancing degradation of connexin 43 by a proteasome-dependent mechanism. The Journal of biological chemistry 279:27219-27224.

Flores CE, Li X, Bennett MV, Nagy JI, Pereda AE (2008) Interaction between connexin35 and zonula occludens-1 and its potential role in the regulation of electrical synapses. Proceedings of the National Academy of Sciences of the United States of America 105:12545-12550.

Flores CE, Nannapaneni S, Davidson KG, Yasumura T, Bennett MV, Rash JE, Pereda AE (2012) Trafficking of gap junction channels at a vertebrate electrical synapse in vivo. Proceedings of the National Academy of Sciences of the United States of America 109:E573-582.

Furshpan EJ, Potter DD (1959) Transmission at the giant motor synapses of the crayfish. The Journal of physiology 145:289-325.

G. Los RL, Natasha Karassina, Chad Zimprich, Mark G. McDougall, Lance P. Encell, Rachel Friedman-Ohana, Monika Wood, Gediminas Vidugiris, Kris Zimmerman, Paul Otto, Soshana Berstock, Dieter Klaubert,and Ketih V. Wood (2006) HaloTag® Technology: Cell Imaging and Protein Analysis. Cell Notes 14:10-14.

Gaietta G, Deerinck TJ, Adams SR, Bouwer J, Tour O, Laird DW, Sosinsky GE, Tsien RY, Ellisman MH (2002) Multicolor and electron microscopic imaging of connexin trafficking. Science 296:503-507.

Gao L, Shao L, Chen BC, Betzig E (2014) 3D live fluorescence imaging of cellular dynamics using Bessel beam plane illumination microscopy. Nature protocols 9:1083-1101.

Gardino AK, Smerdon SJ, Yaffe MB (2006) Structural determinants of 14-3-3 binding specificities and regulation of subcellular localization of 14-3-3-ligand complexes: a comparison of the X-ray crystal structures of all human 14-3-3 isoforms. Semin Cancer Biol 16:173-182.

George CH, Martin PE, Evans WH (1998) Rapid determination of gap junction formation using HeLa cells microinjected with cDNAs encoding wild-type and chimeric connexins. Biochemical and biophysical research communications 247:785-789.

George CH, Kendall JM, Evans WH (1999) Intracellular trafficking pathways in the assembly of connexins into gap junctions. The Journal of biological chemistry 274:8678-8685.

Georgyi V. Los AD, Natasha Karassina, Chad Zimprich, Randall Learish, Mark G. McDougall, Lance P. Encell, Rachel Friedman-Ohana, Monika Wood, Gediminas Vidugiris, Kris Zimmerman, Paul Otto, Dieter H. Klaubert, and Keith V. Wood (2005) HaloTag®

Interchangeable Labeling Technology for Cell Imaging and Protein Capture. Cell Notes 11:2-6.

He LQ, Cai F, Liu Y, Liu MJ, Tan ZP, Pan Q, Fang FY, Liang de S, Wu LQ, Long ZG, Dai HP, Xia K, Xia JH, Zhang ZH (2005) Cx31 is assembled and trafficked to cell surface by ER-Golgi pathway and degraded by proteasomal or lysosomal pathways. Cell research 15:455-464.

Helbig I, Sammler E, Eliava M, Bolshakov AP, Rozov A, Bruzzone R, Monyer H, Hormuzdi SG (2010) In vivo evidence for the involvement of the carboxy terminal domain in assembling connexin 36 at the electrical synapse. Molecular and cellular neurosciences 45:47-58.

Hertlein B, Butterweck A, Haubrich S, Willecke K, Traub O (1998) Phosphorylated carboxy terminal serine residues stabilize the mouse gap junction protein connexin45 against degradation. The Journal of membrane biology 162:247-257.

Hertzberg EL, Saez JC, Corpina RA, Roy C, Kessler JA (2000) Use of antibodies in the analysis of connexin 43 turnover and phosphorylation. Methods 20:129-139.

Herve JC, Derangeon M, Bahbouhi B, Mesnil M, Sarrouilhe D (2007) The connexin turnover, an important modulating factor of the level of cell-to-cell junctional communication: comparison with other integral membrane proteins. The Journal of membrane biology 217:21-33.

Hirschberg K, Miller CM, Ellenberg J, Presley JF, Siggia ED, Phair RD, Lippincott-Schwartz J (1998) Kinetic analysis of secretory protein traffic and characterization of golgi to plasma membrane transport intermediates in living cells. The Journal of cell biology 143:1485-1503.

Hoebe RA, Van Oven CH, Gadella TW, Jr., Dhonukshe PB, Van Noorden CJ, Manders EM (2007) Controlled light-exposure microscopy reduces photobleaching and phototoxicity in fluorescence live-cell imaging. Nature biotechnology 25:249-253.

Hormuzdi SG, Pais I, LeBeau FE, Towers SK, Rozov A, Buhl EH, Whittington MA, Monyer H (2001) Impaired electrical signaling disrupts gamma frequency oscillations in connexin 36-deficient mice. Neuron 31:487-495.

Hunter AW, Barker RJ, Zhu C, Gourdie RG (2005) Zonula occludens-1 alters connexin43 gap junction size and organization by influencing channel accretion. Molecular biology of the cell 16:5686-5698.

Ito S, Sato E, Loewenstein WR (1974) Studies on the formation of a permeable cell membrane junction. I. Coupling under various conditions of membrane contact. Effects of colchicine, cytochalasin B, dinitrophenol. The Journal of membrane biology 19:305-337.

Johnson RG, Meyer RA, Li XR, Preus DM, Tan L, Grunenwald H, Paulson AF, Laird DW, Sheridan JD (2002) Gap junctions assemble in the presence of cytoskeletal inhibitors, but enhanced assembly requires microtubules. Experimental cell research 275:67-80.

Katti C, Butler R, Sekaran S (2013) Diurnal and circadian regulation of connexin 36 transcript and protein in the Mammalian retina. Investigative ophthalmology & visual science 54:821-829.

Kidder GM, Rains J, McKeon J (1987) Gap junction assembly in the preimplantation mouse conceptus is independent of microtubules, microfilaments, cell flattening, and cytokinesis. Proceedings of the National Academy of Sciences of the United States of America 84:3718-3722.

Kothmann WW, Massey SC, O'Brien J (2009) Dopamine-stimulated dephosphorylation of connexin 36 mediates AII amacrine cell uncoupling. The Journal of neuroscience : the official journal of the Society for Neuroscience 29:14903-14911.

Kothmann WW, Li X, Burr GS, O'Brien J (2007) Connexin 35/36 is phosphorylated at regulatory sites in the retina. Visual neuroscience 24:363-375.

Koval M, Harley JE, Hick E, Steinberg TH (1997) Connexin46 is retained as monomers in a trans-Golgi compartment of osteoblastic cells. J Cell Biol 137:847-857.

Kumar NM, Gilula NB (1992) Molecular biology and genetics of gap junction channels. Seminars in cell biology 3:3-16.

Laing JG, Beyer EC (1995) The gap junction protein connexin43 is degraded via the ubiquitin proteasome pathway. The Journal of biological chemistry 270:26399-26403.

Laing JG, Tadros PN, Westphale EM, Beyer EC (1997) Degradation of connexin43 gap junctions involves both the proteasome and the lysosome. Experimental cell research 236:482-492.

Laing JG, Tadros PN, Green K, Saffitz JE, Beyer EC (1998) Proteolysis of connexin43-containing gap junctions in normal and heat-stressed cardiac myocytes. Cardiovascular research 38:711-718.

Laird DW (1996) The life cycle of a connexin: gap junction formation, removal, and degradation. Journal of bioenergetics and biomembranes 28:311-318.

Laird DW, Puranam KL, Revel JP (1991) Turnover and phosphorylation dynamics of connexin43 gap junction protein in cultured cardiac myocytes. The Biochemical journal 273(Pt 1):67-72.

Laird DW, Castillo M, Kasprzak L (1995) Gap junction turnover, intracellular trafficking, and phosphorylation of connexin43 in brefeldin A-treated rat mammary tumor cells. The Journal of cell biology 131:1193-1203.

Lampe PD (1994) Analyzing phorbol ester effects on gap junctional communication: a dramatic inhibition of assembly. The Journal of cell biology 127:1895-1905.

Larson DM, Wrobleski MJ, Sagar GD, Westphale EM, Beyer EC (1997) Differential regulation of connexin43 and connexin37 in endothelial cells by cell density, growth, and TGF-beta1. The American journal of physiology 272:C405-415.

Larson DM, Seul KH, Berthoud VM, Lau AF, Sagar GD, Beyer EC (2000) Functional expression and biochemical characterization of an epitope-tagged connexin37. Mol Cell Biol Res Commun 3:115-121.

Lauf U, Giepmans BN, Lopez P, Braconnot S, Chen SC, Falk MM (2002) Dynamic trafficking and delivery of connexons to the plasma membrane and accretion to gap junctions in living cells. Proc Natl Acad Sci U S A 99:10446-10451.

Lee EJ, Han JW, Kim HJ, Kim IB, Lee MY, Oh SJ, Chung JW, Chun MH (2003) The immunocytochemical localization of connexin 36 at rod and cone gap junctions in the guinea pig retina. The European journal of neuroscience 18:2925-2934.

Li H, Chuang AZ, O'Brien J (2009a) Photoreceptor coupling is controlled by connexin 35 phosphorylation in zebrafish retina. The Journal of neuroscience : the official journal of the Society for Neuroscience 29:15178-15186.

Li H, Zhang Z, Blackburn MR, Wang SW, Ribelayga CP, O'Brien J (2013) Adenosine and dopamine receptors coregulate photoreceptor coupling via gap junction phosphorylation

in mouse retina. The Journal of neuroscience : the official journal of the Society for Neuroscience 33:3135-3150.

Li X, Lu S, Nagy JI (2009b) Direct association of connexin36 with zonula occludens-2 and zonula occludens-3. Neurochem Int 54:393-402.

Li X, Lynn BD, Nagy JI (2012) The effector and scaffolding proteins AF6 and MUPP1 interact with connexin36 and localize at gap junctions that form electrical synapses in rodent brain. The European journal of neuroscience 35:166-181.

Li X, Olson C, Lu S, Kamasawa N, Yasumura T, Rash JE, Nagy JI (2004) Neuronal connexin36 association with zonula occludens-1 protein (ZO-1) in mouse brain and interaction with the first PDZ domain of ZO-1. The European journal of neuroscience 19:2132-2146.

Long MA, Deans MR, Paul DL, Connors BW (2002) Rhythmicity without synchrony in the electrically uncoupled inferior olive. The Journal of neuroscience : the official journal of the Society for Neuroscience 22:10898-10905.

Los GV, Wood K (2007) The HaloTag: a novel technology for cell imaging and protein analysis. Methods in molecular biology 356:195-208.

Los GV, Encell LP, McDougall MG, Hartzell DD, Karassina N, Zimprich C, Wood MG, Learish R, Ohana RF, Urh M, Simpson D, Mendez J, Zimmerman K, Otto P, Vidugiris G, Zhu J, Darzins A, Klaubert DH, Bulleit RF, Wood KV (2008) HaloTag: a novel protein labeling technology for cell imaging and protein analysis. ACS chemical biology 3:373-382.

Magalhaes AC, Dunn H, Ferguson SS (2012) Regulation of GPCR activity, trafficking and localization by GPCR-interacting proteins. British journal of pharmacology 165:1717-1736.

Marandykina A, Palacios-Prado N, Rimkute L, Skeberdis VA, Bukauskas FF (2013) Regulation of Connexin-36 Gap Junction Channels by n-Alkanols and Arachidonic Acid. The Journal of physiology.

Martin PE, Errington RJ, Evans WH (2001) Gap junction assembly: multiple connexin fluorophores identify complex trafficking pathways. Cell communication & adhesion 8:243-248.

May JA, Ratan H, Glenn JR, Losche W, Spangenberg P, Heptinstall S (1998) GPIIb-IIIa antagonists cause rapid disaggregation of platelets pre-treated with cytochalasin D. Evidence that the stability of platelet aggregates depends on normal cytoskeletal assembly. Platelets 9:227-232.

Mills SL, Massey SC (1998) The kinetics of tracer movement through homologous gap junctions in the rabbit retina. Visual neuroscience 15:765-777.

Mundy DI, Machleidt T, Ying YS, Anderson RG, Bloom GS (2002) Dual control of caveolar membrane traffic by microtubules and the actin cytoskeleton. Journal of cell science 115:4327-4339.

Musch A (2004) Microtubule organization and function in epithelial cells. Traffic 5:1-9.

Musil LS, Goodenough DA (1993) Multisubunit assembly of an integral plasma membrane channel protein, gap junction connexin43, occurs after exit from the ER. Cell 74:1065-1077.

Musil LS, Beyer EC, Goodenough DA (1990) Expression of the gap junction protein connexin43 in embryonic chick lens: molecular cloning, ultrastructural localization, and post-translational phosphorylation. The Journal of membrane biology 116:163-175.

O'Brien J (2014) The ever-changing electrical synapse. Curr Opin Neurobiol 29C:64-72.

O'Brien J, Nguyen HB, Mills SL (2004) Cone photoreceptors in bass retina use two connexins to mediate electrical coupling. J Neurosci 24:5632-5642.

O'Brien JJ, Chen X, Macleish PR, O'Brien J, Massey SC (2012) Photoreceptor coupling mediated by connexin36 in the primate retina. The Journal of neuroscience : the official journal of the Society for Neuroscience 32:4675-4687.

Ouyang X, Winbow VM, Patel LS, Burr GS, Mitchell CK, O'Brien J (2005) Protein kinase A mediates regulation of gap junctions containing connexin35 through a complex pathway. Brain research Molecular brain research 135:1-11.

Palmer KJ, Watson P, Stephens DJ (2005) The role of microtubules in transport between the endoplasmic reticulum and Golgi apparatus in mammalian cells. Biochemical Society symposium:1-13.

Paquet M, Asay MJ, Fam SR, Inuzuka H, Castleberry AM, Oller H, Smith Y, Yun CC, Traynelis SF, Hall RA (2006) The PDZ scaffold NHERF-2 interacts with mGluR5 and regulates receptor activity. The Journal of biological chemistry 281:29949-29961.

Park DJ, Freitas TA, Wallick CJ, Guyette CV, Warn-Cramer BJ (2006) Molecular dynamics and in vitro analysis of Connexin43: A new 14-3-3 mode-1 interacting protein. Protein science : a publication of the Protein Society 15:2344-2355.

Park DJ, Wallick CJ, Martyn KD, Lau AF, Jin C, Warn-Cramer BJ (2007) Akt phosphorylates Connexin43 on Ser373, a "mode-1" binding site for 14-3-3. Cell communication & adhesion 14:211-226.

Pereda AE (2015) Neurobiology: all synapses are created equal. Current biology : CB 25:R38-41.

Pereda AE, Curti S, Hoge G, Cachope R, Flores CE, Rash JE (2013) Gap junction-mediated electrical transmission: Regulatory mechanisms and plasticity. Biochim Biophys Acta 1828:134-146.

Piehl M, Lehmann C, Gumpert A, Denizot JP, Segretain D, Falk MM (2007) Internalization of large double-membrane intercellular vesicles by a clathrin-dependent endocytic process. Molecular biology of the cell 18:337-347.

Pollard TD, Borisy GG (2003) Cellular motility driven by assembly and disassembly of actin filaments. Cell 112:453-465.

Roh DS, Funderburgh JL (2011) Rapid changes in connexin-43 in response to genotoxic stress stabilize cell-cell communication in corneal endothelium. Investigative ophthalmology & visual science 52:5174-5182.

Saez JC, Berthoud VM, Branes MC, Martinez AD, Beyer EC (2003) Plasma membrane channels formed by connexins: their regulation and functions. Physiological reviews 83:1359-1400.

Shaw RM, Fay AJ, Puthenveedu MA, von Zastrow M, Jan YN, Jan LY (2007) Microtubule plus-end-tracking proteins target gap junctions directly from the cell interior to adherens junctions. Cell 128:547-560.

Shen V, Rifas L, Kohler G, Peck WA (1986) Prostaglandins change cell shape and increase intercellular gap junctions in osteoblasts cultured from rat fetal calvaria. Journal of bone and mineral research : the official journal of the American Society for Bone and Mineral Research 1:243-249.

Simek J, Churko J, Shao Q, Laird DW (2009) Cx43 has distinct mobility within plasma-membrane domains, indicative of progressive formation of gap-junction plaques. Journal of cell science 122:554-562.

Singh AK, Riederer B, Krabbenhoft A, Rausch B, Bonhagen J, Lehmann U, de Jonge HR, Donowitz M, Yun C, Weinman EJ, Kocher O, Hogema BM, Seidler U (2009) Differential roles of NHERF1, NHERF2, and PDZK1 in regulating CFTR-mediated intestinal anion secretion in mice. The Journal of clinical investigation 119:540-550.

Spector I, Shochet NR, Blasberger D, Kashman Y (1989) Latrunculins--novel marine macrolides that disrupt microfilament organization and affect cell growth: I. Comparison with cytochalasin D. Cell motility and the cytoskeleton 13:127-144.

Takeichi M (1990) Cadherins: a molecular family important in selective cell-cell adhesion. Annual review of biochemistry 59:237-252.

Thomas MA, Zosso N, Scerri I, Demaurex N, Chanson M, Staub O (2003) A tyrosine-based sorting signal is involved in connexin43 stability and gap junction turnover. Journal of cell science 116:2213-2222.

Thomas MA, Huang S, Cokoja A, Riccio O, Staub O, Suter S, Chanson M (2002) Interaction of connexins with protein partners in the control of channel turnover and gating. Biology of the cell / under the auspices of the European Cell Biology Organization 94:445-456.

Thomas T, Jordan K, Simek J, Shao Q, Jedeszko C, Walton P, Laird DW (2005) Mechanisms of Cx43 and Cx26 transport to the plasma membrane and gap junction regeneration. Journal of cell science 118:4451-4462.

Thyberg J, Moskalewski S (1999) Role of microtubules in the organization of the Golgi complex. Experimental cell research 246:263-279.

Tinevez JY, Dragavon J, Baba-Aissa L, Roux P, Perret E, Canivet A, Galy V, Shorte S (2012) A quantitative method for measuring phototoxicity of a live cell imaging microscope. Methods in enzymology 506:291-309.

Traub O, Druge PM, Willecke K (1983) Degradation and resynthesis of gap junction protein in plasma membranes of regenerating liver after partial hepatectomy or cholestasis. Proceedings of the National Academy of Sciences of the United States of America 80:755-759.

Traub O, Look J, Paul D, Willecke K (1987) Cyclic adenosine monophosphate stimulates biosynthesis and phosphorylation of the 26 kDa gap junction protein in cultured mouse hepatocytes. European journal of cell biology 43:48-54.

Traub O, Look J, Dermietzel R, Brummer F, Hulser D, Willecke K (1989) Comparative characterization of the 21-kD and 26-kD gap junction proteins in murine liver and cultured hepatocytes. The Journal of cell biology 108:1039-1051.

Traub RD, Wong RK (1983) Synaptic mechanisms underlying interictal spike initiation in a hippocampal network. Neurology 33:257-266.

van Heusden GP (2005) 14-3-3 proteins: regulators of numerous eukaryotic proteins. IUBMB Life 57:623-629.

VanSlyke JK, Deschenes SM, Musil LS (2000) Intracellular transport, assembly, and degradation of wild-type and disease-linked mutant gap junction proteins. Molecular biology of the cell 11:1933-1946.

Vaughan EE, Dean DA (2006) Intracellular trafficking of plasmids during transfection is mediated by microtubules. Molecular therapy : the journal of the American Society of Gene Therapy 13:422-428.

Vaughan KT (2005) Microtubule plus ends, motors, and traffic of Golgi membranes. Biochimica et biophysica acta 1744:316-324.

Wakatsuki T, Schwab B, Thompson NC, Elson EL (2001) Effects of cytochalasin D and latrunculin B on mechanical properties of cells. Journal of cell science 114:1025-1036.

Wang Y, Rose B (1995) Clustering of Cx43 cell-to-cell channels into gap junction plaques: regulation by cAMP and microfilaments. Journal of cell science 108 (Pt 11):3501-3508.

Wang Y, Newton DC, Marsden PA (1999) Neuronal NOS: gene structure, mRNA diversity, and functional relevance. Critical reviews in neurobiology 13:21-43.

Windoffer R, Beile B, Leibold A, Thomas S, Wilhelm U, Leube RE (2000) Visualization of gap junction mobility in living cells. Cell and tissue research 299:347-362.

Yamaguchi DT, Ma D (2003) Mechanism of pH regulation of connexin 43 expression in MC3T3-E1 cells. Biochemical and biophysical research communications 304:736-739.

Yin X, Jedrzejewski PT, Jiang JX (2000) Casein kinase II phosphorylates lens connexin 45.6 and is involved in its degradation. The Journal of biological chemistry 275:6850-6856.

Zhang JT, Chen M, Foote CI, Nicholson BJ (1996) Membrane integration of in vitro-translated gap junctional proteins: co- and post-translational mechanisms. Molecular biology of the cell 7:471-482.

Zimmerman AL, Rose B (1985) Permeability properties of cell-to-cell channels: kinetics of fluorescent tracer diffusion through a cell junction. The Journal of membrane biology 84:269-283.

VITA

Yanran Wang (Helen) was born in Nanjing, China on October 13th, 1984, the daughter of Xudong Wang, MD and Xianhong Zhou. After completing her work at Dunman High School and Raffles Junior College in Singapore, she entered St. Mary's University in San Antonio, Texas in January 2004. She received the degree of Bachelor of Science, majoring in chemistry and Biology, in 2007. She worked as a research assistant at Texas Biomedical Research Institute (previously known as Southwest Foundation for Biomedical Research) from 2006 to 2007. In May of 2009 she entered the PhD program in neuroscience at The University of Texas Health Science Center at Houston Graduate School of Biomedical Sciences. She received her Master of Science degree in biomedical science in 2013.

Permanent address:

216 Marshall St. Apt 10

Houston, Texas 77006